

**New Approaches to the Determination of Minor Frictional Losses in  
Irrigation Systems**

**Dayton Tagwi  
Students No. 216076837**

**Submitted in partial fulfilment of the academic requirements of**

**Doctor of Philosophy (Engineering)**

**Bioresources Engineering  
School of Engineering  
College of Agriculture, Engineering and Science  
University of KwaZulu-Natal  
Pietermaritzburg  
South Africa**

**August 2022**

## **PREFACE**

The research contained in this thesis was completed by the candidate while based in the Discipline of Bioresources Engineering, School of Engineering, University of KwaZulu-Natal, Pietermaritzburg Campus, South Africa. The research was financially supported by the University of KwaZulu-Natal and the candidate.

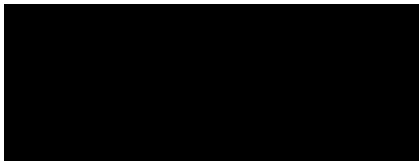
The contents of this work have not been submitted in any form to another University and, except where the work of others is acknowledged in the text, the results reported are due to investigations by the candidate.



---

Signed: Supervisor: Dr Aidan Senzanje

Date: 15<sup>th</sup> of August 2022



Signed: Co-Supervisor: Dr Gareth Lagerwall

Date: 15<sup>th</sup> of August 2022

## DECLARATION 1: PLAGIARISM

I, Dayton Tagwi, declare that:

(i) the research reported in this thesis, except where otherwise indicated or acknowledged, is my original work;

(ii) this thesis has not been submitted in full or in part for any degree or examination to any other university;

(iii) this thesis does not contain other persons' data, pictures, graphs or other information, unless specifically acknowledged as being sourced from other persons;

(iv) this thesis does not contain other persons' writing, unless specifically acknowledged as being sourced from other researchers. Where other written sources have been quoted, then:

a) their words have been re-written but the general information attributed to them has been referenced;

b) where their exact words have been used, their writing has been placed inside quotation marks, and referenced;

(v) where I have used material for which publications followed, I have indicated in detail my role in the work;

(vi) this thesis is primarily a collection of material, prepared by myself, published as journal articles or presented as a poster and oral presentations at conferences. In some cases, additional material has been included;

(vii) this thesis does not contain text, graphics or tables copied and pasted from the internet, unless specifically acknowledged, and the source being detailed in the thesis and in the References sections.



---

Signed: Dayton Tagwi

Date: 15<sup>th</sup> of August 2022

## DECLARATION 2: PUBLICATIONS

My role in each paper and presentation is indicated. The \* indicates corresponding author.

### Chapter 2

1. D Tagwi\*, A. Senzanje and G. Lagerwall (2021) *Secondary Losses in L-Bends in Irrigation Systems*. Manuscript in preparation.
2. Dayton Tagwi wrote the manuscript in consultation with Dr. A. Senzanje and Dr. G. Lagerwall, who supervised the research.

### Chapter 3

3. D Tagwi\*, A. Senzanje and G. Lagerwall (2021) *The Development Of An Empirical Equation For Determining Minor Losses Due To Bends In Smooth Pipes For Irrigation System Design*.
4. Dayton Tagwi wrote the manuscript in consultation with Dr. A. Senzanje and Dr. G. Lagerwall, who supervised the research.
5. Paper was presented at the Postgraduate Research & Innovation Symposium (PRIS) 2021 <https://pris.ukzn.ac.za/> and won an award in the combined Schools of Agriculture, Earth and Environmental Sciences and Engineering.
6. Manuscript submitted to and accepted for publication by the Agricultural Engineering International: CIGR Journal Open. <https://cigrjournal.org/index.php/Ejournal/index>

### Chapter 4

7. D Tagwi\*, A. Senzanje and G. Lagerwall (2021) *Development of the Dynamic Hydraulic Gradient within the Pipe Bend Due To Successive Pipe Bending*. Manuscript under preparation.
8. Dayton Tagwi wrote the manuscript in consultation with Dr. A. Senzanje and Dr. G. Lagerwall, who supervised the research.

### Chapter 5

9. D Tagwi\*, A. Senzanje and G. Lagerwall (2021) *Comparison of Traditional Methods with the Developed Empirical Equation in Determination of Minor Losses*. Manuscript under preparation.

10. Dayton Tagwi wrote the manuscript in consultation with Dr. A. Senzanje and Dr. G. Lagerwall, who supervised the research.

## **Chapter 6**

11. D Tagwi\*, A. Senzanje and G. Lagerwall (2021) *Effect of Two Phase Flow, Slope and Plane on the Bend Pressure Loss*. Manuscript under preparation.

12. Dayton Tagwi wrote the manuscript in consultation with Dr. A. Senzanje and Dr. G. Lagerwall, who supervised the research.



---

Signed: Dayton Tagwi

Date: 15<sup>th</sup> of August 2022

## ABSTRACT

As irrigation system pipe networks become shorter or have more bends, the proportion of losses due to bends increases, contributing significantly to the possible over- and under-sizing of pumps. Bends also inevitably introduce unbalanced thrust forces in pressurized pipelines, which could lead to leakage and possible joint separation. Again, with two phase flow and the combination of slope and plane, potential flow reversal and greater pressure drop may occur with bends. Minor losses though are principally determined using the Equivalent Length, Resistance Coefficient, and Valve Flow Coefficient methods. The use of these approaches in irrigation design is questionable due to the eminent shortcomings identified; namely, fixed flow coefficient (L/D ratio), required complete knowledge of coefficient development for use, and dependency on conversion factors. These shortcomings dictated the need to correctly calculate actual energy losses for efficient irrigation systems. As part of these flaws, these traditional methods do not offer straight forward determination of minor losses with change in bend parameters. Design errors in catering for bends are often encountered, which include incorrect technique usage, estimations of 30 to 50 pipe diameters in equivalent length, and 10, 15 to 25 percent of mainline loss. This research aimed for close approximation of the pressure drop due to the bend section and its peripherals, using a derived Empirical Equation. The attendant hypothesis to the research, was that secondary losses in irrigation systems may be accurately predicted using an Empirical Equation that takes into account the changing bend parameters as input and provides an easy way to calculate losses due to bends during irrigation design.

Development of the Empirical Equation was consequentially by analysis, association, and amalgamation of the behavioural patterns of the bends at relative radius of curvature,  $R_c = 13.545, 27.679, \text{ and } 79.578$  using experimental, and published data. Pressure differentials were measured on the outer and inner sides of straight one meter pipe section(s), bent from  $0^\circ$  to  $22.5^\circ, 45^\circ, 67.5^\circ$ , and ultimately  $90^\circ$  on two opposite axes, at 5 cm intervals within  $\pm 15$  cm peripherals. The two smooth splines of pressure differentials along the pipe bend section and peripherals developed, were related with the change of the main pressure head. This main pressure head behaviour was then graphically and quantitatively described by extrapolating of the smooth spline pressure differentials before, during, and after the bend section. For the traditional approaches, minor frictional losses as determined by the Equivalent Length,

Resistance Coefficient, and Valve Flow Coefficient methods, were compared to the theoretical 19.05 mm pipe (Empirical Equation, as reference). These were also extended to the different relative radii of curvature for the same pipe diameter. Lastly, three pipe diameters were used for assessment of pressure drop owing to two phase flow compared to single phase flow with change in slope and plane of bends from 0° to 90°.

For the investigated bend angles 0° to 90°, the Empirical Equation dynamically determined the best estimate of minor losses without the required thorough knowledge of friction coefficient derivation. It eliminated error by bridging the uncertainty in the use of traditional methods and friction coefficients in determining secondary or minor losses. The Equation's derivation was pragmatic, considering both measurable and immeasurable components and it identified saturation as  $R_c$  exceeded experimental values. A near approximation of the friction coefficient,  $k$  at  $R_c = 0.5$ , often mistaken in the literature is achieved by Equation. The developed Empirical Equation can be satisfactorily employed in irrigation system design methods or as a tool in software for correctly calculating minor losses. The two extremes of the derived dynamic hydraulic gradient lines outside of the bends were linked and from this, the principal restraining forces in the design of thrust blocks should be targeted more at forces related to fluid entering the bend (larger force) and less the exit stream (lesser force). In comparison of traditional methods, the Equivalent Length approach was shown to be fairly accurate for predicting secondary losses during irrigation design, provided the bend length to pipe diameter (L/D) ratio was considered. For the Resistance Coefficient technique, method was seen to be the closest estimate since the published friction coefficients were close to the theoretical 19.05 mm values. For conversion, the Equivalent Length and Resistance Coefficient values must be calculated with regards to changing pipe bend curvature and flow velocity. With bend angles less than 90°, practically all traditional approaches failed to estimate frictional loss. In some cases, air may enter an irrigation system from the suction side with fall in the supply line level and air leaking into the pipeline or chemical build up of air in the irrigation water, or cavitation at the pump. In tests conducted, the pressure drop increased when two phase flow was introduced. Pressure drop was greater at 0° (straight pipe) than for 90° bending. Regardless of pipe size, at low flow rates, the effect of two phase flow outweighs the effect of pressure drop due to bending i.e. for the same extent of bending, the pressure loss due to two-phase flow was less compared to single phase flow about the bend. Pressure drop was found to be unaffected by changes in slope or plane for the bend

angles evaluated. Pressure drop changed owing to change in height of fluid column relative to bend position. From the appraisal done for irrigation system design, air should be removed during normal operation to prevent increased minor losses and potential water hammer. Furthermore, it can be agreed that the influence of change in slope and plane of bends in an irrigation system, can be accounted for in the rise and fall of the straight pipe sections from natural ground, during design calculations.

In summary, the developed Empirical Equation, herein named the Dayton Equation, as hypothesised, can confidently be used for quick, accurate and precise determination of minor losses in irrigation system design as a method or tool for use in spread sheets or irrigation system design software such as IrriMaker (Model Maker Systems) or IRRICAD.

## **ACKNOWLEDGMENTS**

I would like to thank my Supervisor, Dr Aidan Senzanje and Co-Supervisor, Dr Gareth Lagerwall for their helpful insights and valuable time to look into my work.

I would also want to thank the Agricultural Research Council (ARC) Staff, Mr. Milton Petersen and Mr. Bennet Mdaka for the assistance in the construction of the test rig, running tests and recording of data and the outgoing manager Mr. Felix Reinders for granting access to the laboratory for the tests.

I would also like to thank my wife, Dr Aluwani Maiwashe - Tagwi who has always encouraged me and above all, I would like to thank THE LIVING WATER, EMMANUEL, ELOHIM; for the Supernatural UNDERSTANDING, KNOWLEDGE, WISDOM AND MIGHT throughout the journey and EVER.

## TABLE OF CONTENTS

PREFACE.....	
DECLARATION 1: PLAGIARISM.....	i
DECLARATION 2: PUBLICATIONS .....	ii
ABSTRACT .....	iv
ACKNOWLEDGMENTS.....	vii
LIST OF TABLES .....	xiii
LIST OF FIGURES .....	xiv
LIST OF ABBREVIATIONS.....	xvii
LIST OF SYMBOLS .....	xviii
CHAPTER 1: INTRODUCTION .....	1
1.1. Energy Loss due to Change in the Flow Direction.....	1
1.2. Energy Loss due to Fluid Interaction or Shearing Fluid Elements.....	2
1.3. Energy Loss due to Fluid-Wall Interaction .....	3
1.4. Main Purpose of the Research.....	4
1.5. Problem Statement.....	5
1.6. Justification of the Study.....	6
1.7. Aims .....	7
1.7.1. Specific Objectives .....	8
1.8. Originality of the Study.....	8
CHAPTER 2: SECONDARY LOSSES IN L-BENDS IN IRRIGATION SYSTEMS .....	10
2.1. Introduction .....	10
2.2. Limitations of Darcy-Weisbach Friction Equation.....	10
2.3. Colebrook-White / Newton-Raphson, Moody chart, Barr, Wood, Haaland, and Swamee - Jain formulas .....	11

2.4. Hazen-Williams, Blasius, Lamont, Scimemi, Manning and the General Exponential Equations.....	11
2.5. Methods for Determination of Minor Losses .....	12
2.5.1. The Equivalent Length ( $L_e/D$ ) .....	12
2.5.2. The Resistance Coefficient (K) .....	13
2.5.3. Valve Flow Coefficient ( $C_v$ ) .....	14
2.6. Single-Phase Flow Through a Vertical Bend .....	16
2.6.1. Pressure Drop Outside and Inside of Pipe Bend.....	18
2.6.2. Dynamic and Kinematic Viscosity of Water.....	24
2.6.3. Dean Vortices Formation and Secondary Flow Generation Downstream of Bend ...	26
2.7. Two phase Flow through a Bend.....	31
2.7.1. Void Fraction and Two Phase Dynamic Viscosity Models .....	32
2.7.2. Two Phase Flow in Upward, Horizontal, or Downward Arrangement .....	36
2.8. CFD Analysis of Energy Losses on a 90° Bend.....	37
2.9. The Effect of Geometric Parameters on Frictional Losses .....	38
2.10. Discussion .....	41
2.11. Conclusion.....	43
<b>CHAPTER 3: THE DEVELOPMENT OF AN EMPIRICAL EQUATION FOR DETERMINING MINOR LOSSES DUE TO BENDS IN SMOOTH PIPES FOR IRRIGATION SYSTEM DESIGN .....</b>	<b>44</b>
Abstract.....	44
3.1. Introduction .....	45
3.2. Materials and Methods.....	49
3.2.1. Research Site / Laboratory .....	49
3.2.2. Experimental Methodology .....	49
3.3. Theoretical Approach to the Development of the Empirical Equation .....	53
3.3.1. Dimensional Homogeneity and Dimensional Analysis .....	53

3.3.2. Derivation of the Empirical Equation .....	54
3.4. Results and Discussion.....	56
3.4.1. Behaviour of the Relative Radius of Curvature with Bending .....	56
3.4.2. Pressure Drop for Fixed Relative Radius of Curvature with Successive Bending....	57
3.4.3. Friction Coefficients from the Measured Pressure Drop .....	60
3.4.4. Mathematical Relation of Pressure Drop with change in Bend Angle .....	62
3.4.5. Friction Coefficient with changing Pipe Diameter and Bend Angle .....	63
3.4.6. Friction Coefficient with changing $R_c$ and Bend Angle .....	66
3.4.7. Composition of the Empirical Equation.....	68
3.4.8. Validation of the Empirical Equation .....	70
3.5. Conclusions .....	72
APPENDIX A: EXPERIMENTAL DATA FOR PRESSURE DROP DUE TO SUCCESSIVE PIPE BENDING WITH FIXED $R_c$ .....	74
APPENDIX B: AVAILABLE PUBLISHED BEND LOSSES COEFFICIENTS FOR VARIOUS PIPE DIAMETRES TESTED.....	75
APPENDIX C: FITTED COEFFICIENT MULTIPLIER FOR THE “FRICTION COEFFICIENT vs. PIPE DIAMETER CURVE” WITH CHANGING $R_c$ .....	76
CHAPTER 4: DEVELOPMENT OF THE DYNAMIC HYDRAULIC GRADIENT WITHIN THE PIPE BEND DUE TO SUCCESSIVE PIPE BENDING .....	77
Abstract.....	77
4.1. Introduction .....	78
4.2. Materials and Methods.....	80
4.2.1. Study Laboratory .....	80
4.2.2. Experimental Methodology and Equipment.....	81
4.2.3. Experimental Data Analysis .....	84
4.3. Theoretical Approach to the Development of the Dynamic Hydraulic Gradient.....	85
4.4. Results and Discussion.....	86

4.4.1. Pressures differential trends due to Successive Pipe Bending .....	86
4.4.1.1. Outer Pressures due to Successive Pipe Bending .....	90
4.4.1.2. Inner Pressures due to Successive Pipe Bending .....	91
4.4.2. Superimposing of the Inner and Outer Pressures measured over the Successive Pipe Bend.....	92
4.4.3. Change of the Hydraulic Gradient along Bend due to Successive Pipe Bending .....	93
4.4.4. Normalisation of the Change of Hydraulic gradient over Bend Section and Peripherals on a Chart.....	95
4.4.5. Normalisation of the Change of Hydraulic gradient over Bend Section and Peripherals on a MS Excel Tool.....	96
4.5. Conclusions .....	97
APPENDIX D: NORMALISED SMOOTH SPLINE OF EXPERIMENTAL AND THEORETICAL DATA (25mm Ø, 0.1969 ms <sup>-1</sup> ).....	
	99
CHAPTER 5: COMPARISON OF TRADITIONAL METHODS WITH THE DEVELOPED EMPIRICAL EQUATION IN DETERMINATION OF MINOR LOSSES.....	
	101
Abstract .....	101
5.1 Introduction .....	102
5.2 Method of Comparison of the Frictional Loss by Traditional Methods .....	105
5.3 Results and Discussion .....	108
5.3.1 Equivalent Length Method.....	108
5.3.2 Resistance Coefficient Method.....	111
5.3.3 Valve Flow Coefficient .....	112
5.4 Conclusions .....	113
APPENDIX E: FRICTIONAL LOSSES AS DETERMINED BY EMPIRICAL EQUATION FOR THE 19.05 mm DIAMETER PIPE .....	
	115
APPENDIX F: EMPIRICAL EQUATION CALCULATOR BASED ON THE THEORETICAL 19.05 mm DIAMETER PIPE .....	
	116

CHAPTER 6: EFFECT OF TWO PHASE FLOW, SLOPE AND PLANE ON THE BEND PRESSURE LOSS.....	117
Abstract.....	117
6.1 Introduction .....	118
6.2 Materials and Methods.....	120
6.2.1 Study Laboratory .....	120
6.2.2 Experimental Materials and Apparatus.....	120
6.2.3 Experimental Methodology.....	121
6.3 Results And Discussion .....	123
6.3.1 Effects of Two Phase Flow on Pressure Drop.....	123
6.3.2 Effects of the Slope and Plane on Pressure Drop due to Single Phase Flow .....	125
6.4 Conclusions .....	133
CHAPTER 7: CONCLUSIONS AND RECOMMENDATIONS FOR FURTHER RESEARCH.....	135
7.1 Revisiting the Aims and Objectives .....	135
7.2 Contributions to New Knowledge .....	136
7.3 Future Possibilities and Recommendations .....	137
7.4 Final Comments.....	138
REFERENCES.....	139

## LIST OF TABLES

TABLE 3.1 SINGLE PHASE SUPPLY FLOW RATE ( $\text{M}^3\text{S}^{-1}$ ) AND INDIVIDUAL PIPE DIAMETER FLOW VELOCITIES ( $\text{MS}^{-1}$ )	51
TABLE 3.2 FRICTION COEFFICIENTS, $k$ DUE TO PRESSURE DROP AGAINST THE BEND ANGLE FOR THE VARIED SINGLE-PHASE FLOWS TESTED WITH FIGURES IN BOLD USED TO OBTAIN THE AVERAGE VALUES FOR CLOSER APPROXIMATION OF THE FRICTION COEFFICIENTS	61
TABLE 3.3 THEORETICAL FRICTION COEFFICIENTS $k$ , FROM THE DEVELOPED EMPIRICAL EQUATION (IN BOLD ARE THE PUBLISHED VALUES AVAILABLE FROM SPEDDING <i>ET AL.</i> (2004) AND THOSE ADOPTED IN THE IRRIGATION DESIGN MANUAL BY ARC (2003) AND EXPERIMENTAL VALUES AVAILABLE FROM EXPERIMENTAL DATA FOR COMPARISON AND LINKAGE)	70
TABLE 3.4 COMPARISON OF FRICTION COEFFICIENTS, $k$ , PRODUCED BY THE EMPIRICAL EQUATION WITH THE PUBLISHED FRICTION COEFFICIENTS	71
TABLE 3.5 COMPARISON OF FRICTION COEFFICIENTS PRODUCED BY THE EMPIRICAL EQUATION WITH THE EXPERIMENTAL DATA FRICTION COEFFICIENTS	71
TABLE 4.1 SINGLE PHASE SUPPLY PIPE LINE FLOW RATE ( $\text{M}^3\text{S}^{-1}$ ) TESTED AND INDIVIDUAL TEST PIPE DIAMETER FLOW VELOCITIES ( $\text{MS}^{-1}$ )	84
TABLE 5.1 EMPIRICAL EQUATION FRICTION COEFFICIENTS FOR THE 19.05 MM DIAMETER PIPE USED FOR COMPARISON OF THE FRICTIONAL LOSSES	107
TABLE 5.2 EQUIVALENT LENGTHS ( $L/D$ VALUES) FOR THE 19.05 MM DIAMETER PIPE USED FOR COMPARISON OF THE FRICTIONAL LOSSES WHEREIN $H_f = F (L/D)V^2/2G$	107
TABLE 5.3 RESISTANCE COEFFICIENTS ( $k$ VALUES) FOR THE 19.05 MM DIAMETER PIPE USED FOR COMPARISON OF THE FRICTIONAL LOSSES WHEREIN $H_f = kV^2/2G$	108
TABLE 5.4 VALVE FLOW COEFFICIENTS ( $K$ VALUES) FOR THE 19.05 MM DIAMETER PIPE USED FOR COMPARISON OF FRICTIONAL LOSSES WHEREIN $C_v = 1.157K_v$ , $K_v = 0.8646C_v$ ; $H_L = 0.0295 K Q^2/D^4$	108
TABLE 5.5 COMPARISON OF HEAD LOSSES AS DETERMINED BY THE EMPIRICAL EQUATION AND THE EQUIVALENT LENGTH METHOD FOR THE 19.05 MM DIAMETER PIPE	109
TABLE 5.6 COMPARISON OF HEAD LOSSES AS DETERMINED BY THE EMPIRICAL EQUATION EMPIRICAL EQUATION AND THE RESISTANCE COEFFICIENT METHOD FOR THE 19.05 MM DIAMETER PIPE	111
TABLE 5.7 COMPARISON OF HEAD LOSSES AS DETERMINED BY THE EMPIRICAL EQUATION EMPIRICAL EQUATION AND THE VALVE FLOW COEFFICIENT METHOD FOR THE 19.05 MM DIAMETER PIPE	112
TABLE 6.1 PRESSURE DROP WITH CHANGE IN SLOPE FROM $0^\circ$ TO $90^\circ$ WITH FIXED PLANE FOR FLOW VELOCITIES 0.271, 0.197 AND $0.079 \text{ MS}^{-1}$ FOR RESPECTIVE PIPE DIAMETERS	126
TABLE 6.2 PRESSURE DROP WITH CHANGE IN SLOPE FROM $0^\circ$ TO $-90^\circ$ WITH FIXED PLANE FOR FLOW VELOCITIES 0.271, 0.197 AND $0.079 \text{ MS}^{-1}$ FOR RESPECTIVE PIPE DIAMETERS	127
TABLE 6.3 LIQUID DEPTH / LEVEL TO HYDROSTATIC PRESSURE RELATIVE TO THE CHANGE IN SLOPE WITH FIXED PLANE	128
TABLE 6.4 PRESSURE DROP WITH CHANGE IN PLANE FROM $0^\circ$ TO $-90^\circ$ WITH FIXED SLOPE FOR FLOW VELOCITIES 0.271, 0.197 AND $0.079 \text{ MS}^{-1}$ FOR RESPECTIVE PIPE DIAMETERS	131
TABLE 6.5 LIQUID DEPTH / LEVEL TO HYDROSTATIC PRESSURE RELATIVE TO THE CHANGE IN PLANE WITH FIXED SLOPE	132

## LIST OF FIGURES

FIGURE 1. 1 FORCES ON A FLUID ELEMENT AND PRESSURE GRADIENT IN A DUCT AT A 90 DEGREE BEND (NPTEL, 2015).....	2
FIGURE 1. 2 PRESSURE GRADIENT IN A DUCT AT A 90 DEGREE BEND (SUN ET AL., 2012).....	3
FIGURE 2.1 CORKSCREW FLOW IN A BEND: A) SECTION ALONG BEND; B) RECTANGULAR CROSS-SECTION PIPE AND; C) CIRCULAR CROSS-SECTION PIPE (BRILEY, 1974).....	16
FIGURE 2.2 PRESSURE CONTOURS FOR U-BEND WITH BEND-TO-PIPE DIAMETER RATIO 24 AND REYNOLDS NUMBER = 23 6000 (BRILEY, 1974).....	16
FIGURE 2.3 PIPE BEND LOSS COEFFICIENTS (WILCOX, 1978).....	17
FIGURE 2.4 MEAN STATIC PRESSURE OF INCOMPRESSIBLE LIQUID FLOW THROUGH BENDS IN A HORIZONTAL PLANE (AZZI AND FRIEDEL, 2005).....	18
FIGURE 2.5 MEAN VELOCITY PROFILE DEVELOPMENT AT ANGULAR POSITIONS $\phi$ INSIDE A BEND SECTION (RÖHRIG ET AL., 2015).....	19
FIGURE 2.6 INNER AND OUTER ARC PRESSURE COEFFICIENT, $C_p$ ALONG BEND AT, $Re_B = 2\ 4000$ (RÖHRIG ET AL., 2015).....	20
FIGURE 2.7 COMPARISON OF THE FRICTION COEFFICIENT, $C_f$ OF FRICTION OF THE BEND AT $Re_B = 2\ 4000$ (RÖHRIG ET AL., 2015).....	20
FIGURE 2.8 MEAN VELOCITY PROFILE FLUCTUATION ON BEND (DUTTA ET AL., 2016).....	21
FIGURE 2.9 VARIOUS SECTIONS OF LAMINAR SEPARATION BUBBLE FLOW (LIN AND PAULEY, 1996).....	22
FIGURE 2.10 SEPARATION AND REATTACHMENT POINT'S DEPENDENCY ON REYNOLDS NUMBER (DUTTA ET AL., 2016).....	23
FIGURE 2.11 ROOT MEAN SQUARE VELOCITY (RMS) PROFILES OF VELOCITY OSCILLATIONS AT THE BEND EXIT, $U_{RMS}$ IN X DIRECTION AND $V_{RMS}$ IN Y DIRECTION (DUTTA ET AL., 2016).....	23
FIGURE 2.12 WATER RELATIVE VISCOSITY (THE ENGINEERING TOOL BOX.COM, 2018).....	25
FIGURE 2.13 WATER VISCOSITY AT SATURATION PRESSURE (THE ENGINEERING TOOL BOX.COM, 2018).....	25
FIGURE 2.14 SECONDARY FLOW FIELD FOR SMALL AND LARGE DEAN NUMBERS (GHOBADI AND MUZYCHKA, 2016).....	26
FIGURE 2.15 DEGENERATION OF NORMALIZED SWIRL INTENSITY ALONG PIPE FROM ELBOW EXIT WITH $R_c = 3D$ (KIM ET AL., 2014).....	28
FIGURE 2.16 DEPENDENCY OF NORMALIZED SWIRL INTENSITY DEGENERATION ALONG PIPE FROM ELBOW EXIT WITH RADIUS OF CURVATURE (KIM ET AL., 2014).....	29
FIGURE 2.17 SWIRL INTENSITY DEPENDENCY ON REYNOLDS NUMBER AT EXIT OF ELBOW (KIM ET AL., 2014).....	29
FIGURE 2.18 SWIRL INTENSITY DEPENDENCY ON RADIUS OF ELBOW CURVATURE OF AT EXIT OF ELBOW (KIM ET AL., 2014).....	30
FIGURE 2.19 NUMERICAL RESULTS FOR EXPERIMENT (A) STREAM WISE VELOCITY PROFILES, (B).....	31
FIGURE 2.20 TWO PHASE DENSITY DETERMINED BY VOID FRACTION AND TWO PHASE MIXTURE DENSITY IS FOUNDED ON TWO PHASE QUALITY FOUNDED ON THE VALUES OF VOID FRACTION MEASURED AT OKLAHOMA STATE UNIVERSITY, TWO PHASE FLOW LABORATORY (GHAJAR AND BHAGWAT, 2013). .....	34

FIGURE 2.21 STATIC PRESSURE CONTOURS, STREAMLINES DETAILS AT $Re=1 \times 10^5$ AND SECONDARY FLOW PATTERNS AT THE ELBOW CROSS SECTION (DOS SANTOS <i>ET AL.</i> , 2014).....	37
FIGURE 2.22 LOSS COEFFICIENT ( $C_0$ ) WITH THE REYNOLDS NUMBER (DOS SANTOS <i>ET AL.</i> , 2014).....	38
FIGURE 2.23 CONTRAST OF NORMALIZED FRICTION FEATURES OF LAMINAR FLOW WITH MODELS (DAI <i>ET AL.</i> , 2014). .....	39
FIGURE 2.24 VARIATION OF THE FRICTIONAL LOSS COEFFICIENT ( $K_T$ ) WITH BEND ANGLE ( $\theta$ )FOR SMOOTH PIPE BENDS FOR REYNOLDS NUMBER OF $2 \times 10^5$ (ITO, 1960).....	40
FIGURE 2.25 VARIATION OF BEND-LOSS COEFFICIENT WITH RELATIVE RADIUS FOR SMOOTH PIPE BENDS FOR REYNOLDS NUMBER OF $2 \times 10^5$ (ITO, 1960).....	41
FIGURE 3.1 SCHEMATIC DIAGRAM OF EXPERIMENTAL TEST CONFIGURATION DIMENSIONED IN MILLIMETERS SHOWING THE PIPE(S) BEND ANGLES TESTED FOR VARIED FLOW AND GAUGE POSITION.....	50
FIGURE 3.2 RELATIONSHIP BETWEEN RADIUS OF CURVATURE ( $R_c$ ) AND BEND ANGLE FOR THE 8 MM (ID), 23 MM (ID) AND 47 MM (ID) DIAMETER PIPES .....	57
FIGURE 3.3 PRESSURE DROP AS FUNCTION OF THE BEND ANGLE FOR VARIED SINGLE PHASE FLOW FOR THE 47 MM DIAMETER PIPE FOR $R_c = 13.545$ .....	58
FIGURE 3.4 PRESSURE DROP AS FUNCTION OF THE BEND ANGLE FOR VARIED SINGLE PHASE FLOW FOR THE 23 MM DIAMETER PIPE FOR $R_c = 27.679$ .....	59
FIGURE 3.5 PRESSURE DROP AS FUNCTION OF THE BEND ANGLE FOR VARIED SINGLE PHASE FLOW FOR THE 8 MM DIAMETER PIPE FOR $R_c = 79.578$ .....	59
FIGURE 3.6 RELATIONSHIP BETWEEN FRICTION COEFFICIENT AND PIPE DIAMETER FOR $0^\circ$ TO $90^\circ$ BEND .....	64
FIGURE 3.7 FRICTION COEFFICIENT, $k$ , WITH CHANGE IN PIPE DIAMETER FOR FIXED $R_c$ AT $90^\circ$ BEND (SPEDDING <i>ET AL.</i> , 2004). .....	65
FIGURE 3.8 FRICTION COEFFICIENT WITH CHANGE IN $R_c$ FOR FIXED PIPE DIAMETERS FOR THE $90^\circ$ BEND (DATA FROM SPEDDING <i>ET AL.</i> (2004) AND NEUTRIUM (2016)). .....	67
FIGURE 4.1 SCHEMATIC DIAGRAM OF THE TEST APPARATUS SHOWING THE SUCCESSIVE PIPE BENDING ANGLES AND SUCCESSIVE GAUGE POSITIONS FOR THE INNER AND OUTER PRESSURES MEASURED. ....	82
FIGURE 4.2 BEHAVIOUR OF PRESSURE ALONG THE OUTER AND INNER AXIS OF THE PIPE BEND FOR THE 25 MM (OD) PIPE AT $0.197 \text{ ms}^{-1}$ WITH SMOOTHED SPLINE EXPECTED TREND .....	87
FIGURE 4.3 BEHAVIOUR OF PRESSURE ALONG THE OUTER AND INNER AXIS OF THE PIPE BEND FOR THE 25 MM (OD) PIPE AT $0.164 \text{ ms}^{-1}$ WITH SMOOTHED SPLINE EXPECTED TREND .....	88
FIGURE 4.4 BEHAVIOUR OF PRESSURE ALONG THE OUTER AND INNER AXIS OF THE PIPE BEND FOR THE 25 MM (OD) PIPE AT $0.131 \text{ ms}^{-1}$ WITH SMOOTHED SPLINE EXPECTED TREND .....	88
FIGURE 4.5 BEHAVIOUR OF PRESSURE ALONG THE OUTER AND INNER AXIS OF THE PIPE BEND FOR THE 25 MM (OD) PIPE AT $0.0985 \text{ ms}^{-1}$ WITH SMOOTHED SPLINE EXPECTED TREND .....	89
FIGURE 4.6 BEHAVIOUR OF PRESSURE ALONG THE OUTER AND INNER AXIS OF THE PIPE BEND FOR THE 50 MM (OD) PIPE AT $0.0865 \text{ ms}^{-1}$ WITH SMOOTHED SPLINE EXPECTED TREND .....	89
FIGURE 4.7 SMOOTH SPLINE RESULTANT PRESSURE DIFFERENTIALS FOR THE 25 MM (OD) PIPE AT $0.1969 \text{ ms}^{-1}$ ....	92
FIGURE 4.8 CUMULATIVE SMOOTH SPLINE RESULTANT PRESSURE DIFFERENTIALS FOR THE 25 MM (OD) PIPE AT $0.1969 \text{ ms}^{-1}$ OVER THE BEND SECTION AND PERIPHERALS .....	94

FIGURE 4.9 NORMALISED EXTRAPOLATED CHANGE OF THE SUCCESSIVE DYNAMIC HYDRAULIC GRADIENT (MAIN PRESSURE HEAD) FOR THE SUCCESSIVE PIPE BENDING FOR A ONE METER BEND .....	95
FIGURE 6.1 EXPERIMENTAL TEST CONFIGURATION FOR PRESSURE DROP DUE TO TWO PHASE FLOW AND SINGLE PHASE FLOW FOR CHANGE IN SLOPE AND PLANE WITH SUCCESSIVE PIPE BENDING 0° TO 90° .....	121
FIGURE 6.2 INDEPENDENT SLOPE AND PLANE TESTED FOR PRESSURE DROP WITH SINGLE PHASE FLOW FOR SUCCESSIVE PIPE BENDING .....	122
FIGURE 6.3 PRESSURE DROP DUE TO SINGLE AND TWO PHASE FLOW FOR SUCCESSIVE PIPE BENDING FOR THE 50 MM (47 ID) DIAMETER PIPE .....	123
FIGURE 6.4 PRESSURE DROP DUE TO SINGLE AND TWO PHASE FLOW FOR SUCCESSIVE PIPE BENDING FOR THE 25 MM (23 ID) DIAMETER PIPE .....	124
FIGURE 6.5 PRESSURE DROP DUE TO SINGLE AND TWO PHASE FLOW FOR SUCCESSIVE PIPE BENDING FOR THE 10 MM (8 ID) DIAMETER PIPE .....	124
FIGURE 6.6 PERCENTAGE CHANGE IN OVERALL PRESSURE DROP FOR SLOPE -90° TO 90° AND 0° PLANE WITH BENDING .....	129
FIGURE 6.7 PERCENTAGE CHANGE IN OVERALL PRESSURE DROP FOR PLANE -90° TO 90° AND 0° SLOPE WITH BENDING .....	133

## LIST OF ABBREVIATIONS

ARC	Agricultural Research Council.
CFD	Computational Fluid Dynamics.
EVM	Eddy Viscosity Model.
LES	Large Eddy Simulation.
LCD	Liquid Crystal Display.
PRIS	Postgraduate Research & Innovation Symposium.
MS	Microsoft.
NPTEL	National Programme on Technology Enhanced Learning.
PVC	Polyvinyl Chloride.
RMSE	Root Mean Square Error.
RSM	Reynolds-averaged Navier–Stokes.
SABI	South African Irrigation Institute (Afrikaans).
UKZN	University of KwaZulu-Natal.

## LIST OF SYMBOLS

$A$	pipe section area.
$C_v$	Valve Flow Coefficient ( $A_v$ in the S.I. units).
$C_p$	pressure coefficient.
$C_o$	loss coefficient.
$C_f$	friction coefficient.
$D$	pipe diameter.
$D_e$	Dean's number.
$eq$	equivalent.
$f$	Darcy friction factor.
$f_s$	is the Moody friction factor in a straight pipe.
$Fr_\theta$	Froude Number with respect to the bend angle $\theta$ .
$g$	acceleration due to gravity.
$G$	two phase mixture mass flux, ( $G = G_l + G_g$ ), $\text{kg/m}^2\text{s}^{-1}$ .
$H$	flow depth.
$h_f$	head loss.
$h_L$	fluid head.
ID	inside diameter.
$I_s$	swirl intensity.
$I_{s0}$	initial swirl intensity value.
$k$	Resistance Coefficient.
$K$	Crane Resistance Coefficient.
$k_b$	bend loss coefficient.
$k_{LO}$	bend loss coefficient for single phase flow.
$K_v$	$C_v$ in US gallons per minute.
L/D ratio	flow coefficient.
$L$	bend length or pipe section.
$L_e$	equivalent length.
$\hat{n}$	unit vector normal to the pipe section area.
$m$	mixture.
MID	middle point.

OD	outside diameter.
$Q$	volumetric flow rate in $\text{m}^3\text{s}^{-1}$
$r$	Radius of curvature of bend.
$\acute{r}$	pipe radius.
R Squared	the coefficient of determination.
$R_b$	bend centre-line radius.
$R_c$	relative radius of curvature, pipe diameter per bend radius of curvature.
$P$	pressure.
SP	separation point.
SSE	label, residual sum squared.
$R_e$	Reynolds number.
RP	reattachment point.
$t$	total.
TP	two phase.
$u$	mean flow velocity.
$\vec{U}$	flow velocity vector.
$v$	average flow velocity.
$v_d$	Flow velocity with respective pipe diameter.
$x$	quality of phase.
$\alpha$	void fraction.
$\beta_s$	rate of decreases of secondary flow intensity downstream at the elbow.
$\varepsilon$	Pipe roughness.
$\varepsilon/D_h$	relative roughness.
$\rho$	Density of liquid in kg/m.
$\mu_d$	dynamic viscosity.
$\lambda_d$	kinematic viscosity.
$\emptyset$	diameter.
$\theta$	bend angle.
$\Delta P$	change in pressure.
$\Delta P_{TP}$	pressure drop-in two-phase flow.
$\Delta P_{LO}$	pressure drop in a single-phase flow of total mass flux and liquid properties.

## CHAPTER 1: INTRODUCTION

Energy or pressure loss in irrigation systems is due to the contribution of fluid elements colliding and fluid wall friction in the straight pipe sections. There are, however many methods used in the determination of frictional losses along the straight pipe sections, for example the approaches by; Darcy-Weisbach developed in 1845, Hazen-Williams developed in 1906, Newton-Raphson developed in 1911 or Colebrook-White developed in 1939, Moody chart developed in 1944, Wood developed in 1966, Swamee - Jain developed in 1976, Barr developed in 1981, Haaland developed in 1983, Lamont and General Exponential equation developed in 1998 (Wilson, 2012). In addition to these losses in the irrigation systems, there are secondary or minor losses that are attributed to by the fittings, i.e., bends, Tee pieces, sluice valves, ball valves, reducers, reflux valves, foot valves and screens. These, however, are regarded as minor losses but contribute significantly to the head requirement when sizing a pump in the irrigation design process. The minor (frictional) losses due to the bends and fittings collectively contribute to the pressure drop along the supply line and overall loss of system pressure (Yasmina and Rachid, 2015). Application of the above mentioned straight pipe frictional loss approaches is applicable to some extent with some level of limitation in the case of a bend or fitting.

Energy or pressure losses (secondary or minor losses also) in this case are mainly due to fluid-wall frictional and dynamic (fluid elements interactions) losses within the section of fitting involved. Energy or pressure losses are also seen to occur as a result of the collision and shear stress of the water with the pipe wall or fitting and eddies produced in the turbulence (dos Santos *et al.*, 2014). Secondary frictional losses, however, occur because of three factors: firstly, the change in the direction of flow, secondly due to the fluid interaction in itself (fluid element(s) friction) i.e. cohesion forces and thirdly, differential pipe wall-fluid interaction i.e. adhesion forces about the bend, and in some cases, the enlargement and or constriction of the pipe section at the bend (Jayanti, 2011).

### **1.1. Energy Loss due to Change in the Flow Direction**

Bends in irrigation pipe lines are introduced essentially to redirect the flow to the required blocks for irrigation purposes. The energy losses relative to the bend in the pipe sections are

mainly dependent on the pipe diameter, angle of the bend, radius of curvature of the bend and the flow velocity. Change in flow direction introduces pressure differentials and flow separation resulting in the formation of eddies. As the angle of the bend increases the energy losses inevitably increase, and as the bend radius of curvature increases, the energy losses reduce (Azzi and Friedel, 2005; NPTEL, 2015).

## 1.2. Energy Loss due to Fluid Interaction or Shearing Fluid Elements

Inevitably due to the introduction of the bend, there are energy losses within the shearing fluid elements due to the change in the flow streamlines. As the fluid column flows past the pipe bend, fluid element(s) close to the inside of the bend experience a pull radial to the centre of curvature of the bend that is defined as centripetal acceleration (Azzi and Friedel, 2005; NPTEL, 2015). Due to the curved duct and change in flow path, the fluid element(s) also encounter centrifugal acceleration due to self-weight from the momentaneous centre of curvature of the bend to the outer wall, resulting in the swirling and mixing of the fluid. The fluid flowing through a bend in an irrigation system typically flows in a similar manner as shown in Figure 1.1.

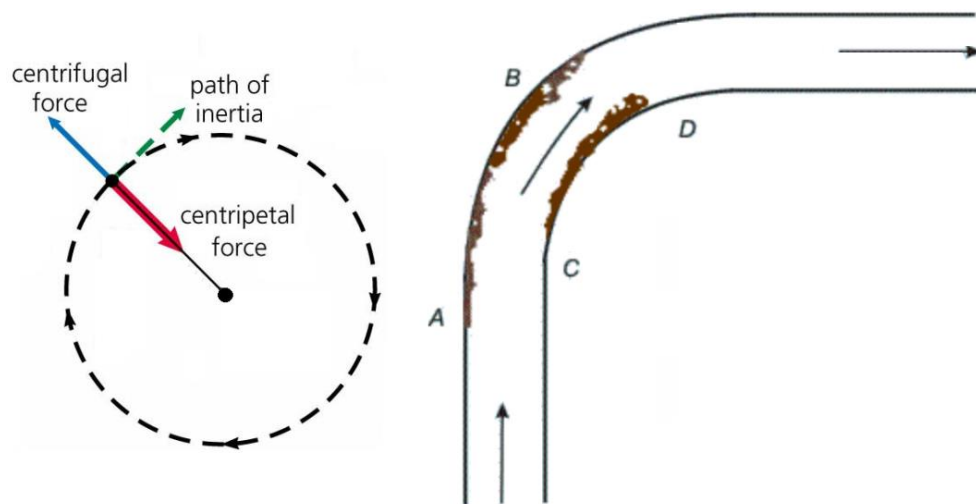


**Figure 1. 1 Forces on a fluid element and pressure gradient in a duct at a 90 degree bend (NPTEL, 2015)**

Due to the bending, pressure increases on the inner wall of the pipe from point A, and gradually increases to a maximum at point B. Consequently, on the opposite end of the pipe, the fluid column encounters centripetal acceleration and pressure falls from C to a minimum

at point D and the water flowing in the middle inevitably experiences some pressure gradients also causing secondary losses in the plane radial to the pipe. The retarded flow close to the wall C to D also experiences a vacuum and coupled with the influence of the swirling fluid from the outside of the bend, resulting in the formation of the eddy currents, causing energy losses (NPTEL, 2015). Figure 1.2 shows the differential pressures (pressure contours) observed experimentally in a 90° bend.

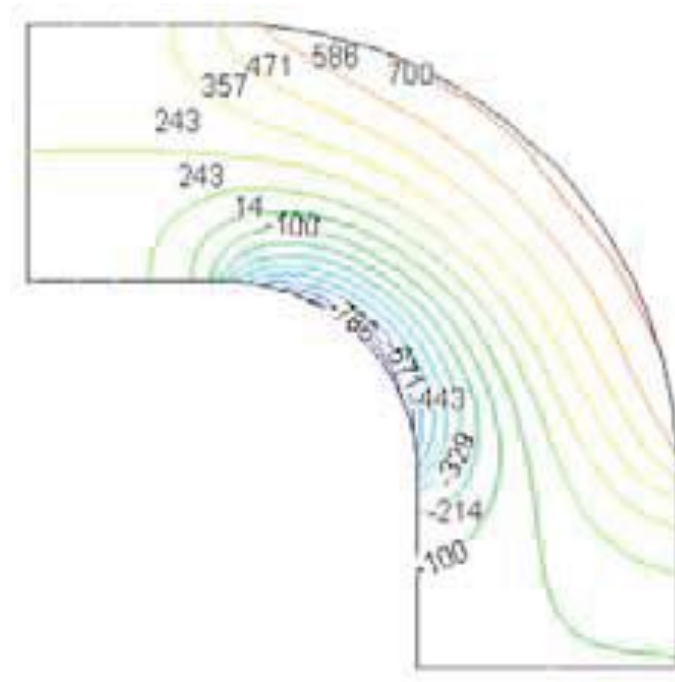


**Figure 1. 2 Pressure gradient in a duct at a 90 degree bend (Sun *et al.*, 2012)**

The pressure differentials together with the fluid-wall interactions primarily result in the start of separation and formation of eddy currents in the fluid with the accompanied oscillation of the fluid column as it exits the bend, causing pressure losses. As flow continues downstream of the 90° bend pipe, it continues to spiral and oscillate along the pipe until it stabilises at fifty times the pipe diameter length along the pipe from the central plane of the bend (Sun *et al.*, 2012).

### **1.3. Energy Loss due to Fluid-Wall Interaction**

In amalgamation with the explained energy losses to include all other unknown effects of bending, there is energy lost due to the differential fluid to wall interaction articulated in terms of the velocity of flow;

$$Kv^2/2g \quad (1. 1)$$

Where  $K$  is a Resistance Coefficient dependent of pipe total bend length and the ratio of radius of curvature of bend ( $r$ ) to pipe diameter ( $D$ ) i.e.  $r/D$  taken at the centre plane of the bend;

$v$  is the average flow velocity; and  $g$  is acceleration due to gravity.

$K$  varies marginally with the Reynolds number ( $R_e$ ) but increases as surfaces roughness increases (Wilson, 2012). The accuracy of the  $K$  values is largely dependent on the foundational formulas. These could be Colebrook-White / Newton-Raphson, Moody chart, Barr, Wood, Haaland, and Swamee and Jain formulas (Babatola *et al.*, 2008). The summation of all the factors contributing to the pressure drop, the change in the direction of flow, the fluid interaction itself (fluid element(s) friction) or eddies and pipe wall-fluid interactions, need to be correctly quantified with respect to the change in the bend angle, radius of curvature, flow velocity and pipe diameter, to precisely and accurately quantify (best approximate of) the secondary losses. The focus on accurately determining frictional losses in this study is to enable quick, accurate and precise flow calculation in the hydraulic design of efficient irrigation systems.

#### **1.4. Main Purpose of the Research**

The purpose of this research is to rapidly, accurately and precisely quantify the frictional losses (secondary or minor losses) at the bends in the process of undertaking design of irrigation systems. Losses are largely due to the fluid molecular-wall collisions with pipe roughness and the dynamic forces resulting in the inter-particle collisions by the moving fluid as it passes through the bend with respect to diameter and curvature. Smooth pipes (PVC) in particular are under consideration in this research. This research aims to achieve its purpose with the derivation of a simple Empirical Equation for accurately and precisely calculating the frictional losses for different bend angles (special bends normally found when designing irrigation systems) and also apply the concept to standard bends as used in irrigation system design, tools and or software.

For one to calculate the frictional loss due to a bend, friction factors are often used as the closest approximation as seen in the literature reviewed and normal design practice with the use of tables or predetermined coefficients, which is lengthy and often erroneous as estimations are often used. This also requires a thorough knowledge of how a friction coefficient was derived to align the friction coefficient used to the varied bend angles and pipe diameters encountered during design, leaving room for error and time consuming (Wilson, 2012). Most friction resistance friction coefficients were derived relative to the fixed 90° bend angle and different radius of curvature introducing the inaccuracies in using the same coefficients with change or different pipe diameters and curvature as may be required in the irrigation design process (ARC, 2003). The analysis and generation of an Empirical Equation for the calculation of the precise and accurate frictional losses, bridges the gap between the uncertainties in the use of the various friction coefficients and the different methods used to determine minor losses. Methods include estimation with the Equivalent Length, Resistance and Valve flow Coefficient methods, as change in the bend angle, radius and pipe diameter occur with varied flow. The Empirical Equation will in essence introduce a quick, accurate and precise method of calculating the frictional losses in the design of irrigation systems also improving system efficiency.

### **1.5. Problem Statement**

In irrigation systems, the frictional losses are largely due to the long pipe sections and to some extent the fittings, i.e., minor losses. As the irrigation system pipe network gets to shorter lengths with smaller block widths and long-rectangular block lengths, the irrigation system gets complicated and the proportion of losses due to the fittings and the valves increases, but these are by convention termed minor losses (Wilson, 2012). Over the years, there has been development of formulas and methods of determining minor losses in irrigation systems to a great degree of accuracy mainly with the Equivalent Length, Resistance Coefficient and the Valve Flow Coefficient Methods (Wilson, 2012). However, this has not been as much accurate as compared to the determination of frictional losses along the straight pipe sections due to the complexity in how coefficients or equivalent lengths are determined and used to estimate the pressure losses with changing bend parameters (mainly bend angle, bend length, bend radius and respective flow velocity). It has also been found that there are seemingly no reliable methods for quickly determining the pressure drop in bends

(Spedding *et al.*, 2004). The relatively inaccurate determination of the minor losses results in the under sizing of the irrigation pumps which can result in the failure of the irrigation system or poor system performance (Wilson, 2012). Over sizing of the irrigation systems, though operational may occur, that is, bigger pipe diameters, valves and respective components of the system design are used, which lead to a higher capital cost.

To enable the improved determination of minor losses, it is needful to correctly determine the frictional loss contribution due to individual influences or elements instead of combining everything in the friction coefficient for changing bend parameters (which will require a good knowledge of the development of coefficient) or approximating an equivalent length. The changing bend parameters to be considered would be the influences due to the roughness (for smooth pipes in this case), Reynolds number, radius of curvature, bend angle, pipe diameter, wall hydraulic area of interaction (bend length) and pressure differentials (incorporating the energy losses due to change in direction of the fluid elements) in the fluid flow about the bend. The best approximate or accurate determination of frictional loss can be more reliable and precise when the determination of frictional loss is a function of the specific bend parameters as mentioned earlier.

## **1.6. Justification of the Study**

The validity of Darcy's law when considering frictional losses has been a subject of interest for many years (Wilson, 2012). This has also been seen in the inapplicability of the Darcy formula with large Reynolds numbers that is turbulent instead of laminar flow. Questions have also arisen in the use of the fitting friction factors and the pipe friction factors (Wilson, 2012). Very little attention is given to the effect of the individual parameters in the fluid flow and fittings during the design phase, though they give rise to significant pressure drop and are often estimated at 30 to 50 pipe-diameters in length of an equivalent straight pipe (Spedding *et al.*, 2004). Accurately determining the losses due to pipe bends, T pieces, sluice valves, ball valves, reducers, reflux valves and foot valves with screens will also reduce the cost incurred in over sizing of pumps and possible over and under designing. Generally, there is a saving in the capital and pumping cost, i.e., the saving in pipe sizes and electricity consumed by the ideal system. The existence of the minor losses in the irrigation systems calls for a need to accurately determine the actual energy losses for designing of efficient irrigation

systems, for critical operation and at times plant safety in the case of a downstream hydraulic values relief system which need instantaneous response (Ito, 1960). This can be done with careful consideration of the bend length or parameters, incorporating the energy losses due to change in direction of the fluid elements and eddies. In essences, determining frictional losses as a function of roughness, Reynolds number, radius of curvature, bend angle, pipe diameter, wall area interaction and pressure differentials in the fluid flow about the bend, instead of estimating them at 10% to 15% and at times 25% of the main losses as by Savva and Frenken (2002), designers in industry will give more timely, accurate and precise frictional losses, designing efficient irrigation systems. To achieve this, a new correlation needs to be developed in relation to the curvature multiplier and the momentum change due to the bend. This is also essential with the current introduction of low pressure (operating pressure) emitters and possible use of special bends (unique bends made specifically for an irrigation system or cases of applying the bending schedule according to the pipe manufacturing bend limits) in an irrigation system.

### **1.7. Aims**

The main objective of this research is to obtain an easy to apply method and tool for quickly, accurately, and precisely quantifying the minor losses due to bends. This is with respect to the dynamic forces acting on fluid, inter-particle collisions and the molecular-wall collisions due to the pipe diameter, roughness, flow velocity(s), bend angle(s) and bend radii. These can however be correctly approximated with the development of an Empirical Equation, method, and tool, which will offer the input of the changing bend parameters and give an easy way of determining minor losses due to bends, during the irrigation design process. This concept can then be applied to short, standard, long radius and specialized bends as used in irrigation system design.

Hypotheses: Pressure loss in irrigation systems largely due to the collective turns the fluid is subjected to in bends and the resulting generation of two secondary helical vortex flows, oscillating downstream of the pipe when the irrigation system is in operation which can be precisely and accurately determined.

### 1.7.1. Specific Objectives

The specific objectives of the study are as follows:

- i. To develop an Empirical Equation for determining minor losses in irrigation pipe bends as a function of pipe roughness, diameter and radius of curvature with flow;
- ii. To develop the successive dynamic hydraulic gradient before, about and after the bend with successive introduction of curvature, a chart and a spread sheet tool;
- iii. To compare minor frictional losses as determined by the Empirical Equation in above objective for accuracy or extent of error, repeatability, and reliability of traditional methods in estimation of minor loss.
- iv. To determine the effect of two-phase flow on pressure loss due to bends and the effect of the slope (gradient) and plane (incline) of bend.

### 1.8. Originality of the Study

Determination of pressure drop is important for the improvement of the performance of irrigation systems as we move towards the use of low-pressure drip systems or emitters and the use of special bends in irrigation systems. Most of the research work undertaken has not been able to bridge the gap between the use of various coefficients with reference to the change in bend angle, curvature (bend radius and pipe diameter) with varied flow without a thorough understanding of the coefficients by the user, resulting in untimely and often erroneous use of coefficients. This research will narrow in on the individual practical components contributing to pressure drop to produce an Empirical Equation of the form  $f(\theta, D, L, R_e, r, v_d, \rho, \varepsilon, \lambda_d, \mu_d)$  wherein;

$\theta$  - Bend angle;

$D$  - Pipe diameter;

$L$  - Bend length;

$R_e$  - Reynolds number;

$r$  - Radius of curvature of bend;

$\rho$  - Density;

$v_d$  - Flow velocity with respective pipe diameter;

$\varepsilon$  - Pipe roughness;

$\mu_d$  - Dynamic viscosity;

$\lambda_d$  - Kinematic viscosity, for the successive determination of

secondary or minor losses due to bends. This is in attempt to improve the accuracy and precision while saving time in designing efficient irrigation systems.

The following points provide an overview of what is contained in this thesis:

- Chapter 2 provides the literature reviewed on the limitations of the different straight pipe friction equations and methods and those also developed specifically for bends. The different phase of flow through bends and pressure drop outside and inside of pipe bends. The influence of dynamic and kinematic viscosity properties of water, Dean vortices formation and secondary flow generation downstream of a bend. CFD Analysis of a 90° bend and the effect of geometric parameters on frictional losses on bends.
- Chapter 3 is on the development of an Empirical Equation for quick, accurately and precisely determining of minor losses for bends from 0° to 90° with respect to the varied bend parameters and varied flow.
- Chapter 4 looks at the development of the successive dynamic hydraulic gradient within the pipe bend, due to successive pipe bending and expresses findings in the form of a chart for manually determining the dynamic hydraulic gradient or a MS Excel spread sheet tool within the bend section and the peripherals.
- Chapter 5 compares the minor friction losses determined by the Empirical Equation and the available traditional methods to check their accuracy or extent of error, repeatability and reliability in the estimation of secondary losses for use in irrigation design and any other applications.
- Chapter 6 focuses on the effect of two phase flow on pressure loss and the effect of the slope and plane of the bend for single phase flow on pressure loss.
- Chapter 7 summarises this research, ties the various objectives into a connected body of research and then highlights the conclusions of the study, including the acceptance or rejection of the hypothesis postulated. Identifies future possibilities of future research, recommendations and improvements, and final comments on research done.

## CHAPTER 2: SECONDARY LOSSES IN L-BENDS IN IRRIGATION SYSTEMS

### 2.1. Introduction

Frictional losses in pipe sections though measured with the Darcy-Weisbach developed in 1845, Hazen-Williams developed in 1906, Newton-Raphson developed in 1911 or Colebrook-White developed in 1939, Moody chart developed in 1944, Wood developed in 1966, Swamee - Jain developed in 1976, Barr developed in 1981, Haaland developed in 1983, Lamont and General Exponential equation developed in 1998, have limitations in the measurement of the pressure drop in bends and fittings since their application is on straight pipe sections (Wilson, 2012). These methods only focus on the frictional loss due to the fluid interaction with the internal wall of the pipe per given length, with the partial contribution by the fluid elements mixing with no change in the pipe geometry. Pragmatic methods have been discovered but lack ease of application with changing pipe geometry introducing inaccuracies in the irrigation design process (ARC, 2003). As a result of bending introduced to a pipe section, pressure contours about the bends were found to occur, investigated and explicitly spelt out, but there were no explicit relations to the pressure losses due to the bending brought to light (Jayanti, 2011). To some degree, the fluid phases have also been deemed to play a role in the overall pressure loss about bends, and again most findings were centred on the 90° elbow only (Ghajar and Bhagwat, 2013). These have been to date modelled with computational fluid dynamics but do not accurately and precisely determine bend losses as and when require in the design processes (dos Santos *et al.*, 2014).

### 2.2. Limitations of Darcy-Weisbach Friction Equation

At high flow rates, during the transition flow and turbulent flow in smooth and rough pipes, the measurement of pressure drop was found not to satisfy the Darcy equation with large Reynolds numbers (from laminar to turbulent flow), which called for the inclusion of additional parameters to accurately measure pressure drop (Tek, 1957). Considering the experimental data, the generalized Darcy equation seemed to satisfy pressure drop reasonably within a range of Reynolds numbers, but as the Reynolds number increased the Darcy equation was found to lose its predictability on the actual pressure drop. This is so because,

since the Darcy law considers that the drag force is linearly proportional to the flow velocity and holds for low flows velocities (Awad, 2016; Fourar *et al.*, 2004). These findings called for a need to develop new methods of determining pressure drop.

### **2.3. Colebrook-White / Newton-Raphson, Moody chart, Barr, Wood, Haaland, and Swamee - Jain formulas**

These equations are merely the Darcy-Weisbach friction equation with the consideration of the pipe roughness, hydraulic radius and the Reynolds number, and are capable of estimating frictional losses at higher levels of Reynolds number or turbulent fluid-flow. Using statistical methods, Babatola *et al.* (2008) checked the accuracy, analysed the rationality and goodness of fit for the formulas. The methods gave different levels of error 1.0%, 1.0%, 1.0%, 0.9999%, 0.9997%, and 0.9991% for the Colebrook-White, Swamee - Jain, Moody, Barr, Haaland, and Wood, respectively. The first three methods were deemed to be the best options because the high coefficient of determination. However, the Moody method was deemed the best due to its explicit chart in the absence of software packages to calculate the frictional losses. These methods however are specifically for determining the frictional losses in straight pipe lengths and to some extent are not applicable to the losses due to specialised (unique bends made specifically for an irrigation system or cases of applying the bending schedule according to the pipe manufacturing bend limits) and L-bends as used in other sections of irrigation systems.

### **2.4. Hazen-Williams, Blasius, Lamont, Scimeni, Manning and the General Exponential Equations**

The Darcy-Weisbach equation and the Colebrook-White formula are rational and dimensionally homogeneous, while the Hazen-Williams equation is dimensionally not homogeneous with a limited range of applicability although it caters for the cases of sloping pipes as opposed to the horizontal pipe of the later mentioned two formula (Valiantzas, 2005). Likewise, the Blasius, Lamont, Scimeni, Manning and the General Exponential equations are not dimensionally homogeneous, and all these methods focus on a straight pipe section, which means they fall short when we look at the accurate determination of secondary or minor head losses due to changes in the pipe geometry, such as a bend (Wilson, 2012).

## 2.5. Methods for Determination of Minor Losses

Methods deemed accurate for the determination of secondary or minor losses in pipe bends and fittings can be classified within three categories. These are the Equivalent Length ( $L_e$ ), the Resistance Coefficient (K), and the Valve Flow Coefficient method ( $C_v$ ) though the Valve Flow Coefficient method is mostly used for valves. The Resistance Coefficient method however has many ways of defining the coefficient making it necessary for one to know the way in which it was developed and its conditions of application (Wilson, 2012). It makes extensive use of tables that one must understand in its application to avoid errors (Neutrium, 2016).

### 2.5.1. The Equivalent Length ( $L_e/D$ )

This method is the least accurate compared to all other methods. It is more reliable when they are tables of data available to determine frictional losses relative to the pipe diameter, roughness and Reynolds number. The pressure drop across a fitting would be equivalent to a straight pipe length,  $L_e$ , giving a slight increase to the multiplier  $\frac{fL}{D}$  such that the overall drop across a fitting would be regarded as  $(L + L_e)/D$ . Wherein L is the length of a straight pipe with a diameter D. The head multiplier would then be taken to be  $f(L + L_e)/D$  for the frictional loss in the fitting (Wilson, 2012). However, when one is using an Equivalent Length measured from a fitting of a different dimension, the approach assumes that the relative proportions of the fitting size remain constant as the pipe size varies. This is however rarely the case, and as a result, there is some error in the pressure drop that occurs. Since the flow coefficient (L/D ratio) decreases as the fitting size increases, the pressure drop would be overestimated at pipe sizes greater than those for which the fittings Equivalent Length was calculated. The pressure drop would be underestimated at smaller pipe sizes than those for which the Equivalent Length was measured. The Equivalent Length method has the advantage of being very easy to calculate (Neutrium, 2016). Both pipe runs and fittings can be added together to create a single total length, from which the pressure loss can be measured.

The Equivalent Length equation combines the losses due to the differential pressures within the fluid as it turns about the bend, the wall surface area in contact with the water, entrances and exit losses of the fluid into the bend and change in direction, treating the losses as existing in one straight pipe. Generally, the pressure drop when using the Equivalent Length method tries to sum up all contributions to the frictional losses over the curved flow path through the bend, equating all pressure drops to that of an Equivalent Length of straight pipe loss leaving room for inaccuracies due to estimations made for different bend parameters involved in the design process, calling for the need for research on better methods (Wilson, 2012).

### 2.5.2. The Resistance Coefficient (K)

Since this method is characterised against varying flow conditions (i.e., Reynolds number), it is more reliable than the Equivalent Length method. It is, however, less reliable than other approaches because it lacks the different geometries of fittings of various sizes (Neutrium, 2016). Unlike the Equivalent Length method, the Resistance Coefficient method sums up the resistance coefficients giving the form (Perry, 1950):

$$h_L = \left( \frac{fL}{D} + \sum_{i=0}^n K \right) \left( \frac{v^2}{2g} \right) \quad (2. 1)$$

Wherein  $f$  is the the Darcy friction factor;  $D$  is the pipe diameter;  
 $L$  is the length of a straight pipe;  $v$  is the flow velocity;  
 $g$  is the acceleration due to gravity;and  $K$  is the friction coefficient.

The Resistance Coefficient method, as used by the Chemical Engineers Handbook in by Perry (1950) had the intention of using a Resistance Coefficient as though it were the same for different diameters (bend parameters) again, introducing inaccuracies. It was found thought that generally the Resistance Coefficient decreased as the fitting size increased. The K value was used in the fully turbulent flow conditions and not on laminar flow to date (Perry, 1950). In a bid to improve the friction factor K, the Crane 2 friction factor was introduced with a range of K factors for each fitting, with the provision of adjusting the K values per fitting, which also brought more confusion. It was also discovered that at Reynolds numbers less than 2 000, there was an express increase in the K values (Silverberg, 2001).

Hooper (1981) modified the K value to include the fitting size and the Reynolds number ( $R_e$ ) such that (Albright, 2008):

$$K = \frac{K_1}{R_e} + K_\infty \left(1 + \frac{1}{D}\right) \quad (2. 2)$$

Where  $K_\infty = K$  infinity.

Advancement on the work by Hooper (1981) gave the three-K equation which could fit the data well (Darby *et al.*, 2001):

$$K = \frac{K_m}{R_e} + K_i \left(1 + \frac{K_d}{D^{0.3}}\right) \quad (2. 3)$$

The seemingly best method in use to date, the SABI Irrigation Design Manual for designing irrigation systems when determining the minor losses, is on the basis that minor losses are proportional to the velocity head component  $\left(k \frac{v^2}{2g}\right)$  as in a straight pipe, considering the Darcy-Weisbach equation (ARC, 2003):

$$h_L = \frac{fL}{D} \frac{v^2}{2g} \quad (2. 4)$$

where;  $h_L$  is the fluid head;

$f$  is the Moody friction factor or Darcy-Weisbach friction factor;

$L$  is the straight pipe length;

$D$  is the internal pipe diameter;

$v$  is the average fluid velocity; and

$g$  is the acceleration due to gravity.

Again, there is no consideration of the change in the bend parameters when calculating the minor frictional losses. However the method, it remains quite accurate since the coefficients are pragmatically determined.

### 2.5.3. Valve Flow Coefficient ( $C_v$ )

Though used mainly for valves  $C_v$  ( $A_v$  in the S.I. units) values can be easily converted to K values. The methods outlined earlier use the multiplier with the velocity head term giving a likelihood of the same results and with the Valve Flow Coefficient method (Wilson, 2012).

$$Q = A_v \sqrt{(\Delta P / \rho)} \quad (2.5)$$

Where:  $Q$  – volumetric flow rate in  $\text{m}^3\text{s}^{-1}$        $\Delta P$  – pressure drop in  $\text{N/m}^2$   
 $\rho$  – density of liquid in  $\text{kg/m}^3$

The Equivalent Length ( $L_e/D$ ) and the Resistance Coefficient (K) use the same velocity head multiplier when predicting the frictional losses allowing conversion between the two, considering the fitting dimensions are known in either case when using the length ( $L_e/D$ ) or the Resistance Coefficient (K) method. The argument however, pertaining to the two methods is how the length ( $L_e/D$ ) and the Resistance Coefficient (K) method are compared with different Reynolds numbers and pipe roughness (Wilson, 2012). Despite the efforts to correctly quantify the secondary losses, friction factors smaller than those obtained by the Moody, Prandtl, White-Colebrook, or Nikuradse smooth pipe rule (or Blasius law) have been calculated in large diameter pipes, according to findings in literature (Berlamont, 2014). It is shown that a small amount of rotation or swirl, such as that induced by curvature, will continue downstream of a straight pipe, decreasing the apparent friction factor premeditated using the nominal Reynolds number. The Blasius rule can also hold true if the friction factor is measured using the real Reynolds number and rotation is taken into account. For rotation numbers less than 1 to 2, the reduction in friction factor is usually in the 5 to 10% range. Only big diameter pipes and/or strong Reynolds numbers are prone to experience the phenomena.

The use of the Darcy-Weisbach, Colebrook-White / Newton-Raphson, Moody chart, Barr, Wood, Haaland, Swamee - Jain Hazen-Williams, Lamont and General exponential equation have some limitations in the application of the formulas when measuring the pressure drop in bends and fittings since focus is on straight pipe sections. They therefore cannot be used to determine the best estimate of frictional losses due to bends or fittings. The methods deemed accurate for the determination of minor losses in pipe bends are the Equivalent Length and the Resistance Coefficient; however, these lack the ease of application with specific changes in the bend parameters when one needs to quickly apply them in the design process, which brings about the inaccuracies that research aims to address. The Valve Flow Coefficient method, though mostly used for valves, remains mainly for conversion when one understands how the coefficients are derived.

## 2.6. Single-Phase Flow Through a Vertical Bend

Single phase flow is characterised by one state of matter, gas (steam or vapour) or liquid (water) as is the case with irrigation water, the primary variables being, velocity, pressure, enthalpy and density. As irrigation water flows through a bend, it experiences a radial pressure gradient generated by the centrifugal force acting on the fluid due to the bend. The water partially splits from the centre and spirals as it moves sideways past the bend forming a double flow field as shown in Figure 2.1 (Briley, 1974). Pressure contours are about a bend are also shown in Figure 2.2.

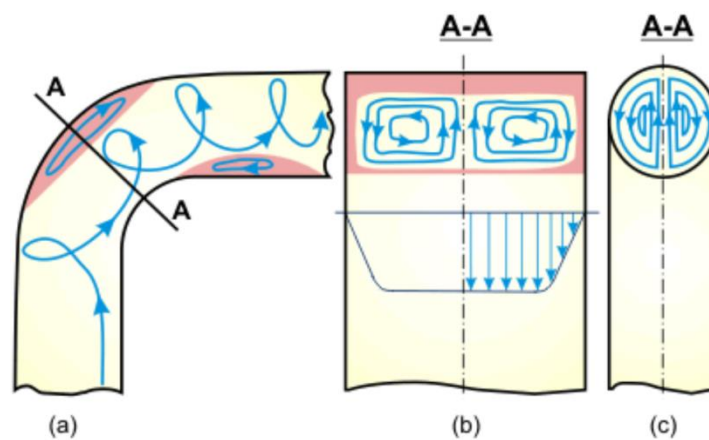


**Figure 2.1 Corkscrew flow in a bend: a) Section along bend; b) Rectangular cross-section pipe and; c) Circular cross-section pipe (Briley, 1974)**

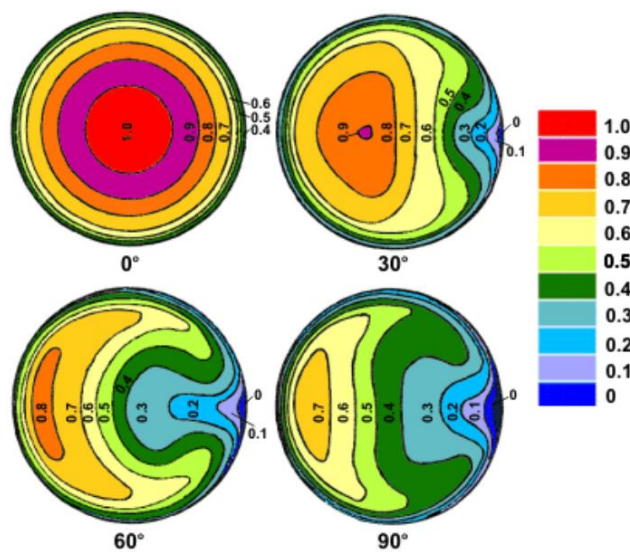


**Figure 2.2 Pressure contours for U-bend with bend-to-pipe diameter ratio 24 and Reynolds number = 23 6000 (Briley, 1974)**

Flow separation was also seen to be adverse with sharp bend angles, increasing the pressure losses (Jayanti, 2011). This flow pattern was also seen to be similar even with large bend angle pipes. The pressure losses at the bend were concluded to be a result of change in fluid momentum due to the bend and dynamic viscosity, wall friction and varying Reynolds number as it collides, and swirls as influenced by the bend angle and radius of curvature of the bend. Jayanti (2011) expressed pressure drop as a sum of two components, firstly frictional loss due to the straight pipe section or equivalent loss because of the Reynolds number and the pipe roughness. Secondly, pressure loss due to the change in flow direction. The bend loss coefficient due to the curvature ratio and bend angle was expressed as:

$$\Delta P = \frac{1}{2} f_s \rho u^2 \frac{\pi R_b}{D} \frac{\theta}{180} + \frac{1}{2} k_b \rho u^2 \quad (2.6)$$

Where:  $f_s$  is the Moody friction factor in a straight pipe;  $\rho$  is the density;  
 $u$  is the mean flow velocity;  $R_b$  is the bend radius;  
 $D$  is the tube diameter;  $\theta$  is the bend angle; and  
 $k_b$  is the bend loss coefficient obtained from Figure 2.3.

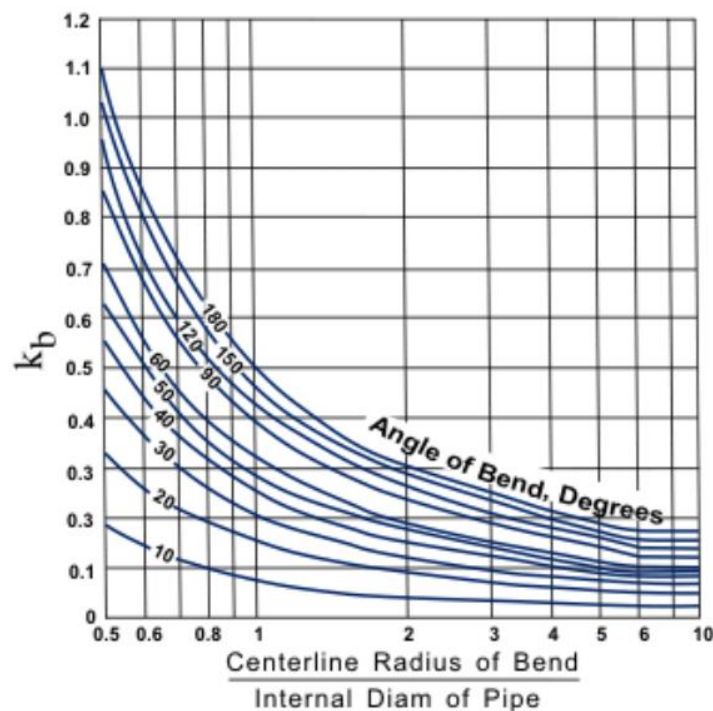
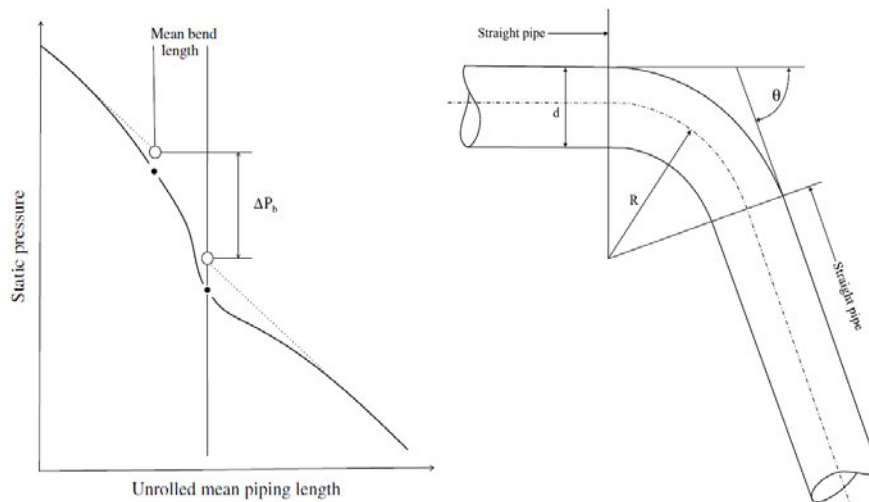


Figure 2.3 Pipe bend loss coefficients (Wilcox, 1978)

The above relationship though seemingly close, does not allow for centreline radius of bend per internal diameter or pipe of more than ten for easy determination. In other experiments conducted, the frictional loss in a single-phase flow bend was found to be composed of the fluid-wall friction, the vortex detachment, secondary flow generation and downstream tangent for the two symmetrical velocity profiles developed at the bend (Azzi and Friedel, 2005). The pressure loss in a 90° bend was also expressed graphically by Azzi and Friedel (2005) as shown in Figure 2.4.



**Figure 2.4 Mean static pressure of incompressible liquid flow through bends in a horizontal plane (Azzi and Friedel, 2005)**

The dynamic viscosity components of the pressure drop excluding the acceleration due to gravity, hydrostatic pressure drop, and secondary flow generation are ruled by dissimilar contributing factors. However, the actual pressure drop often needed in the design of an irrigation system can be found from the resultant of all the pressures about the bend and influence region. This is the sum of all the pressure contours (pressure differentials) and the downstream oscillation of the two symmetrical vortices due to the bending.

### **2.6.1. Pressure Drop Outside and Inside of Pipe Bend**

Frictional pressure drop outside of the bend within the pipe can practically be seen to be due to the impact of the straight flowing streamlines of fluid with respect to the pipe bend. Ideally there exists a half cylinder hydraulic area of collision instigating a variation in the angular

momentum with the outer wall and a half cylinder hydraulic area of detachment and attachment of flow also creating vacuum, thus pressure loss on the inner wall at the bend. The concave outer wall of pipe bend, due to impact, causes the change in the streamlines of flow and the mean angular momentum. Contrary to the outer wall, the convex inner wall due to the vacuum created, acts as the starting point of the generation and direction of the vortices (due to the mean shearing of the fluid) giving the mean angular motion. The two effects due to the bend angle and radius of curvature give the characteristics of the turbulence development (Röhrig *et al.*, 2015). The development of the mean stream wise velocity due to the concave outer wall and the convex inner wall were illustrated in a study by Röhrig *et al.* (2015) at  $0^\circ$ ,  $22.5^\circ$ ,  $45^\circ$ ,  $67.5^\circ$  and  $90^\circ$  along pipe bend. A computational study using the Large Eddy Simulation (LES) and various Reynolds-averaged Navier–Stokes (RSM) were used and calculated by the low Reynolds number Eddy Viscosity Model (EVM), as seen in Figure 2.5. For pipe radius,  $\hat{r}$  and bend radius,  $R$ . The  $\hat{r}/R_b = 0$  indicates the centre through the bend with  $\hat{r}/R_b = -1$ , the outer and  $\hat{r}/R_b = 1$ , the inner bend contour.

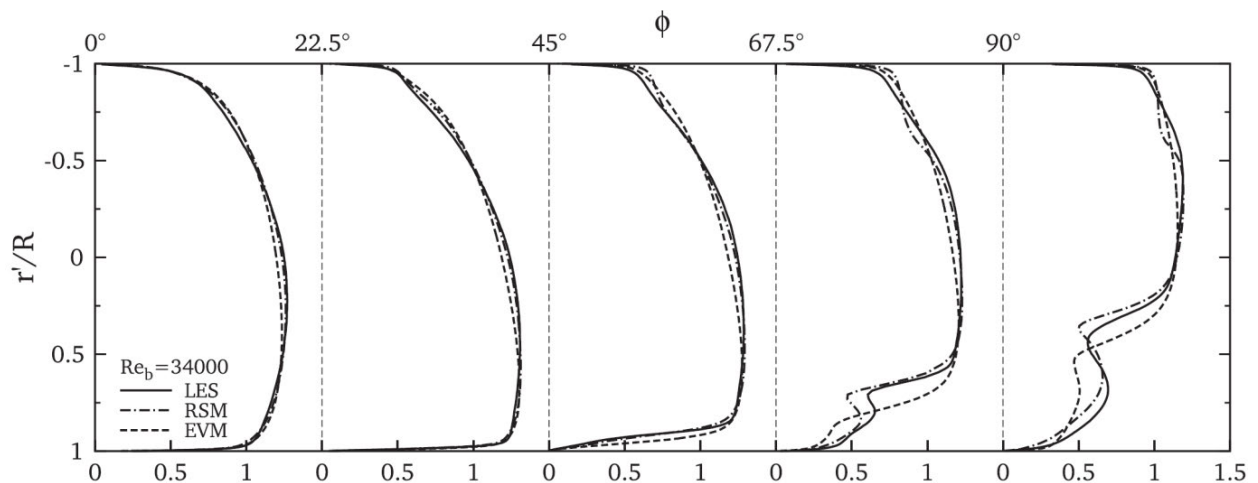


**Figure 2.5 Mean velocity profile development at angular positions  $\phi$  inside a bend section (Röhrig *et al.*, 2015)**

The development of the mean stream wise velocity field with the profiles at the different bend positions was shown for the different computational methods employed in the study. It was pragmatically seen that the velocity profile progressively became unequal. It was also observed that acceleration of the fluid with substantial pressure decrease occurred on the fore part of the inner concave side as opposed to the outer convex part as seen in Figure 2.6. The shaded region  $0^\circ$  to  $90^\circ$  indicates pipe bend length over the whole pipe length,  $\bar{s}$ .

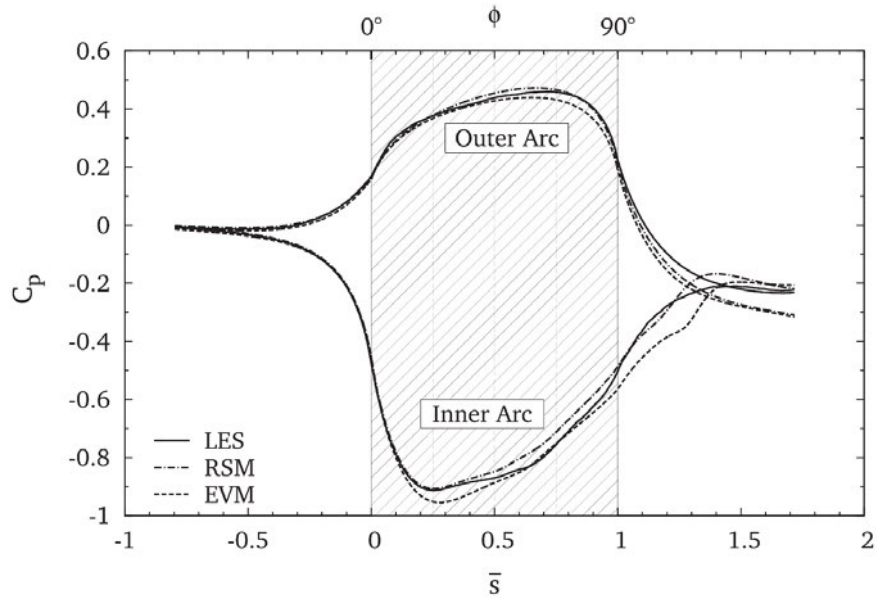


**Figure 2.6 Inner and outer arc pressure coefficient,  $C_p$  along bend at,  $Re_b = 2\ 4000$  (Röhrig *et al.*, 2015)**

Further comparison was also done for the coefficient of friction for the inner concave side as well as the inner convex part of the bend as shown in Figure 2.7.

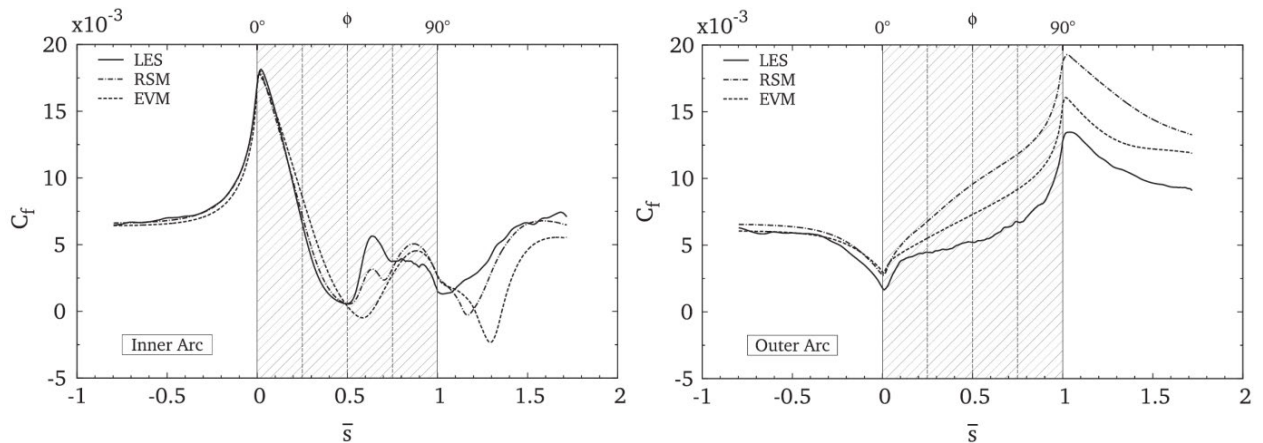


**Figure 2.7 Comparison of the friction coefficient,  $C_f$  of friction of the bend at  $Re_b = 2\ 4000$  (Röhrig *et al.*, 2015)**

Comparable numerical studies were also undertaken by Dutta *et al.* (2016) to characterize the effects of various Reynolds numbers ( $Re = 1 \times 10^5$  to  $10 \times 10^5$ ) on the flow separation on the inner bend with Numerical simulation. Similar results were obtained for the normalized mean

velocity profile fluctuation as seen in Figure 2.8 where  $U_x/U_{in}$  refers to the mean velocity and inlet velocity, respectively.

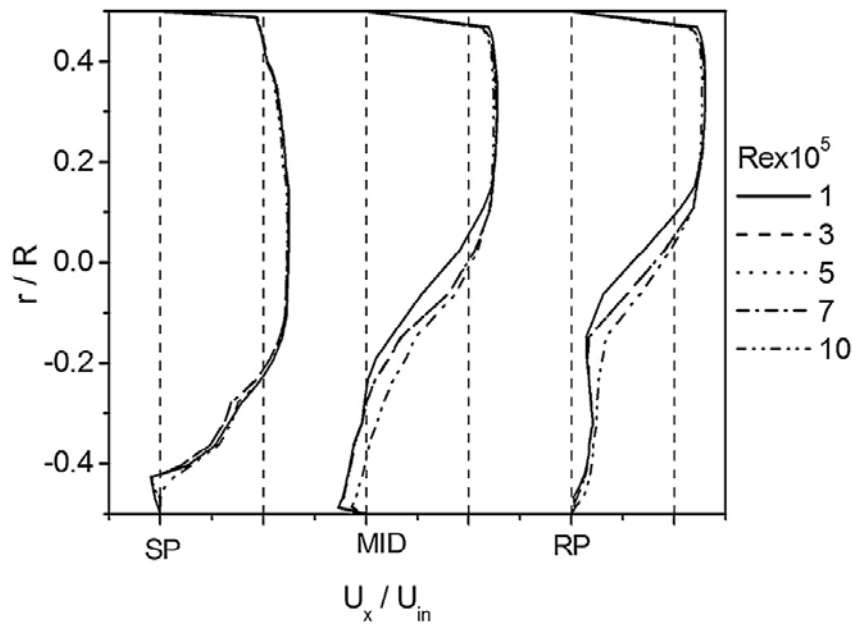


**Figure 2.8 Mean velocity profile fluctuation on bend (Dutta *et al.*, 2016)**

Velocity acceleration on the outer part of the bend was also perceived to be higher as expected. Separation and reattachment points were also observed for the dissimilar Reynolds numbers at diverse positions of the pipe bend in the central symmetry plane. The negative hydrostatic pressure drop as the case of a non-aerated nappe was formed mainly due to the separation point (SP), middle point (MID) and the reattachment point (RP) in the inner part of the bend. SP, MID and the RP features are expressed in bubble flow as seen in Figure 2.9.

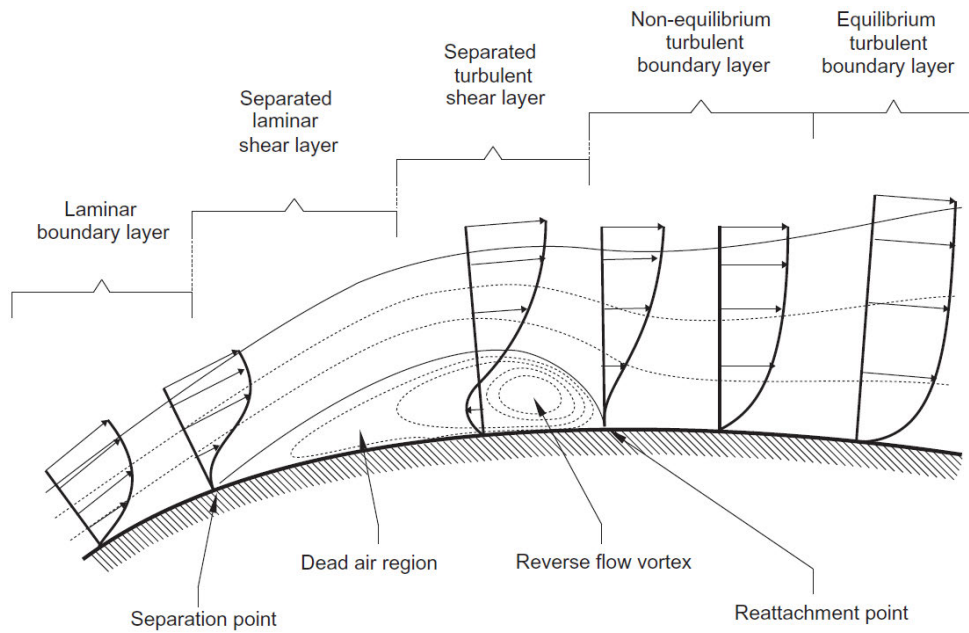


**Figure 2.9 Various sections of laminar separation bubble flow (Lin and Pauley, 1996)**

In the numerical simulation undertaken, as the Reynolds number increased the velocity profile close to the inner part of the bend tried to recuperate to the fully developed flow form. This was achieved by the slowing down of flow in the outer core and accelerating effects in the inner part of the bend, giving rise to the assumption that pipe curvature effects are reduced (Dutta *et al.*, 2016). Studies were also done by Dutta *et al.* (2016) to get an understanding of the dependence of separation and reattachment points on the Reynolds number from the bend outlet. These are shown in Figure 2.10 as “Present analysis”.

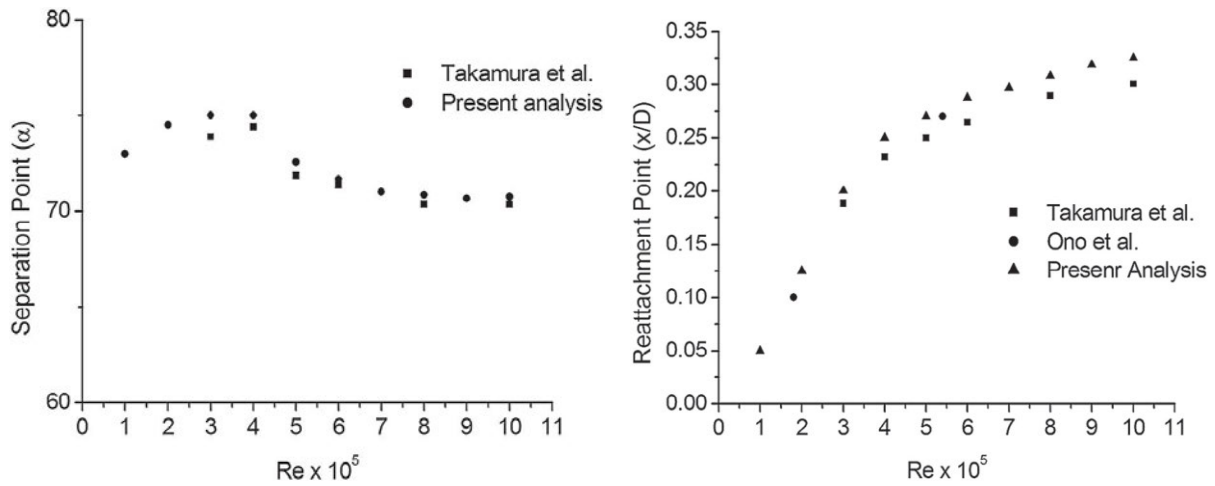


**Figure 2.10 Separation and reattachment point's dependency on Reynolds number (Dutta *et al.*, 2016)**

As the Reynolds number increased, the separation point travelled upstream of the bend before it started to decrease, and the reattachment point generally increased. Again, with bend  $R_c/D = 1$ , for radius of curvature  $R_c$  and pipe diameter  $D$ . The different Reynolds numbers, velocity fluctuations in the  $x$  and  $y$  directions were also seen as shown in Figure 2.11, with the negative and positive values ( $r/R$ ) representing the inner and outer core respectively at the separation region. Where,  $r$  is the pipe radius and  $R$ , the bend radius.

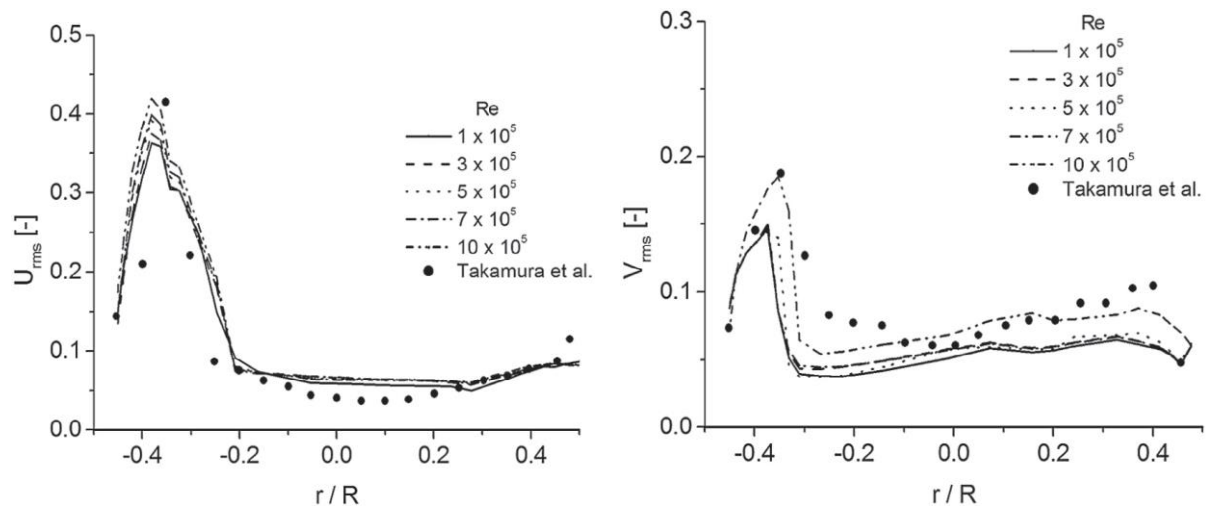


**Figure 2.11 Root mean square velocity (rms) profiles of velocity oscillations at the bend exit,  $U_{rms}$  in  $x$  direction and  $V_{rms}$  in  $y$  direction (Dutta *et al.*, 2016)**

The strength of oscillation was larger in the  $x$  compared to the  $y$  direction, and  $U_{rms}$  profiles did not demonstrate considerable dependency on the Reynolds number change, compared to

the clear dependency of  $V_{rms}$  profiles, with peak value becoming larger, moving from the centre to the outer part as the Reynolds number increased (Dutta *et al.*, 2016).

Due to the existence of the bend or curvature, it can be concluded that the change in flow direction produces a centrifugal force that makes the denser water phase travel away from the centre of curvature of bend, and at the same time, the less dense phase traverses to the centre of curvature of bend. Concurrently, the maximum axial velocity traverses to the outside of the bend with the formation of a proportioned pair of counter-rotating helical vortices (Autee and Giri, 2016).

### **2.6.2. Dynamic and Kinematic Viscosity of Water**

Viscosity, as a measure of the resistance of the flowing water as it deforms passing the bend, contributing to the differential pressure loss; that is the "thickness" or "internal friction". This is largely due to shear stress and tensile stress in the flowing fluid (Maheshwar, 2018). Being a tensorial quantity, viscosity can be represented in two independent components. These are two viscosity coefficients which are also defined as the Dynamic or Absolute viscosity and kinematic viscosity or dynamic viscosity per density of fluid. These yield the most important Shear viscosity, often referred to as the viscosity of the fluid in general, which is simply the fluid reaction to applied force (ratio of the pressure applied to fluid in the axial direction ( $x$ ,  $y$ ,  $z$  axis) on fluid surface to the resultant change in velocity) or velocity gradient. Secondly, Volume viscosity which is also called the bulk viscosity, normally applicable to compressible fluid and Extensional viscosity, a combination of shear and bulk viscosity which also occur with compressible fluids (Ismael, 2015). Figures 2.12 and 2.13 shows the water relative viscosity and the viscosity of water at saturation pressure.

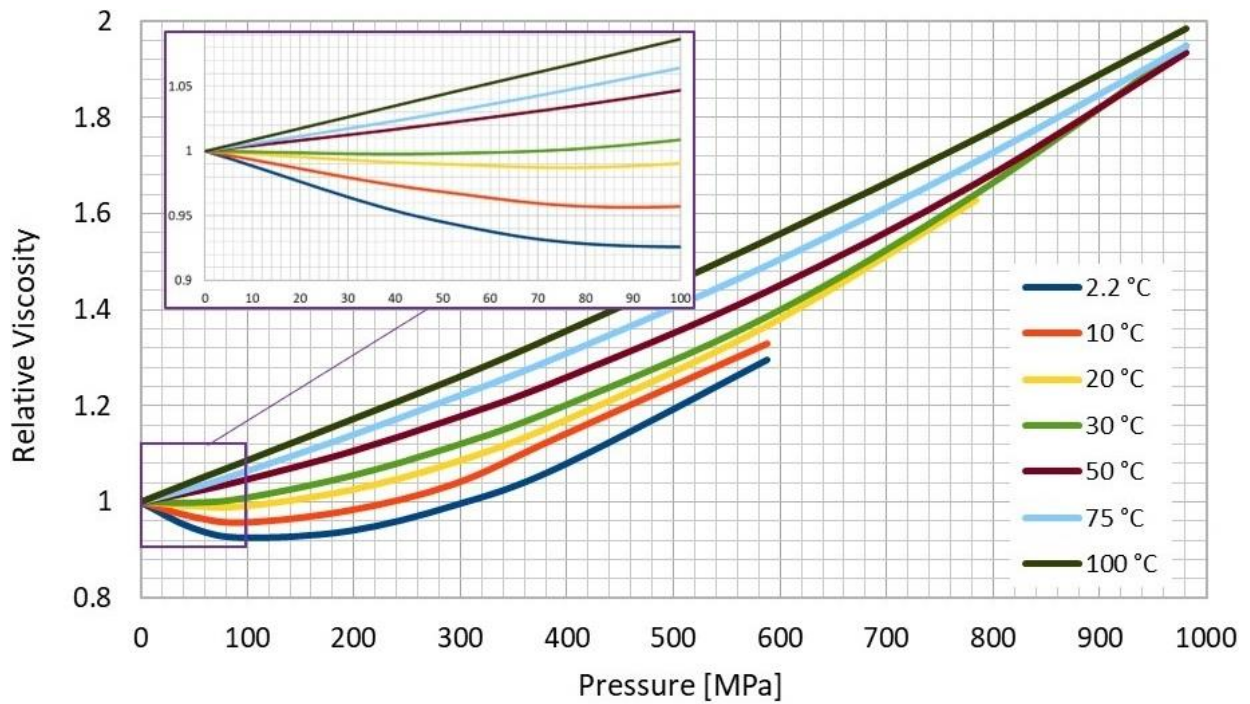


**Figure 2.12 Water relative viscosity (The Engineering tool box.com, 2018)**

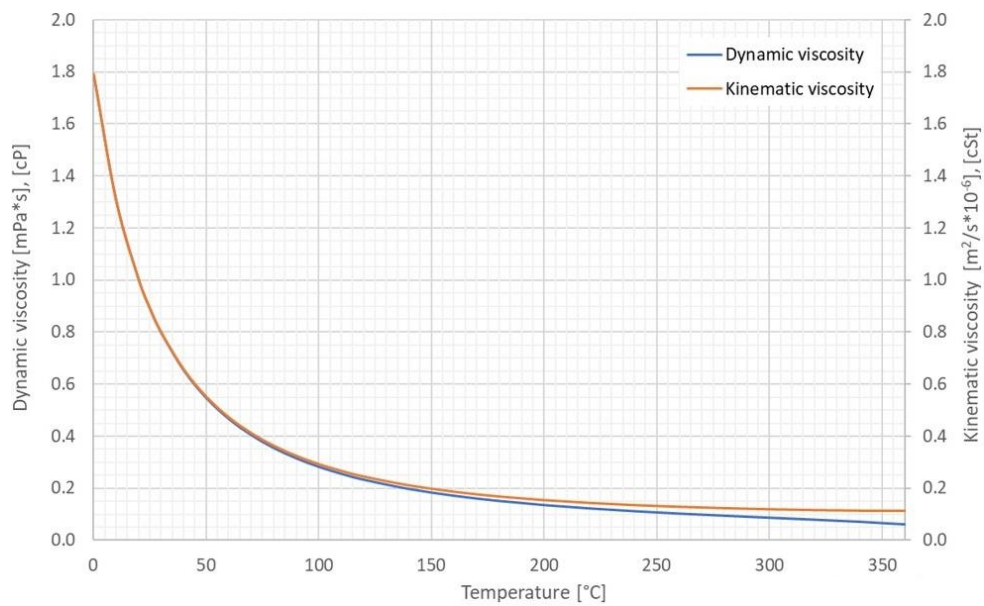


**Figure 2.13 Water viscosity at saturation pressure (The Engineering tool box.com, 2018)**

The change in Kinematic viscosity with a change in temperature (Viscosity index) is used in cases with significant temperature differences but is not the case with irrigation water. It can clearly be seen with temperature and pressure ranges investigated, the dynamic and kinematic viscosities in irrigation water, which is normally room temperature and lower does not change significantly.

### 2.6.3. Dean Vortices Formation and Secondary Flow Generation Downstream of Bend

Flow in the pipe bend consists of recirculating regions with curved streamlines generally characterised by the Dean's number, ( $D_e$ ) (Dean, 1928). This was defined relative to the pipe bend diameter with centre line radius. Dean's number considers the viscous, inertia and curvature due to the pipe bend. Dean's number ( $D_e$ ), gives the ratio of the square root of the product of the inertia and centrifugal forces to the viscous forces:

$$D_e = \left(\frac{dv\rho}{\mu}\right) \left(\frac{r}{R_b}\right)^{\frac{1}{2}} = R_e \sqrt{\frac{d}{2R_b}} = R_e / \sqrt{\frac{R_b}{r}} \quad (2.7)$$

Where:  $D_e$  – Dean's number;

$d$  – pipe diameter;

$v$  – velocity;

$\rho$  – density;

$\mu$  – dynamic viscosity;

$r$  – pipe radius;

$R_b$  – pipe bend centre-line radius.

$R_e$  – Reynold's number; and

$D$  – the diameter for non-circular geometry, and equivalent diameter in use.

The relationship between pressure gradient and flow rate was found to be independent of the bend curvature but on Dean's number. This was shown by various authors using different definitions of the Dean's number (Vashisth *et al.*, 2008). The curvature,  $1/R$  was seen to affect the flow pattern. Figure 2.14 shows the two secondary helical vortex flow fields or flow streamline contours for low and high Dean Numbers (Ghobadi and Muzychka, 2016).

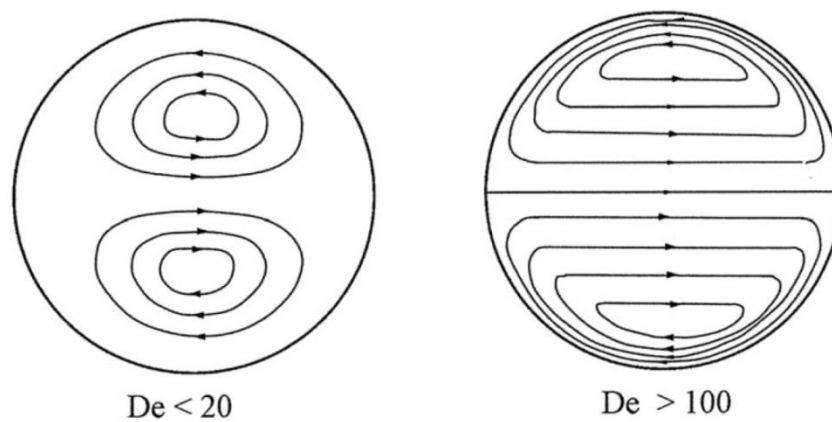


**Figure 2.14 Secondary flow field for small and large Dean Numbers (Ghobadi and Muzychka, 2016)**

For curvature ratios greater than 5, the flow field in circular cross-section bend was found to be solely due to the Dean Number in tests conducted, wherein curvature ratios is defined as the bend's radius of curvature per tube radius. Secondary boundary layers were also observed on the wall for turbulent flow with at high Dean Number  $> 370$ . Fluid was also seen entering and exiting these boundary layers between the outer and inner bends respectively. At a higher Dean Number, and therefore a higher centrifugal force, the axial velocity increased, and more fluid was sucked into the secondary boundary layers along the outer bend. The secondary boundary layers thinned near the outer bend and thickened near the inner bend as they adjusted. Instantaneously, the maximum axial velocity moved towards the outside of the bend. A symmetrical pair of counter-rotating helical vortices were eventually created as a consequence (Berger *et al.*, 1983).

To better quantify pressure drop in two phase flow situations, Sánchez Silva *et al.* (2010) developed two correlations based on experimental data. The first was a tweak to the traditional Chisholm model that resulted in a more accurate prediction for a broader variety of scenarios. Again, the use of the Dean Number,  $D_e = R_e (D/2R_bR)^{0.5}$ , was obtained by combining the curvature ratio  $(2R_b/D)$  with the liquid Reynolds number ( $R_e = GD/\mu L$ ) (Hsu *et al.*, 2015).

Two phase pressure drop in a  $90^\circ$  bend was also found to be independent of pipe diameter but dependent on curvature ratio,  $R/D$  in a way similar to that observed for single phase flow in an experimental study (Hsu *et al.*, 2015). Secondary flow generated due to the inequality of the pressure at bend and the centrifugal force radial to the bend curvature is reliant on the bend radius of curvature and Reynolds number relative to the pipe diameter and bulk velocity, and when the radius of curvature  $R_c/D > 1.5$ . A secondary flow pairs of counter rotating Dean vortices were produced within the bend and at the same instant, stream wise flow starts to distort and shift from the centre of curvature (Weske, 1948).

The strength of a swirl about the axis of flow, swirl number, is the area-averaged flux of angular momentum. This was represented by Equation 2.8 as shown (Kim *et al.*, 2014).

$$I_s = \frac{\int [\vec{U} - (\vec{U} \cdot \hat{n}) \hat{n}]^2 dA}{U_b^2 \int dA} \quad (2.8)$$

Wherein  $I_s$  – swirl intensity;  
 $\vec{U}$  – flow velocity vector;  
 $\hat{n}$  – unit vector normal to the pipe section area; and  
 $A$  – pipe section area.

Jongtae *et al.* (2014) also expressed the exponential decay of the swirl as a decreasing function:

$$\frac{I_s}{I_{s0}} = \exp(1 - \beta_s \frac{L}{D}) \quad (2.9)$$

Where  $\beta_s$  – the rate of decreases of secondary flow intensity downstream at the elbow; and  
 $I_{s0}$  – Initial swirl intensity value.

This was seen to be 0.21 from the finest fit amid the experimental data and correlation (Kim *et al.*, 2014). This is expressed graphically in Figure 2.15.

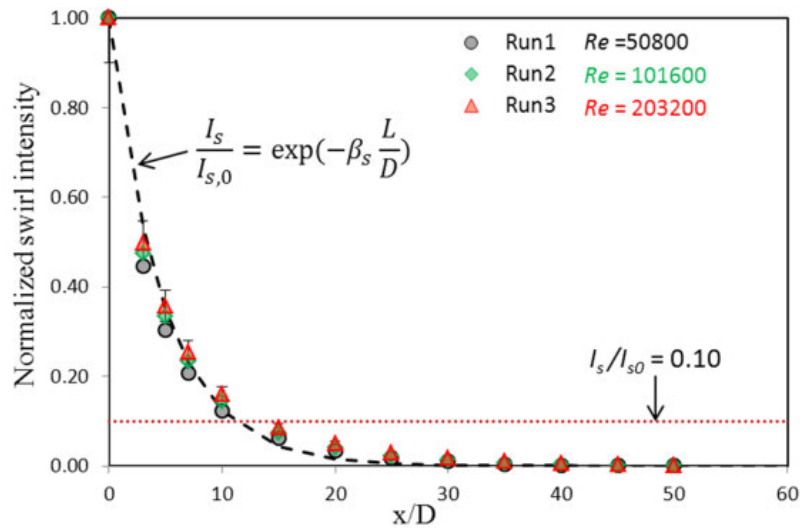


**Figure 2.15 Degeneration of normalized swirl intensity along pipe from elbow exit with  $R_c = 3D$  (Kim *et al.*, 2014)**

Based on Equation 2.9,  $I_s$  was found to dissipate 10% of its original value which is approximated at  $11D$  downstream of the elbow or  $90^\circ$ . To find out the effects of other

geometric parameters, the results were compared to the previous velocity measurements and expressed as in Figures 2.16 to 2.18.

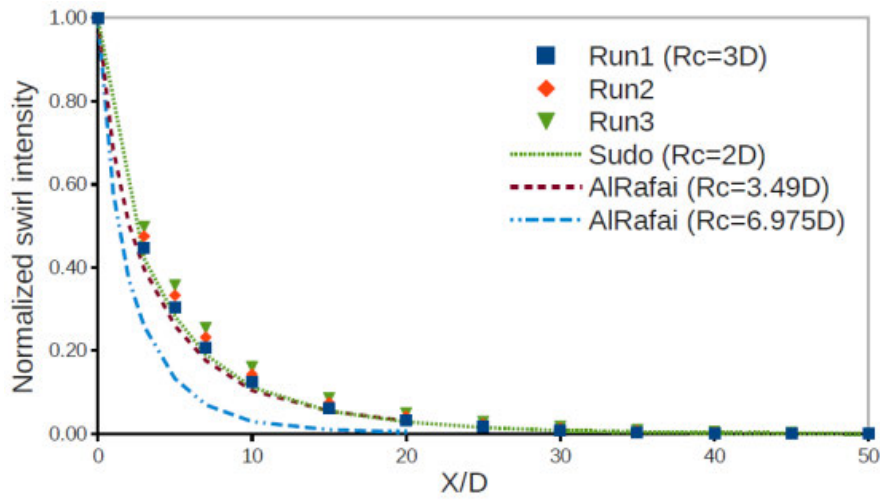


**Figure 2.16** Dependency of normalized swirl intensity degeneration along pipe from elbow exit with radius of curvature (Kim *et al.*, 2014)

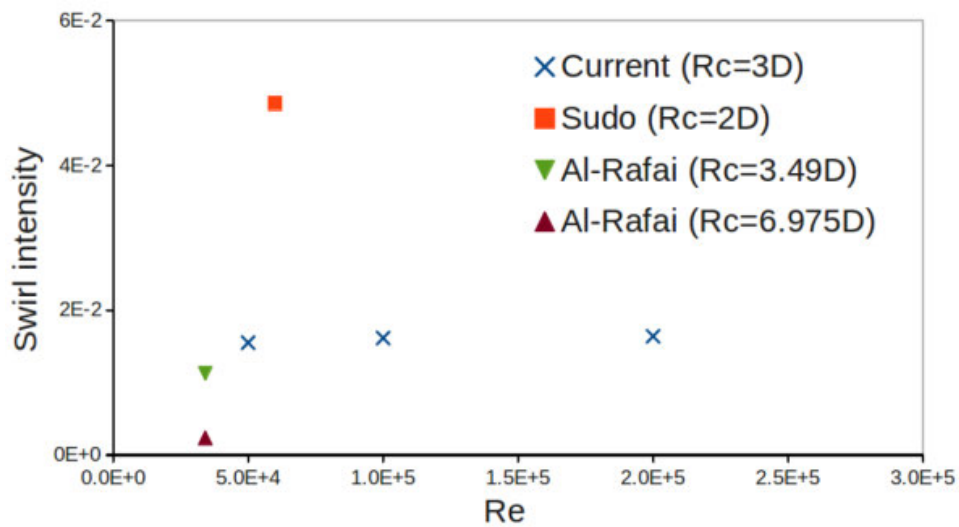


**Figure 2.17** Swirl intensity dependency on Reynolds number at exit of elbow (Kim *et al.*, 2014)

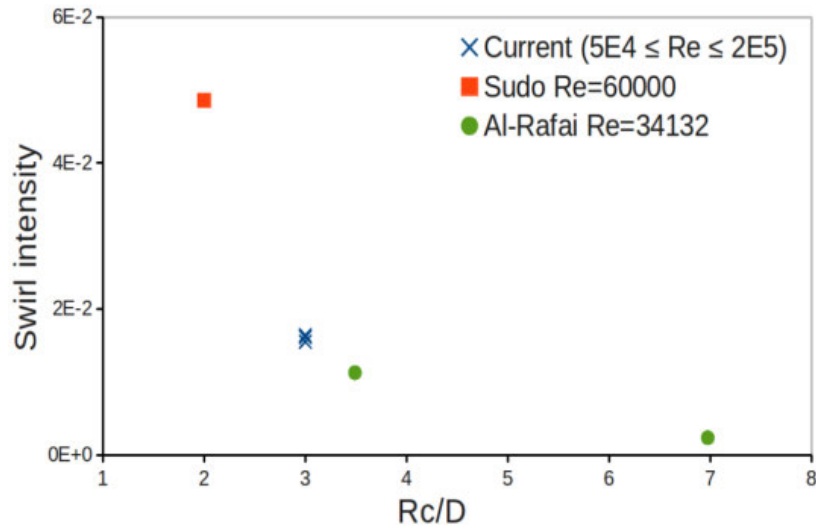


**Figure 2.18 Swirl intensity dependency on radius of elbow curvature of at exit of elbow (Kim *et al.*, 2014)**

Swirl intensity due to the vortices formed was also found to be greatly reliant on the radius of curvature and less on the Reynolds number. Swirl intensity (secondary flow generated) dissipation was also found to be exponential in nature and signified by the swirl number as well (Chigier and Beer, 1964). Kim *et al.* (2014) concluded that swirl intensity does not have much dependency on the Reynolds number but shows greater dependency on the radius of curvature of the bend and that studies needed to be undertaken to give the relationship between swirl intensity and the elbow radius of curvature. This was achieved with the use of the numerical method and turbulence model. In conclusion to the study by Kim *et al.* (2014), swirl intensity, defined as the area averaged tangential velocity, decreased exponentially on exit of the bend or elbow, dissipated faster as the radius of the elbow curvature grew bigger. Figure 2.19 shows a schematic diagram of the swirl decay and the streamline flow as described in the modelling.

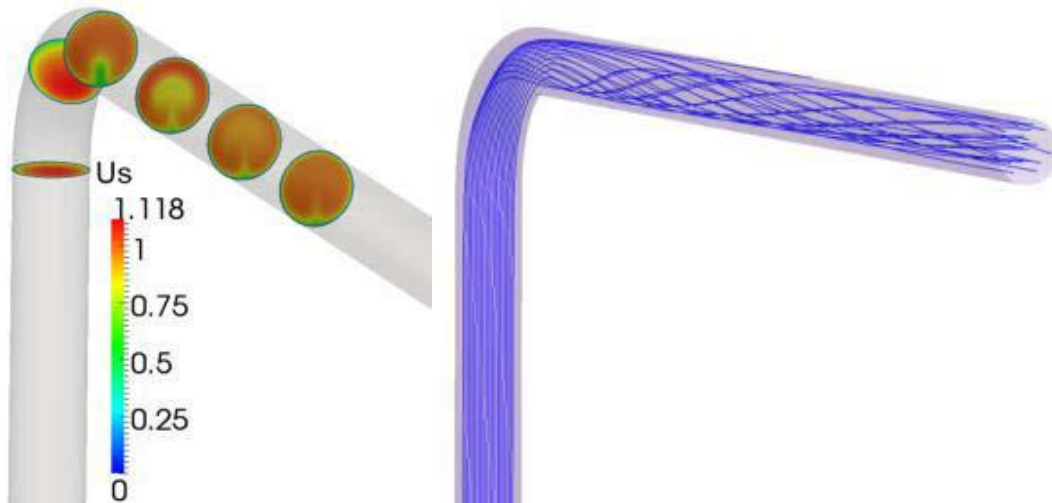


**Figure 2.19 Numerical results for experiment (a) Stream wise velocity profiles, (b) Streamline (Sudo *et al.*, 1998)**

Based on pressure gradient analysis with 90° bends, least downstream recovery length was found to be 150 times (Azzi and Friedel, 2005). Frictional losses within two phase fluid were also undertaken to shed more light on frictional loss due to bends. In the case of two phase flow, pressure loss was found to increase due to energy dissipation with momentum exchange amid the phases together with the separation and mingling of the gas-liquid phase.

## **2.7. Two phase Flow through a Bend**

In the situation of the two phase flow, primary variables are still the same as the single-phase flow with the addition of the mass and void fraction. As irrigation water flows through the bend or fitting, mass is conserved, and the process is adiabatic. Two phase flow through a bend is associated with a centrifugal-force-induced stratification of two phases with a process of migration of bubbles near the internal side of the bend (Jayanti, 2011). The complex interaction between the inertia, pressure, centrifugal forces, viscous, surface tension, adhesion and gravitational forces, leads to the heavier phase migrating to the outside of the bend, a process defined as film inversion (Hewitt and Jayanti, 1992). It was also observed that the gravitational force also affects the flow form (Azzi and Friedel, 2005). As for the instance of bubble or slug flow in a vertical bend, gas was seen to flow on the inner side of the bend owing to the equilibrium of the centrifugal forces pulling the liquid phase to the outside and gravity pulling it down. The relationship between the two phases due to the radius of

curvature, bend angle and mixture mean velocities is expressed by the Froude Number,  $Fr_\theta$  which is given as follows:

$$Fr_\theta = v^2 / gR_b \sin\theta \quad (2. 10)$$

wherein the Froude Number is unity at radial equilibrium and the gas phase changes to the inner side of bend and less than unit with the converse (Azzi and Friedel, 2005). The method of measuring two phase flow through bends is deemed impossible although it has been proposed as in Equation 2.11, which employs a method of multiplying the single phase pressure losses by a two phase multiplier (Chisholm, 1980).

$$\frac{\Delta P_{TP}}{\Delta P_{LO}} = 1 + \left( \frac{\rho_L}{\rho_G} - 1 \right) \times \left[ \left\{ 1 + \frac{2.2}{k_{LO} \left( 2 + \frac{R_B}{D} \right)} \right\} x(1-x) + x^2 \right] \quad (2. 11)$$

Where:  $\Delta P_{TP}$  is the pressure drop in two phase flow;

$\Delta P_{LO}$  is the pressure drop in a single-phase flow of total mass flux and liquid properties;

$k_{LO}$  is the bend loss coefficient for single phase flow; and

$x$  is the quality of phase.

Pressure drop in the two phase is more than that of the single-phase due to the reduction in flow area for the two phases and this is what potentially takes place in an irrigation system at times (Coleman and Garimella, 1999). Estimation of the two phase density and the subsequent hydrostatic pressure drop for a vertical tube with a bend, depends very much on the void fraction and is very much affected by the void fraction error (Ghajar and Bhagwat, 2013). Ghajar and Bhagwat (2013) analysed the dependency of the two phase density on void fraction using the slip ratio and drift flux model-based correlations and found the drift flux model-based correlations performed better than the slip ratio.

### 2.7.1. Void Fraction and Two Phase Dynamic Viscosity Models

The entire pressure drop in a liquid-gas mixture entails the hydrostatic, frictional and acceleration vectors of the pressure drop (Ghajar and Bhagwat, 2013). Knowledge of the two

phase mixture density which is dependent on the accurate prediction of void fraction is needed for the calculation of the total pressure drop in a liquid-gas mixture . This is expressed in Equation 2.12 with mixture density and void fraction of alternatively two phase quality (Ghajar and Bhagwat, 2013). The approach assumes no slip between the two phases in the homogeneous flow model.

$$\left(\frac{dP}{dL}\right)_{t,TP} = \left(\frac{dP}{dL}\right)_{h,TP} + \left(\frac{dP}{dL}\right)_{f,TP} + \left(\frac{dP}{dL}\right)_{a,TP} \quad (2. 12)$$

When  $\left(\frac{dP}{dL}\right)_{h,TP} = \rho_m g \sin\theta$  (mixture density)

and  $\rho_m = \rho_g \alpha + \rho_l (1 - \alpha)$  (void fraction)

and  $\rho_m = \left(\frac{x}{\rho_g} + \frac{1-x}{\rho_l}\right)^{-1}$  (alternative two phase quality)

Where:  $L$  – pipe length, m;  $P$  – pressure, Pa;  
 $g$  – acceleration due to gravity, ms<sup>-2</sup>;  $x$  – quality  
 $\alpha$  – void fraction;

and subscripts:  $a$  – acceleration;  $h$  – hydrostatic;  $f$  – friction;  
 $g$  – gas phase;  $l$  – liquid phase;  $m$  – mixture;  
 $t$  – total; and  $TP$  – two phase.

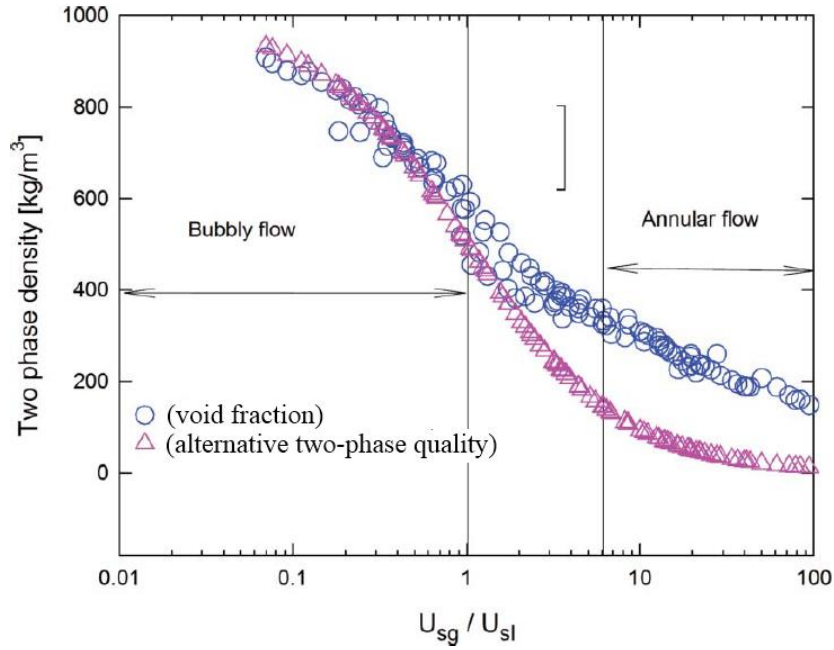


**Figure 2.20 Two phase density determined by void fraction and two phase mixture density is founded on two phase quality founded on the values of void fraction measured at Oklahoma State University, Two phase Flow Laboratory (Ghajar and Bhagwat, 2013).**

The two phase density expressed by way of a void fraction and the alternative two phase quality are in good agreement for bubbly flow but significantly differ for the annular flow regime as seen above. Based on visual observation, the alternative two phase quality method under predicts two phase density and resultant hydrostatic pressure drop. For non-boiling liquid-gas as in irrigation water, we can disregard the influence of the acceleration constituent to the two phase pressure drop (Ghajar and Bhagwat, 2013). Overly, the friction or pressure drop is considered for the fluid wall interaction and the liquid-gas interface expressed in Equation 2.13 (Ghajar and Bhagwat, 2013).

$$\left(\frac{dP}{dL}\right)_{f,TP} = \frac{f_{TP}G^2}{2D\rho_m} \quad (2.13)$$

Where:  $G$  – two phase mixture mass flux, ( $G = G_l + G_g$ ),  $\text{kg/m}^2\text{s}^{-1}$ ; and

$D$  – pipe diameter, m

This two phase friction factor equation is dependent on the two phase Reynolds number,  $Re_m = \frac{GD}{\mu_m}$ ,  $\mu$  being phase dynamic viscosity,  $\text{Pas}^{-1}$ , which also depends on the two phase dynamic viscosity. The two phase dynamic viscosity requires the formulation of a two phase equivalent mass flux, (*eq* - equivalent), expressed in Equation 2.14 (Akers *et al.*, 1958).

$$G_{eq} = G \left( (1 - x) + x \sqrt{\frac{\rho_l}{\rho_g}} \right) \quad (2.14)$$

Many methods of predicting pressure drops at bends have been developed, validation of which can only be done when practical tests have been undertaken. Autee and Giri (2016) made a comparative study of the leading methods in the determination of pressure drop through the bends. In the study, it was found that the applicability of the pressure drop correlations differed by  $\pm 50\%$ . Most literature reports have either used the Blasius or Colebrook equation on the calculation of the two phase friction factor also founded on the two phase Reynolds number. However, the Blasius equation is used in smooth pipes and does not take into consideration the transition between laminar and turbulent flow whereas the Colebrook equation is mainly for turbulent flow regimes. The Churchill friction factor correlation, (Equation 2.15), was deemed more accurate as it takes in to account the effects of pipe roughness ( $\epsilon$ ) and the smooth transition between laminar and turbulent flow with the variables A and B, expressed in Equation 2.15.

$$f_{TP} = 8 \left[ \left( \frac{8}{Re_m} \right)^{12} + \frac{1}{(A+B)^{1.5}} \right]^{\frac{1}{12}} \quad (2.15)$$

Where,

$$A = \left[ 2.457 \ln \left( \frac{1}{\left( \frac{7}{Re_m} \right)^{0.9} + (0.27\epsilon/D)} \right) \right]^{16}$$

And,

$$B = \left( \frac{37530}{Re_m} \right)^{16}$$

### 2.7.2. Two Phase Flow in Upward, Horizontal, or Downward Arrangement

With the use of long inlet and outlet pipes, it is presumed the flow is fully developed. An upward, horizontal, and downward arrangement with a 90° bend test on the single-phase pressure drop and flow pattern was conducted (Ghajar and Bhagwat, 2013). It was discovered that for the single-phase flow, friction factor due to the 90° bend was more than that of a straight pipe length for the same Reynolds number. Friction factor for a smaller curvature ratio (2R/D) was found to be greater than that of a bigger curvature ratio bend. For two phase pressure drop, the pressure drop in the upward arrangement of the 90° bend is more than that of the horizontal configuration due to the swirled motion and liquid flow reversal in the pipe bend (Hsu *et al.*, 2015). However, this happens in the upward arrangement only at specific flow patterns (Reynolds number) and pressure gradient, and none in the downward configuration. As the mass flux and quality increased in all cases (two phase to single-phase), the difference in pressure drop for all three scenarios became insignificant due to the rising flow inertia. This is also the case of flow in irrigation systems. Liquid flow reversal was more evident in the larger pipe diameter used in the test but there exists threshold velocities in each case, after which there is no more liquid flow reversal occurring. Threshold flow velocities were found to be 2 ms<sup>-1</sup> for a 5.5 mm diameter pipe bend and 4 ms<sup>-1</sup> for a 5.9 mm diameter pipe bend (Ghajar and Bhagwat, 2013).

In other experiments on a 90° bend with a horizontal inlet and upward outlet, the frictional losses were equivalent to the flow in the reverse, that is, a vertical inlet and a horizontal outlet. In the case of a horizontal inlet and downward outlet, a 35% decrease in the frictional loss was experienced at the bend (Deobald, 1962). An investigation was also done on the influence of the plane on the bend. The frictional losses on a 90° bend in the vertical plane was found to be 30% less than in a horizontal plane (Grant and Cotchin, 1989).

The total pressure drop in a liquid-gas mixture in a horizontal pipe entails of the hydrostatic (gravity), frictional and acceleration components of the pressure drop, with the pipe bend being horizontal. The effects of gravity can be neglected as supported by the result of error in two phase hydrostatic pressure drop with prediction of void fraction by Ghajar and Bhagwat (2013). Likewise, a pipe having a uniform size at bend, the momentum change or acceleration component was said to be insignificant (Autee and Giri, 2016). Change in

momentum or acceleration as fluid impacts the bend the resultant change in flow direction, the nappe or vortex detachment, secondary flow generation and downstream tangent for the two symmetrical velocity profiles developed at the bend, adding to the observed pressure drop. In some instances, it was also concluded that there are two separate effects that result in the pressure drop due to a bend, the pressure gradient which leads to excessive friction on the outer wall of bend inside the pipe bend and the secondary flow due to the bend geometry (Crawford *et al.*, 2003).

## 2.8. CFD Analysis of Energy Losses on a 90° Bend

dos Santos *et al.* (2014) examined flow through a 90° bend with incompressible airflow in turbulent conditions. Using the finite volume method, the mass, momentum, and the turbulence kinetic energy and dissipation rate equations, (turbulence equations), were developed to determine the friction loss coefficient of the bend and the effect of Reynolds number on the coefficient. Pressure drop was found to be attributed to by the fluid wall interaction and the dynamic losses. Static pressure contours were developed showing the streamline of flow. Flow was characterised by high pressure on the external of the bend and low pressure on the inside as flow close to the inner side of the bend tends to proceed straight with the outer flow spiralling as seen in Figure 2.21.

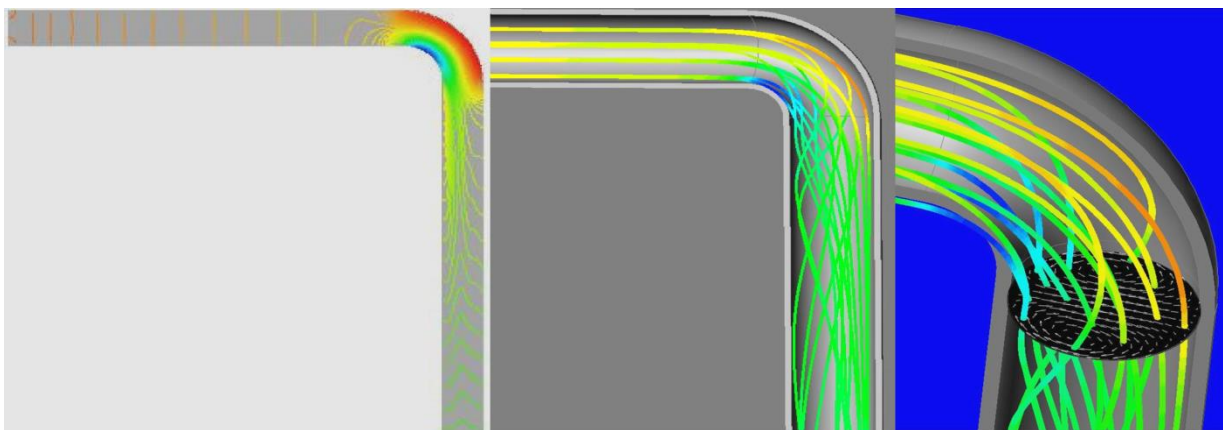


**Figure 2.21 Static pressure contours, Streamlines details at  $Re=1 \times 10^5$  and Secondary flow patterns at the elbow cross section (dos Santos *et al.*, 2014)**

The frictional loss coefficient decayed over the Reynolds number  $1 \times 10^4 \leq Re \leq 1 \times 10^6$  and were fitted to give the coefficient of friction, ( $C_o$ ) to give Equation 2.16 and shown in Figure 2.22 graphically;

$$C_o = \frac{264.56}{126.23 + Re^{0.7345}} + 0.079 \quad (2.16)$$

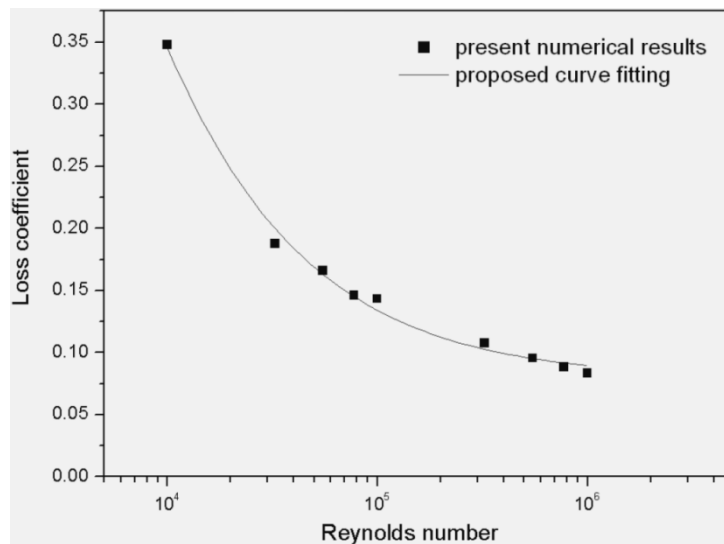


**Figure 2.22 Loss coefficient ( $C_o$ ) with the Reynolds number (dos Santos *et al.*, 2014)**

Determination of pressure loss in this instance, though it can be a close approximation with fixed parameters of a bend, it cannot be applied in a situation of varying bend parameters, compromising the applicability in the irrigation design process.

## 2.9. The Effect of Geometric Parameters on Frictional Losses

The energy losses due to the fluid wall interaction happen as fluid flows before and after the bend. This will always be the case in an irrigation system, pressurised in its normal operation. The contribution of pipe roughness, geometry (shape), bend angle, curvature radius and change in pipe diameter contribute significantly to the frictional losses.

Effectively there will always be a component of fluid wall friction which will hinge on the roughness of the pipe (Farshad *et al.*, 2001). The effect of pipe roughness on frictional losses is influenced by the flow velocity in the pipe. The change in flow velocity influences the flow profile with the accompanied change in the Reynolds number (Tezuka *et al.*, 2008). Pipe

roughness is also influenced by the hydraulic diameter flow area with its variation and the extent of wall shear stress (impact) by the flowing fluid, which also affects the rate at which flow turns turbulent from laminar flow. The more the roughness the sooner flow turns turbulent compared to a smoother pipe with respective flows (Kandlikar *et al.*, 2005). Experimental study on fully developed flow as seen in an irrigation pipe in use, showed that the roughness played only a slight effect on the flow features that is, the friction factor and critical Reynolds number of fluid when considering the relative roughness  $0\% < \varepsilon/D_h \leq 1\%$  as seen in Figure 2.23 (Dai *et al.*, 2014).

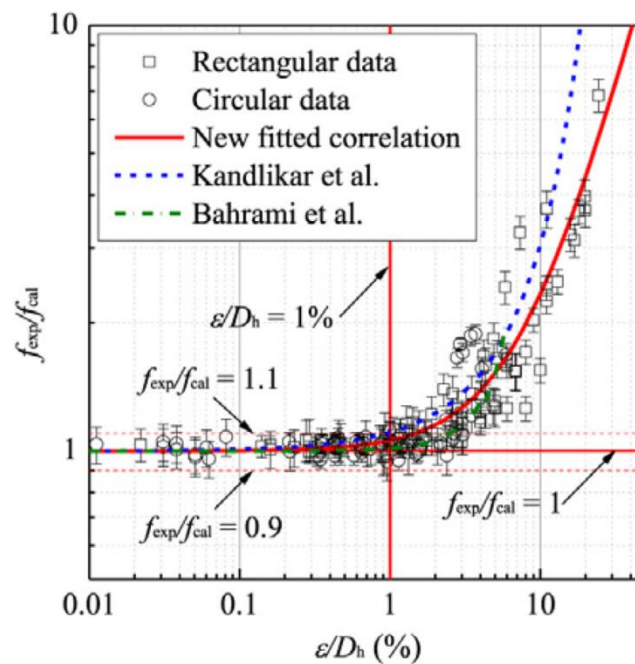


**Figure 2.23 Contrast of normalized friction features of laminar flow with models (Dai *et al.*, 2014).**

The geometry of the channel was seen to have little to no effect on the threshold (Dai *et al.*, 2014). At relative roughness over 1%, the friction factor and the critical Reynolds number progressively are at variance with the predicted values. At relative roughness  $\varepsilon/D_h = 1\%$  a threshold was recommended to differentiate between smooth and rough flow in micro- and mini- channels. In a study of a water distribution network as of the principle of an irrigation system, pipe roughness may be detrimental to the pumping energy, with a saving of 0.7 to - 0.2 % of the total pumping energy (Speight, 2014). In some other scientific work undertaken, at pipe relative roughness below 5%, it was found that the incompressible fluid had no effect on the flow resistance (Li, 2003). As the irrigation water flows past the bend, the degree of

fluid wall interaction (differential pressure) varies with the angle and shape of the bend, introducing the effect of the bend angle and radius of curvature.

Generally, as the angle of the bend increases the energy losses inevitably increase (NPTEL, 2015). With the exception of the long-radius pipe bends, the frictional loss was found not to be comparative to the refraction or bend angle for a given  $R/r$  value (Ito, 1960). This is illustrated in Figure 2.24 with different bend angles tested.

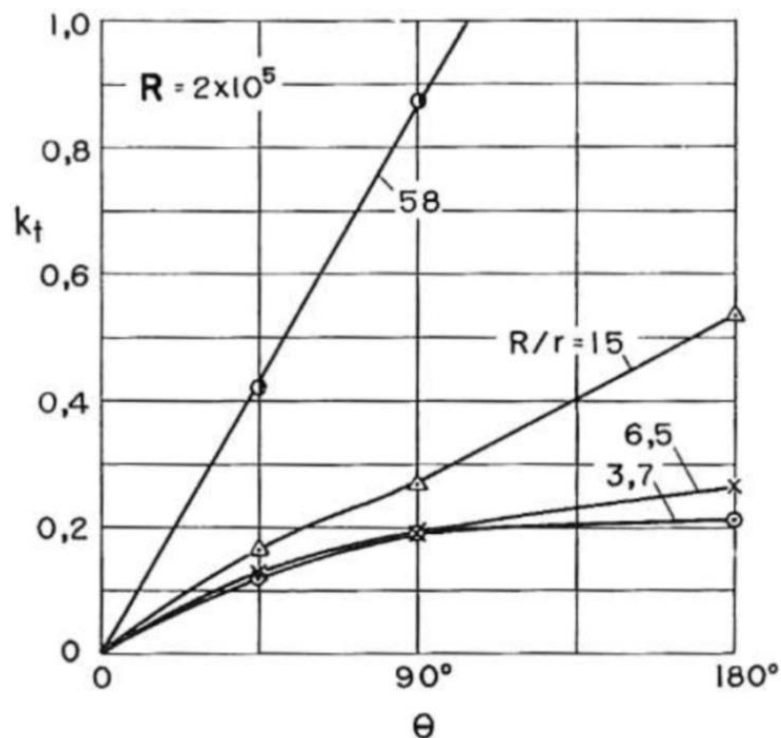


**Figure 2.24 Variation of the frictional loss coefficient ( $k_t$ ) with bend angle ( $\theta$ ) for smooth pipe bends for Reynolds number of  $2 \times 10^5$  (Ito, 1960)**

Again, generally as the bend radius of curvature increases, the energy losses reduce (NPTEL, 2015). A minimum value of the frictional loss coefficient,  $k_t$ , was seen for  $R/r \approx 5$  for the  $45^\circ$  and  $90^\circ$  bends, and  $\approx 4$  for  $180^\circ$  bends. This is also shown graphically Figure 2.25 by experimental test undertaken.

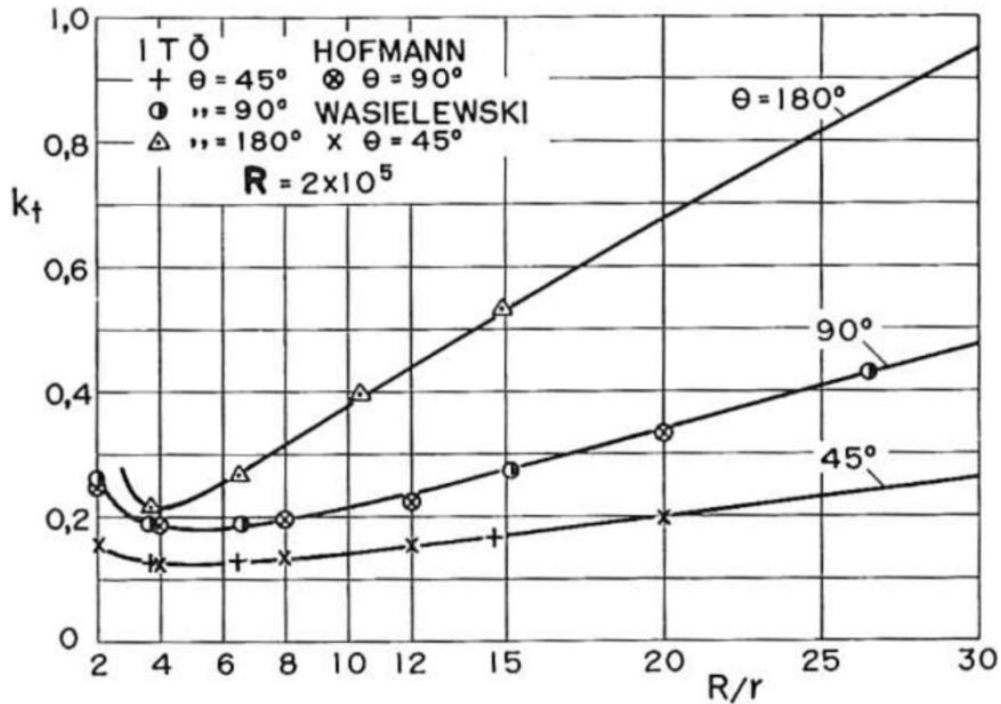


**Figure 2.25 Variation of bend-loss coefficient with relative radius for smooth pipe bends for Reynolds number of  $2 \times 10^5$  (Ito, 1960)**

With the impact of flow depth ( $H$ ) to center line radius ( $R = R_b$ ) of curvature ratio,  $H/R$ , on the development of secondary flow, energy loss and turbulence were also investigated for an open channel, as with the principle of flow in a pipe bend on horizontal ground. In linear models, secondary flow is realized to increase with increase in curvature according to low-amplitude perturbation models, but it was found that it either hardly increases with curvature or it was not proportional (Blanckaert, 2009). This phenomenon termed “saturation” was also seen for turbulence and energy loss. Secondary flow was found to develop because of the curvature resulting in the formation of turbulence, leading to energy loss which lagged behind the turbulence formation.

## 2.10. Discussion

In view of the literature reviewed, pressure losses due to straight pipe sections can easily be determined with the developed equations though one may encounter changing pipe diameters and varied flow. When secondary losses are considered, there have been limitations identified with the use of the straight pipe friction equations. This has led to the development of the Equivalent Length, Resistance and Valve Flow Coefficient Methods but is not often easily

understood for on application when determining pressure drop. Though methods were developed not all the equivalent lengths and coefficients have been practically determined for ease of application. Often a thorough knowledge of how the equivalent lengths and coefficients is needed, and this has led to estimations due to the uncertainties involved in incorporating changing pipe geometry and flow.

Pressure drop was found to occur in three sections of a pipe bend, the straight pipe section just before the bend, within the bend and after the bend. Pressure drop is firstly due to perturbation that occurs before the bend, after which pressure drop continues to occur again inside the bend as the column of flowing fluid is split into two, generating Dean vortices. Fluid simultaneously undergoes differential forces as it splits and combines, with collision and adhesion on the outside and inside of the bend, respectively. Pressure drop again occurs on exit of the pipe bend due to perturbation and the generated secondary flow in the straight pipe section downstream. Pressure drop finally continues downstream of the bend with decaying intensity as fluid oscillates downstream.

The dynamic and kinematic viscosity component of water also plays part to the viscosity of the fluid with temperature and overall pressure drop. These are however insignificant considering irrigation water at room temperature. The effect of pressure drop due to bending is further enhanced with the change from a single-phase fluid to two phase fluid with some component of contribution by the plane of the bend. The general flow pattern of the flow field due to bending was also seen remarkably well with the use of CFD showing clear streamline of flow. This flow phenomenon about the bends was consider similar by many authors and expressed in different ways as described with the Dean Number. Simply put, the ratio of pipe diameter to bend length ( $L/D$ ) and the use of the relative radius of curvature ( $R_c$ ), better describes flow about a bend. Despite the vast knowledge available, determination of pressure losses due to bending is often made complicated with changing bend geometries and varying flows, requiring more information or knowledge on the equivalent lengths and friction coefficients, and this has led to the over or under estimations of pressure drop due to bending.

## 2.11. Conclusion

From the undertaken studies as seen in above literature, there has been some work done to incorporate changes in the pipe dimensions when determining frictional losses due to straight pipes. This has made straight pipe friction equations simple and easy to apply when working with them giving precise and accurate values. When a bend is introduced to a pipe section, though good analyses and methods have been done for determining frictional losses, it becomes complicated with the change in pipe diameter, bend angle, radius of curvature and varied flows.

When using the Equivalent length method, a thorough knowledge of how the equivalent lengths were derived is needed to use them, creating a gap for ease of application of method. Similarly, a thorough knowledge of how friction coefficients are derived is also needed with the use of the Resistance and Valve Flow Coefficient method. Limitations also occur with the pragmatic coefficients published creating gaps in the available data. Due to absence of experimentally determined equivalent lengths and coefficients with at times varying bend angles results in the element of error due to estimations eventually made in the calculation of the pressure losses about bends, and likewise the Valve Flow method.

Due to the lack of ease, quick, accurate and precise applicability for calculation of minor losses as the need arises in the design of irrigation systems, designers often resort to estimation of 10% to 15% and at most 25% of the mainline losses to cater for secondary losses due to bends. This gap can only be bridge with the use of the correct equivalent length and or correct friction coefficient with changing pipe geometries unless pragmatically determined. Gap calls for the need of development of an Empirical friction Equation, catering for the change in the pipe diameter, bend angle and radius of curvature with respect to flow. With this, designers could easily and rapidly give better estimates of the precise and accurate secondary losses as needed in the process of designing irrigation systems. The extent of bending considered in this research when designing of irrigation systems is the Short, Standard, Long and Specialised radius bends for bend angle  $0^\circ$  to  $90^\circ$ .

## **CHAPTER 3: THE DEVELOPMENT OF AN EMPIRICAL EQUATION FOR DETERMINING MINOR LOSSES DUE TO BENDS IN SMOOTH PIPES FOR IRRIGATION SYSTEM DESIGN**

Manuscript submitted to and accepted for publication, after review, by the *Agricultural Engineering International: CIGR Journal*: <sup>ab</sup>D. Tagwi<sup>1</sup>, <sup>a</sup>A. Senzanje and <sup>a</sup>G. Lagerwall  
<sup>a</sup>Bioresources Engineering Programme, School of Engineering, University of KwaZulu-Natal, Pietermaritzburg, 3201. South Africa. <sup>b</sup> Water Resource Development Planning, Department of Water and Sanitation, Head Office, Pretoria, 0001. South Africa.

### **Abstract**

As pipe networks get to shorter lengths or the number of bends increase, the proportion of losses due to bends increases contributing significantly to possible over- and under-sizing of pumps, especially for low operating pressure systems. Methods used for determining minor losses in smooth pipes for irrigation system design consist of mainly the Equivalent Length, Resistance Coefficient and Valve Flow Coefficient method. Without a thorough knowledge of their development, the methods do not offer easy, quick, accurate and precise determination of minor losses as bend parameters change in the design process. The resulting incorrect use of methods and estimations of 30 to 50 pipe-diameters in length of equivalent straight pipe, 10% to 15% and at times 25% of mainline losses by designers in industry, leaves room for error.

An Empirical Equation for determining minor losses based on the Resistance Coefficient method deemed the most accurate, was derived from analysis, association, and amalgamation of behavioural patterns of pressure drop due to change of individual bend parameters that contribute to pressure drop. Changing bend angles and key components defining bends, pipe diameter per bend radius of curvature (relative radius of curvature),  $R_c$ , and the flow coefficient, bend length per pipe diameter ratio (L/D ratio) were used in the derivation of the Empirical Equation. Behavioural patterns at  $R_c$  values of 13.545, 27.679 and 79.578 were obtained experimentally and the Short, Standard and Long radius, from published data.

The derived Empirical Equation (based on the theoretical 19.05 mm Standard radius for friction coefficient,  $k = 0.7395$ ) dynamically determined the best estimate of minor losses due to bend angles  $0^\circ$  to  $90^\circ$  without need of a thorough knowledge of derivation of coefficient, eliminating error. It catered for finding  $k$  for pipe diameters outside the experimental and published data. The pragmatic basis for its derivation catered for all the constant parameters, easily measured and the unseen or immeasurable parameters also validating the equation. The equation allowed for the identification of the phenomenon of saturation as  $R_c$  continued beyond experimental values. It confirmed the difference between the Short and Standard radius bends ( $k = 0.8976$ ) often confused in the literature reviewed by close approximation of  $k$  at  $R_c = 0.5$ . The derived Empirical Equation can satisfactorily be used in irrigation system design procedure and as a tool in software for correctly estimating the minor losses.

**Keywords:** *Pressure drop, Friction coefficient, Bend radius, Relative radius of curvature, Minor losses.*

### **3.1. Introduction**

Determination of the secondary losses is critical since the introduction of drip and micro irrigation systems has reduced the operating pressure of the old systems (Chirgwin and Sutton, 2019). With the current and future introduction of low-pressure emitters (operating pressure) and possible use of special bends (unique bends made specifically for an irrigation system or cases of applying the bending schedule according to the pipe manufacturing bend limits) in irrigation systems, it is essential that determination of minor losses be as accurate as possible for efficient systems. This will also enable farmers or users to realise a saving in the capital costs, pumping costs, and eventually a green economy.

Considering the different methods used for determining minor or secondary losses in pipe networks, the Equivalent Length, Resistance Coefficient and the Valve Flow Coefficient method (Wilson, 2012), the first two methods are ideal for determining pressure drop since they are based on experimental findings to validate them. The Valve Flow Coefficient method is often best used for conversion of coefficients.

Comparing the Equivalent Length and the Resistance Coefficient methods, the former though accurate, the pressure drop is likely to be underestimated at smaller pipe diameters than those for which the Equivalent Length was measured. This is because the flow coefficient (bend length (L) per pipe diameter (D), L/D ratio) decreases as the fittings size increases. The pressure drop would be overestimated at pipe sizes greater than those for which the fitting's equivalent length was calculated (Papavinasam, 2013). The Equivalent Length method however has the advantage of being very easy to calculate but as a consequence, evaluating small or dynamic pressure losses in pipes is better achieved using the Resistance Coefficient process (Sabet, 2016).

With regards to the published experimental findings, bends are classified into three categories, Short Radius, Standard Radius and Long Radius as described by Dhodapkar *et al.* (2009). In a case the diameter of the elbow is D, and the radius is R, the outer diameter of a tube with a radius of curvature equal to 1.5 times its outer diameter, or  $R = 1.5D$ , is referred to as a Long Radius elbow. A Standard Radius elbow has a radius of curvature equal to the tube's outer diameter, i.e.  $R = D$  as also confirmed by Spedding *et al.* (2004). However, in the literature reviewed there seems to be confusion between Short and Standard Radius because the two names are often referred interchangeably (ARC, 2003; Spedding *et al.*, 2004; Spellman, 2013; Escudier, 2017; net, 2022; Neutrium, 2016; Permanent-Steel-Manufacturing, 2017; Steeljrv, 2018; Haihio-group, 2020).

To date, the SABI Irrigation Design Manual (South African Norms and Standards) revised edition June 2003 by ARC (2003) for designing irrigation systems when determining the minor losses is on the basis that minor losses are proportional to the velocity head component. This is such that a friction coefficient,  $k$ , is multiplied with the velocity head,  $\left(k \frac{v^2}{2g}\right)$ , similar to the straight pipe equation considering the Darcy-Weisbach equation (ARC, 2003). The friction coefficients used are the same and do not carry the changing pipe diameter, which is often the case during the design process. This approach was adopted so as not to confuse the designer but lacks the inclusion of the changing L/D ratio and resulting relative radius of curvature,  $R_c$  for closer approximation of the friction coefficient. The use of the friction coefficient,  $k$ , as a Resistance Coefficient method suffices for one to get the correct pressure drop while undertaking the irrigation design process with changing bend

parameters (mainly bend angle, bend length, bend radius and respective flow velocity). This is true, provided the correct  $k$  value is used following a thorough understanding of how the friction coefficient was derived (Wilson, 2012).

In practice, not all the  $k$  values are given for the change in the relative radius of curvature and pipe diameter. This leaves the designers to estimate the correct friction coefficient from the tables or work with the incorrect coefficients on estimation. In the process this brings about the inaccuracies and uncertainties in the determination of secondary losses in the irrigation system design process. Often estimations of a safety factor of 30 to 50 pipe-diameters in length of equivalent straight pipe, 10% or 15% and up to 25% of the mainline losses (minor losses due to the pipe bends along the main line to the point requiring the most head in the system) in the irrigation system design, is done in the industry to cater for the grey area in the calculation of the minor losses (Savva and Frenken, 2002; Spedding *et al.*, 2004).

Avoiding the estimation or inclusion of the minor losses leaves the designer with the risk of a just failing system and the cost on the possible resizing of the pump as this is normally the key component affecting the performance or design of an efficient irrigation system in general experience. The existence or presence of the minor losses and the inaccuracies that are involved in determining them also affect the possible saving on pipe sizes, pumping cost or electricity consumed by the pump sized. This situation calls for a need to have a closer approximation method for the actual energy or pressure lost due to bends. This is also the case for critical operation and at times plant safety in downstream hydraulic valves relief systems (Spedding *et al.*, 2004).

The seemingly best method to determine minor or secondary losses due to bends must be based on pragmatic findings validated by experimental results giving a good basis for the design of an irrigation distribution network or system (Yasmina and Rachid, 2015). Despite the accuracy of this method, the main issue would be the need to find a multiplier or coefficient which carries or applies the effect of the changing or transforming bend parameters. This will enable easy and correct assignment of the friction coefficient or equivalent length without a thorough knowledge for the bend parameters in question during the irrigation design process (Pei *et al.*, 2016).

To solve this problem, the development of an Empirical Equation is needed to allow for the designers to input the changing bend or specialized bend parameters significantly sensitive to affecting pressure drop or secondary losses. Developing an Empirical Equation for minor losses as a function of the bend parameters requires the breaking up or disaggregating or elaboration of the friction coefficient,  $k$  in the expression  $\left(k \frac{v^2}{2g}\right)$ , which will only need to align or allow for one to effect the changing bend parameters for the correct  $k$  value. Of little significance is the roughness of the pipe, and geometry (square or circular tube) which may be ignored (Li, 2003). These, like other dynamic properties (which cannot easily be measured and at times are three- or multi-dimensional in nature) resulting from the introduction of a bend, are at times easily accounted for in the process of determination of the significant measurable bend parameters.

With future developments, the introduction of much lower operating pressure emitters will continue to push for the accurate and precise determination of the secondary losses, requiring designers to move away from estimations. This pushes designers to the extreme of having to accurately calculate minor losses with the use of correct equivalent lengths and coefficients since the major or primary loss determination methods are quite accurate (Wilson, 2012).

Despite the accuracies involved in the use of the traditional methods, there have been limitations in the use of the methods due to their reliance on pragmatic findings, requiring more tests to be done to determine equivalent lengths and friction coefficients (Spedding *et al.*, 2004). This means traditional methods are only applicable to the extent of the testing conditions done (ARC, 2003). In contrast, the development of an Empirical Equation as the main aim of the research is not limited to the extent of pragmatic finds. It also has the ease of inserting or inputting in the changing bend parameters catering for the Short, Standard and Long or specialised bends involved during the design process. In essence, pressure drop is determined due to the respective curvature that is the bend Length to Diameter (L/D) ratio with respective flow velocity, replacing the difficulties or complexities in the use of the traditional methods, introducing error. This will also enable the designer to arrive at the closest approximate of pressure drop due to bending with the use of the correct friction coefficient without a thorough knowledge of derivation of the friction coefficient required.

The Empirical Equation will give a simple, easy, and quick mathematical tool for the precise and accurate determination of pressure drop due to bends as well as specialised bends.

The main purpose of this research is to develop an Empirical Equation for correctly determining minor losses due to bends in smooth pipes for irrigation design. This will offer a simple, easy, and quick way (mathematical tool) for precise and accurate determination (closest approximation) of minor losses due to bends as well as specialised bends. It is hypothesised that the friction coefficient approaches saturation or a constant as the  $Re$  increases.

### **3.2. Materials and Methods**

Research site / laboratory and experimental methodology are looked at in the following subsections.

#### **3.2.1. Research Site / Laboratory**

All experimental work was carried out in the HydroLab of the Agricultural Research Council – Institute for Agricultural Engineering (ARC-IAE) accredited laboratory in South Africa.

#### **3.2.2. Experimental Methodology**

The build-up of fully developed flow was critical in the determination of pressure loss only due to the bends. Fully developed flow before the bend voided the measurement of any other frictional loss due to secondary effects but only the introduction of the bend in all instances measured. In the measurements done, this was achieved using an inlet and outlet pipe to the bend not less than 151 cm in all cases tested. Additionally, the single phase (water only) supply line was also made at least 2.5 m long and straight before supplying the test configurations. In all the tests undertaken single phase flow (water at room temperature) was used for the tests for simulating the scenarios as in the normal operation of an irrigation system and the test scenarios were repeated five times in each case to learn or ascertain the correctness of the measured values.

Pressure measurements were then done specifically to determine pressure drop due to the bending introduced, that is, the behavioural change due to the pressure contours shortly after the bend of an open-end pipe to determine the actual pressure drop. The schematic diagram in Figure 3.1 shows the test configuration of the experimental apparatus used with flexible straight plastic pipes to successively form the required one-meter bend(s) section from 0° to 90° in increments of 22.5°, and subjected to varied supply flow velocities as tabulated in Table 3.1.

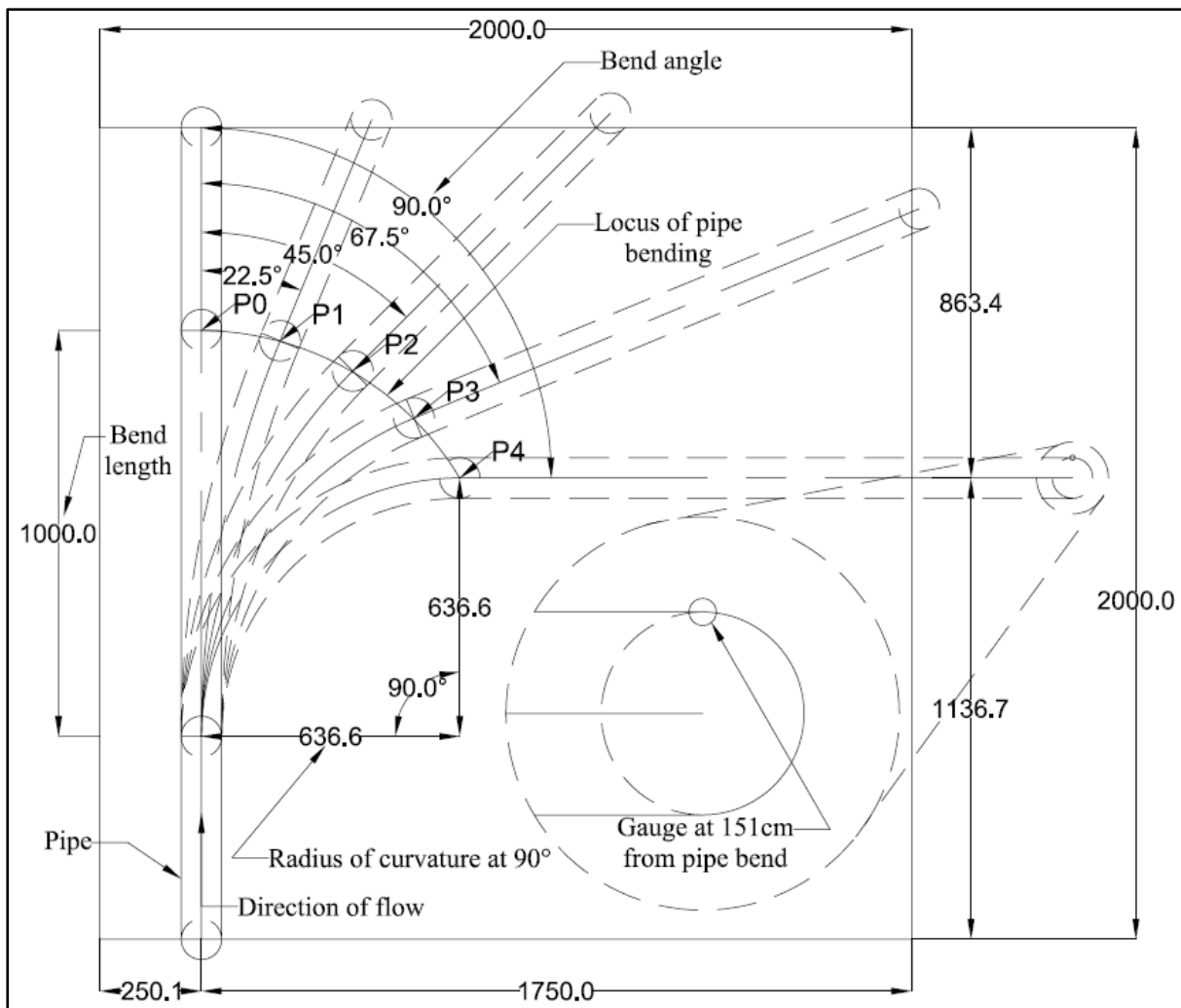


**Figure 3.1 Schematic diagram of experimental test configuration dimensioned in millimeters showing the pipe(s) bend angles tested for varied flow and gauge position**

During the experiments, the lowest flow supply to each pipe tested reached the limits when water supplied could not fill the pipe. Just above this flow, the testing of the pipes could be achieved but testing was however done at intervals from  $0.0000136 \text{ m}^3\text{s}^{-1}$  to  $0.0001500 \text{ m}^3\text{s}^{-1}$

of the supply line flow rate, which translated to the various flow velocities with the change in pipe diameter (Table 3.1).

**Table 3.1 Single phase supply flow rate ( $\text{m}^3\text{s}^{-1}$ ) and individual pipe diameter flow velocities ( $\text{ms}^{-1}$ )**

Main supply line flow rate with flow meter Outside pipe diameter, 100 mm (OD) Internal pipe diameter, 97 mm (ID)		Actual flow velocity in each pipe ( $\text{ms}^{-1}$ )		
		10mm (OD) 8mm (ID)	25mm (OD) 23 mm (ID)	50mm (OD) 47mm (ID)
( $\text{m}^3\text{s}^{-1}$ )	(LPM)			
0.0000136	0.82	0.271	0.033	0.008
0.0000273	1.64	0.543	0.066	0.016
0.0000409	2.45	0.814	0.098	0.024
0.0000545	3.27	1.085	0.131	0.031
0.0000682	4.09	1.356	0.164	0.039
0.0000818	4.91	1.628	0.197	0.047
0.0000955	5.73	1.899	0.230	0.055
0.0001091	6.55	2.170	0.263	0.063
0.0001227	7.36	2.442	0.295	0.071
0.0001364	8.18	2.713	0.328	0.079
0.0001500	9.00	2.984	0.361	0.086
Flow	Too low flow relative to the pipe size (open channel flow)			
Flow	Too high flow, relative to the pipe size (tests not done)			

The clear PVC pipe diameters were taken as given by the manufacturer and verified with Vernier callipers, considering the wall thickness of the pipe. Varied pipe diameters 10 mm (8 mm ID), 25 mm (23 mm ID) and 50 mm (47 mm ID) were individually fed water from a 100 mm (97 mm ID) pipe through a flow meter (ZJ-LCD-M Digital Display Water Flow Sensor Meter, 0.01 LPM, 1% accuracy), to determine the relationship between different flows and pressure drop introduced in each test. Instantaneous measurements of the bend parameters taken include the pressure drop, bend angle and bend radius for the respective flow tested per pipe diameter tested for the one meter bend.

With the change in bend angle from position P0 to P1 to P2 then P3 and finally P4 (0°, 22.5°, 45°, 67.5°, 90°, respectively) as seen in Figure 3.1, pressure drop was successively introduced and measured, with change in the bend radii. Changes to the test pipe, radius of curvature and pipe diameter were applied for each fixed length pipe or bend length while the supply flow rate was varied from 0.0000136 m<sup>3</sup>s<sup>-1</sup> to 0.0001500 m<sup>3</sup>s<sup>-1</sup> (Table 3.1), permissible with the pipe diameter to achieve the varied flows and resultant pressure drop.

Pressure drop was measured with the WIKA CPG1500 series precision digital pneumatic pressure gauge (-1 to +5 ×10<sup>2</sup> kPa 0.1% accuracy) taking the average pressure readings for the piezometric pressure from the pipe wall with flowing fluid. The release of the fluid from the test apparatus was not controlled (open-ended). The test set up was performed relative to the atmospheric pressure, allowing for low operating pressure catering for the sensitivity of the pressure gauge used. Since water is relatively incompressible, the assumption was that the normal operation of an irrigation system would be catered for.

The way the pressure drop changed with change in the bend angle for the three pipe diameters was further used to give the mathematical way and manner in which the bend angle alone affected the pressure or friction coefficient in the development of the Empirical Equation. The behaviour of pressure drop with bend angle, as displayed by the results of the three pipes tested, was finally used but linked with the R<sub>c</sub> and the L/D ratio in developing the Empirical Equation.

Converting the pressure drop to the friction coefficients was done by removing the  $\frac{v^2}{2g}$  term in the pressure drop measured. As a result of the differences in the point of measurement of the pressure drop downstream of the bend for experimental and published coefficients, a manometric correction factor of approximately 0.19 due to the estimated decay of the main pressure head was used. This was relative to the point of pressure measurement, based on initial swirl intensity value of 0.21 seen from the finest fit amid the data and correlation by Kim *et al.* (2014). Correction is due to the different pressure contours or pressure regions as we move downstream of the bend also shown by Jayanti (2011). This showed that in the future tests, pressure drop should be measured at least 50 pipe diameters or more from the

bend and based on pressure gradient analysis with 90° bends, least downstream recovery length was found to be 150 times by Azzi and Friedel (2005).

### **3.3. Theoretical Approach to the Development of the Empirical Equation**

In the development of the Empirical Equation, measurement of the pressure drop due to successive pipe bending was done at  $R_c$  values 13.545, 27.679 and 79.578 for the 90° bend to gain an understanding of the parameters leading to the friction coefficients and validation with the experimental work. These are larger than the already published Short, Standard and Long radii. The experimental data obtained was then mathematically associated with the published data for a chosen theoretical 19.05 mm diameter pipe friction coefficient for convention and basis of the Empirical Equation for a Standard radius. The theoretical 19.05 mm pipe diameter, Standard radius was used due to the availability of data for comparison from the published and the experimental friction coefficients.

Observations of the behaviour of the individual bend parameters during each test (instantaneous parameters) were noted for association with the change of the resulting friction coefficients. The corresponding experimental data was fitted to establish the various relationships between the different bend parameters over the successive formation of the different bends (0° to 90°). In analysing of fluid problems, the simplest and most desirable method at times is a direct mathematical solution (Farhat and Lesoinne, 2000).

A mathematical relationship which established the relationship between the different bend parameters was finally determined to give the expanded or disaggregated resistance or friction coefficient  $k$ , due to the constant and immeasurable quantities (e.g., instantaneous roughness, dynamic viscosity, and kinematic viscosity) included. The actual pressure drop was then found by including the  $\frac{v^2}{2g}$  term lastly. This in essence was finally the derived Empirical Equation for a chosen theoretical 19.05 mm diameter pipe friction coefficient.

#### **3.3.1. Dimensional Homogeneity and Dimensional Analysis**

Having understood that the pressure drop in all cases can best be expressed as  $\left(k \frac{v^2}{2g}\right)$  only with the correct make-up of the parameters to give the correct friction coefficient,  $k$  value (ARC, 2003), it is essential that dimensional homogeneity is considered (Fenner *et al.*, 2018). Dimensional homogeneity and dimensional analysis needs to be considered for the consistency of both sides of the Empirical Equation. Dimensional homogeneity requires that an equation with quantities on both sides of the equal sign have the same units and this means a dimensionless  $k$  value (Fenner *et al.*, 2018). The dimensional analysis of an equation has the main advantage of reducing the number of variables in the problem as it combines dimensional variables to form non-dimensional parameters.

### 3.3.2. Derivation of the Empirical Equation

In all cases in the formation of a bend, there is always a change in the measured bend parameters such that the change is always a function,  $f(\theta, D, L, R_e, r, v_d, \rho, \varepsilon, \lambda_d, \mu_d)$ , which influences the value of the coefficient to give the correct pressure drop. Wherein;  $\theta$  - bend angle;  $D$  - pipe diameter;  $L$  - bend length;  $R_e$  - reynolds number;  $r$  - raduis of curvature;  $\rho$  - density;  $v_d$  - flow velocity with respective pipe diameter;  $\varepsilon$  – pipe roughness;  $\mu_d$  - dynamic viscosity and;  $\lambda_d$  - kinematic viscosity.

Looking at the behaviour of the bend from the experimental findings by Ito (1960), Chisholm (1983), Fitzsimmons (1964), Sekoda (1969), Pigott (1950), Keulegan and Beij (1937) as cited by Spedding *et al.* (2004), we can express the pressure loss due to the bend,  $\Delta P$  (ARC, 2003) as;

$$\Delta P = k \frac{v^2}{2g} \quad (3.1)$$

Wherein  $k = f(\theta, D, L, R_e, r, v_d, \rho, \varepsilon, \lambda_d, \mu_d)$

Considering the related parameters  $R_e, v_d$  which speak to the flow in general, it would suffice to have the velocity head numerator term,  $v^2$ , only to account for flow in the overall equation (ARC, 2003) (Spedding *et al.*, 2004);

then

$$\Delta P = f(\theta, D, L, r, \rho, \varepsilon, \lambda_d, \mu_d) \frac{v^2}{2g} \quad (3.2)$$

Looking at each parameter individually with the exclusion of the relatively constant parameters, ( $\rho, \varepsilon, \lambda_d, \mu_d$  which have insignificant influence on the coefficient considering smooth PVC pipe under investigation with water for irrigation design purposes), in the formation of the  $k$  value for the conditions desired (The Engineering tool box.com, 2018);

then

$$\Delta P = f(\theta, D, L, r) \frac{v^2}{2g} \quad (3.3)$$

A mathematical expression which gives us  $f(\theta, D, L, r)$  can best estimate the friction coefficient,  $k$  value given that  $\theta, D, L, r$  are known during each design stage of an irrigation system design. This would give the precise and accurate pressure drop friction coefficient, or rather the closest estimate of the  $k$  value. Derivation of the Empirical formula took three key steps governed by the relationships found with the main parameters  $\theta, D, L$  and  $r$  with respect to the extent of bending. When broken down, this is mainly due to the bend angle  $\theta$ ,  $L/D$  ratio and  $R_c$ . Focus will be on the behaviour of the  $90^\circ$  bend since a similar effect was seen in the experimental findings across the lower bend angles only at lower magnitudes and translation was also done through the change in the bend angle  $\theta$ .

Since the value of  $\Delta P$  is based on the pragmatic or real values from experimental data, it can be agreed that  $\Delta P$  considers the actual extent of losses (head loss) due to the bend to include the constant and immeasurable parameters.  $\Delta P$  is made up of the contribution of the complicated issues due to the dynamic pressures differentials within the bend resulting in the energy losses due to change in direction, Dean vortices or vortex formation (Azzi and Friedel, 2005). These result in the generation of the secondary effects with swirl intensity generation as seen by Kim *et al.* (2014), looked at in the next chapter.

In theory  $\Delta P$ , considers the pressure loss or the minor losses due to a pipe bend with an inlet and outlet of infinity length on analysis (Dutta *et al.*, 2016).  $\Delta P$  considers the 30 to 50 pipe-diameters in length of an equivalent straight pipe length for actual pressure drop as identified

by Spedding *et al.* (2004). Also, based on pressure gradient analysis with 90° bends, it caters for the least downstream recovery length found to be 150 times pipe diameter of the bend (Azzi and Friedel, 2005). Lastly, the magnitude of  $\Delta P$  also includes the concept of decay as given by the initial swirl intensity value of 0.21 which was seen from the finest fit amid the data and correlation by Kim *et al.* (2014).

### **3.4. Results and Discussion**

The behaviour of the relative radius of curvature with bending, pressure drop for fixed relative radius of curvature with successive bending, friction coefficients derived from the measured pressure drop, mathematical relation of pressure drop with change in bend angle, friction coefficient with changing pipe diameter and bend angle, friction coefficient with changing  $R_c$  and bend angle, composition of the Empirical Equation and the validation of the Empirical Equation is presented and discussed the following subsections.

#### **3.4.1. Behaviour of the Relative Radius of Curvature with Bending**

For all the pipe diameters tested, the transition of the bend angle parameters as bending was introduced from 0° to 90°, brought about considerable changes in bend angle ( $\theta$ ) and radius of curvature ( $r$ ) for the fixed bend length ( $L$ ) and pipe diameter ( $D$ ). This brought about the key relationships identified between the different measured parameters  $\theta, D, L, r$ , essential for the development of the Empirical Equation. The relationship of bend angle with the relative radius of curvature,  $R_c$  ( $R_c = \text{radius of curvature, } r / \text{pipe diameter for bend, } D$ , which is unit less) for the fixed bend length for all the pipes tested is expressed graphically in Figure 3.2.

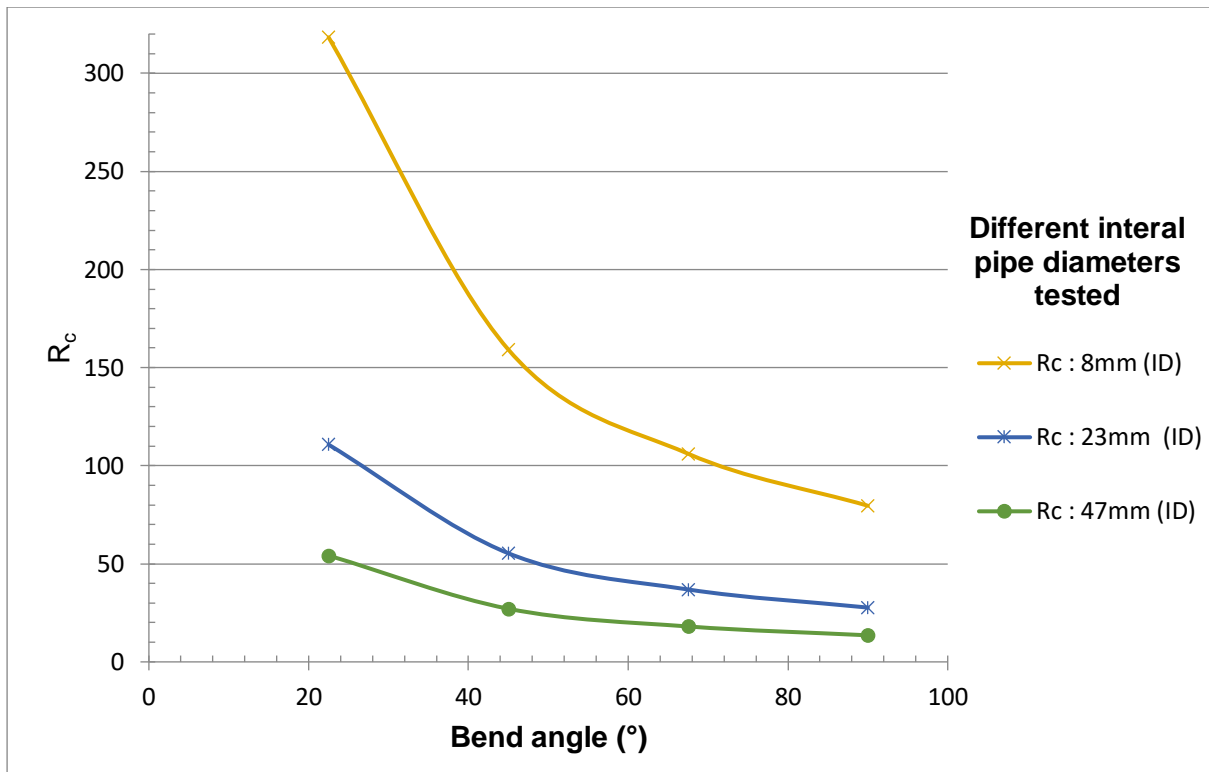


**Figure 3.2 Relationship between radius of curvature ( $R_c$ ) and bend angle for the 8 mm (ID), 23 mm (ID) and 47 mm (ID) diameter pipes**

Generally, it can be seen from each pipe tested that  $R_c$  can be increased due to the decrease in the bend angle and the decrease in the pipe diameter. This is because as we approach the straight pipe condition with reduction in bend angle, the radius of the bending approaches infinity as the pipe diameter remains constant. This agrees with the work by Zhan *et al.* (2006). Fundamentally, despite the different pipe diameters used in the tests, the change appeared the same, that is a similar response is seen for the change in  $R_c$  for each pipe tested, except on visual analysis there is seen to be a multiplier or scaling-up to combine or overlay the three pipe diameters tested which was also found out by Beck (1960). This relationship was used in expressing the measured results and is further expressed mathematically to combine the individual bend angles to the pipe diameters tested on the last steps of the development of the Empirical Equation.

### 3.4.2. Pressure Drop for Fixed Relative Radius of Curvature with Successive Bending

On conducting the tests on the pressure drop due to the successive pipe bending with the varied flows, the general trend seen was that the pressure drop increased with the increase in

the bend angle and expressed for fixed  $R_c$ . These results are tabulated in Appendix A and graphically shown in Figures 3.3, 3.4 and 3.5 for the varied flows velocities tested.

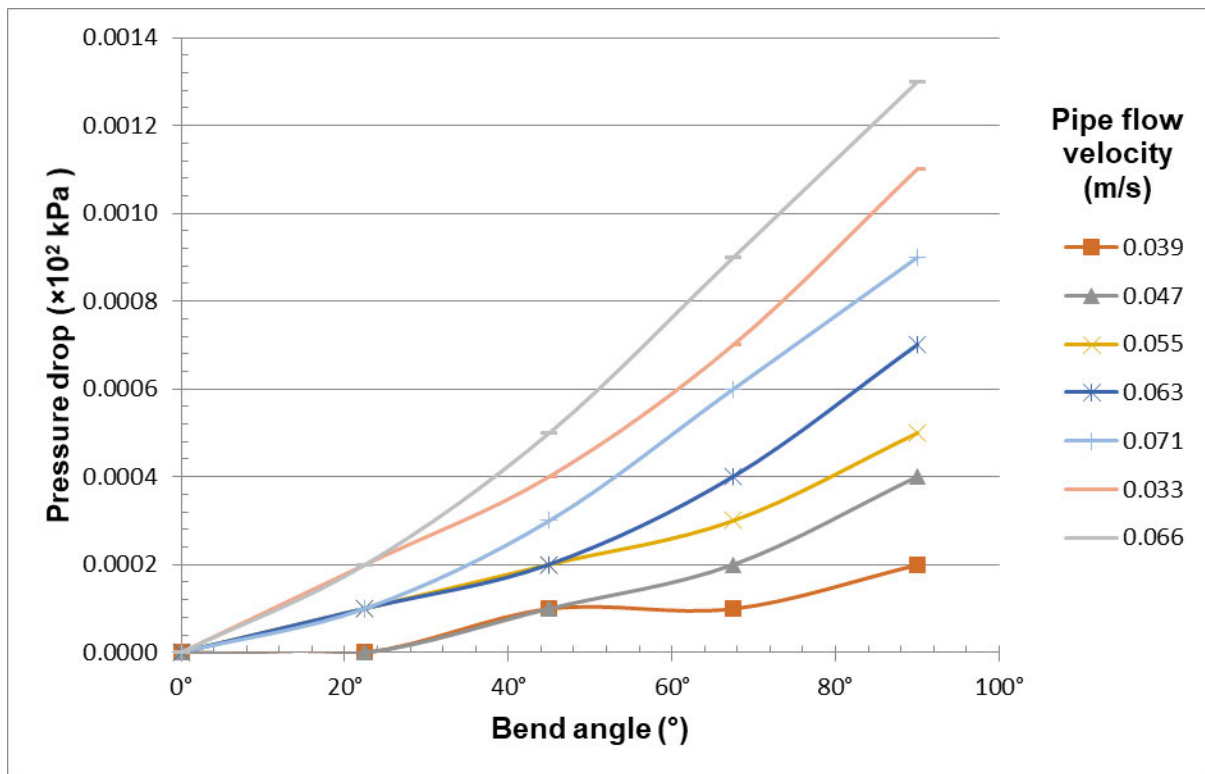


**Figure 3.3 Pressure drop as function of the bend angle for varied single phase flow for the 47 mm diameter pipe for  $R_c = 13.545$**

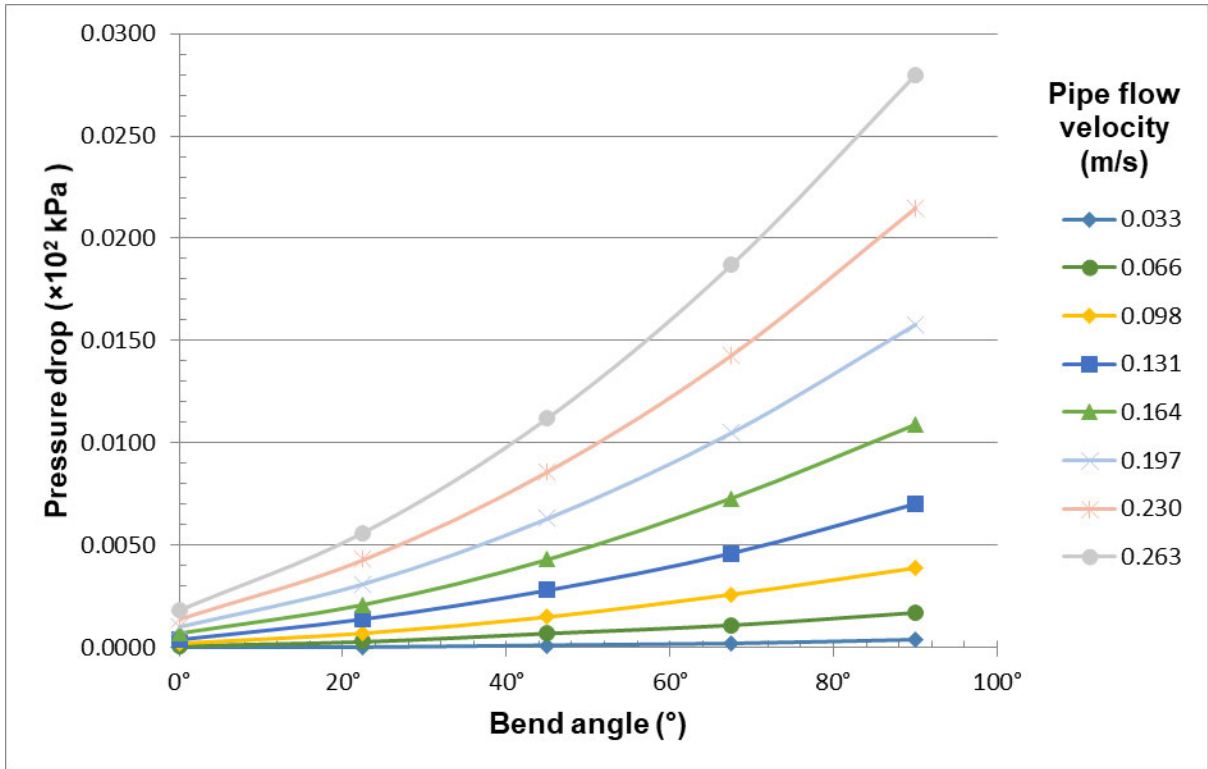


Figure 3.4 Pressure drop as function of the bend angle for varied single phase flow for the 23 mm diameter pipe for  $R_e = 27.679$

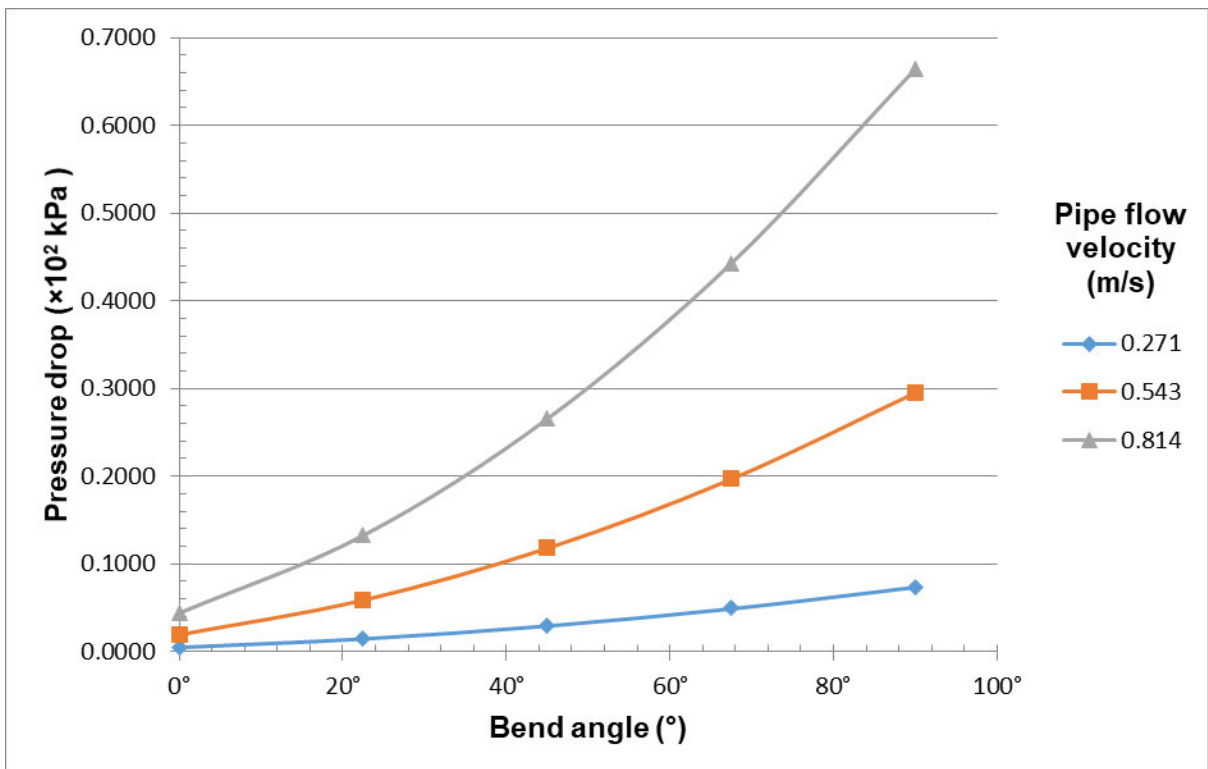


Figure 3.5 Pressure drop as function of the bend angle for varied single phase flow for the 8 mm diameter pipe for  $R_e = 79.578$

Generally, as the flow velocity increased with mass flux of the flowing fluid, the consequent pressure loss increased even as bend angle increased (Figures 3.3, 3.4 and 3.5). From the different pipe diameters tested, a general trend is seen on the influence of the bend angle on the pressure drop.

As the pipe diameter increased, the overall pressure drop decreased and lower pressure readings were seen in the larger (47 mm) pipe due to a larger flow cross sectional area compared to all other pipes tested (see Figure 3.3). Increasing the pipe diameter effectively reduced the flow velocity of the fluid elements resulting in fewer collisions as seen by Sommerfeld and Lain (2015). The smaller pipe diameter (8 mm) expressed fairly large pressure drop readings compared to all the others tested (see Figure 3.5). Higher flows velocities were also seen with the smaller pipe due to the much reduced pipe diameter in relation to the 100 mm diameter main supply line wherein the flow-meter was connected for all tests.

### **3.4.3. Friction Coefficients from the Measured Pressure Drop**

The pressure drop measured was found to give an indication of the actual head loss due to the extent of bending involved in each test. To get a better understanding of the pressure drop recorded, it was necessary again to convert the values to a friction coefficient as expressed by other authors: Ito (1960), Chisholm (1983), Fitzsimmons (1964), Sekoda (1969), Pigott (1950), Keulegan and Beij (1937) as published by Spedding *et al.* (2004) and also adopted in the Irrigation Design Manual by ARC (2003) for comparison. The friction coefficients as a result of the pressure drop measured for the pipes tested are shown in Table 3.2. The friction coefficient is seen to be fairly constant in each case especially with the 50 mm and the 25 mm pipe despite the case of the lower flows ignored.

**Table 3.2 Friction coefficients,  $k$  due to pressure drop against the bend angle for the varied single-phase flows tested with figures in bold used to obtain the average values for closer approximation of the friction coefficients**

Bend angle	0°	22.5°	45°	67.5°	90°	0°	22.5°	45°	67.5°	90°	0°	22.5°	45°	67.5°	90°
Velocity (ms <sup>-1</sup> )	Diameter 0.047 m					Diameter 0.023 m					Diameter 0.008 m				
0.033	Too low flow relative to the pipe size, pipe not full					0.0000	0.0000	0.3465	0.6931	1.3861	Flow below tested range				
0.039	0.0000	0.0000	0.2424	0.2424	0.4834										
0.047	0.0000	0.0000	0.1674	0.3348	<b>0.6714</b>										
0.055	0.0000	0.1231	0.2462	0.3692	<b>0.6166</b>										
0.063	0.0000	0.0943	0.1886	0.3772	<b>0.6609</b>										
0.066						0.0866	0.2599	0.6064	0.9529	1.4727					
0.071	0.0000	0.0745	0.2236	0.4472	<b>0.6714</b>										
0.079	0.0000	0.1208	0.2416	0.4228	<b>0.6647</b>										
0.086	0.0000	0.0999	0.2496	0.4494	<b>0.6492</b>										
0.098	Too high flow, relative to the pipe size					0.0770	0.2695	0.5775	1.0011	<b>1.5016</b>					
0.131						0.0866	0.3032	0.6064	0.9963	<b>1.5161</b>					
0.164						0.0970	0.2911	0.5960	1.0119	<b>1.5109</b>					
0.197						0.0963	0.2984	0.6064	1.0107	<b>1.5209</b>					
0.230						0.0990	0.3041	0.6082	1.0113	<b>1.5205</b>					
0.263						0.0975	0.3032	0.6064	1.0125	<b>1.5161</b>					
0.271						Too high flow, relative to the pipe size					0.2536	0.7507	1.5013	2.4955	<b>3.7432</b>
0.543											0.2498	0.7494	1.4975	2.4955	<b>3.7419</b>
0.814	0.2497	0.7484	1.4968	2.4949	<b>3.7421</b>										
<b>Average <math>k</math></b>	0.0000	0.0854	0.2195	0.4001	<b>0.6557</b>	0.0545	0.1765	0.5102	0.8824	<b>1.5143</b>	0.2510	0.7495	1.4986	2.4953	<b>3.7424</b>

From experimental results, clearly the friction coefficient is relatively constant for the extent of bending involved as for the 90° bends in all cases in bold (see Table 3.2). This is also seen across with the lower bend angles, respectively, and averages thereof at the bottom (see Table 3.2). The constant nature of the friction coefficients for the head losses is also confirmed by the published results on the 90° bends by Spedding *et al.* (2004). The friction coefficients due to the lower levels of bending (bend angle) exhibited a successive decrease which is also later expanded on and shown to have a mathematical relation for all.

#### 3.4.4. Mathematical Relation of Pressure Drop with change in Bend Angle

On analysis of the changing friction coefficients with the respective bend angles tested (0° to 22.5° to 45° to 67.5° and finally to 90°) from all the experimental results, a relationship was found to exist for the pressure drop. Generally, the experimental friction coefficient for each test done for the transitional bending 0° to 90° was found to be related to the other flows for the different pipe diameters tested by simply a multiplier to a fitted mathematical relationship for a Linear Model Poly2 as given in Equation 3.4 using the MATLAB R2014a curve fitting tool for a function  $p(\theta)$ :

$$p(\theta) = p1 * \theta^2 + p2 * \theta + p3 \quad (3.4)$$

Wherein  $\theta$  = bend angle, with coefficients (with 95% confidence bounds):

$$p1 = 4.869e^{-05}, p2 = 0.003287 \text{ and } p3 = 0.0493$$

Then

$$p(\theta) = 4.869e^{-05}\theta^2 + 0.003287\theta + 0.0493 \quad (3.5)$$

*Goodness of fit: SSE: 1.676e<sup>-31</sup>; Adjusted R-square: 1; RMSE: 2.895e<sup>-16</sup>*

$p(\theta)$  is a result of the gradual decrease in pressure drop as we move from the 90° bend to the straight pipe condition (0°). This equation was used to define the spread of the friction coefficient with the changing bend angle for the developed Empirical Equation.

From Equation 3.3,  $\Delta P = f(\theta, D, L, r) \frac{v^2}{2g}$ , the first component of the friction coefficient (bend angle,  $\theta$ ) is considered found in Equations 3.4 and 3.5. All that remains is the change due to the  $D, L$  and  $r$ , the two elements left in development of the Empirical Equation as will be shown. With Equation 3.5 the relation established, focus was then given to the behaviour of the 90° bend for the rest of the analysis and development of the Empirical Equation with the understanding that the same effect, but different magnitude will be spread to the lower angles of bending in a similar fashion.

It is understood that the key relationship to all bends is the bend length to pipe diameter ratio ( $L/D$ ) as cited by Spedding *et al.* (2004) and used by Poirier and Geiger (2016). This meant that understanding the influence of diameter coupled with  $L/D$  ratio would give the second component of the friction coefficient. Lastly, the third component could be established due to the behaviour of the  $R_c$  which entails  $r$  since  $R_c =$  radius of curvature,  $r$  per pipe diameter,  $D$ . The two last components were then combined with the first,  $p(\theta)$ , completing the friction coefficient. Multiplication was used in almost all instances to combine the different relations observed. This was mainly due to the horizontal and vertical translation (scaling) seen on the friction coefficient with the changing bend parameters to combine or overlay the effect of changing bend parameters.

It was clear that a good understanding of the behaviour or change in each bend parameter could help understand the phenomenon of pressure drop to the bend and thence the resistance or friction coefficient for the different bend parameters as shown in the make of the Empirical Equation.

#### **3.4.5. Friction Coefficient with changing Pipe Diameter and Bend Angle**

Again, for the fixed  $R_c$ , consideration of the 90° bend behaviour was done for analysis of the three pipes diameters tested. This is because the same behaviour occurred but of a lesser magnitude with the decrease in the bend angle and this is catered for in the first relation established Equation (3.5). The fixed  $R_c$  with bend angle behaviour was plotted for the changing friction coefficient (average friction coefficients used) for each pipe diameter tested

as shown in Figure 3.6. On analysis, this behaviour was also linked (mathematically) to each other and the published friction coefficients by the  $L/D$  ratio and the  $R_c$  lastly shown.

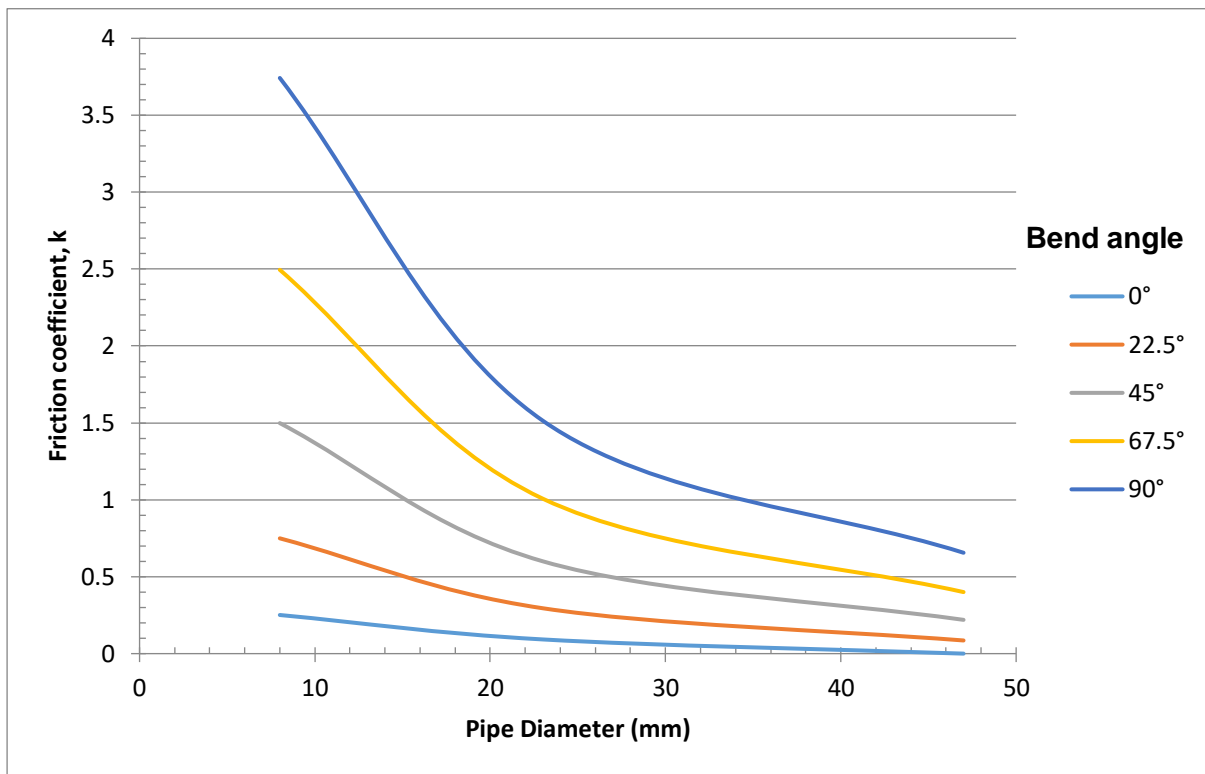


**Figure 3.6 Relationship between friction coefficient and pipe diameter for 0° to 90° bend**

In general, as the pipe diameter increases the friction coefficient decreased, this again is the case for the lower levels of bending plotted in Figure 3.6 for the smaller angles. This is because as we increase the pipe diameter until infinity, we approach the straight pipe conditions. Clearly from the graph considering the transition of the friction coefficient with the change in bend angle, mathematically the  $k$  is asymptotic (approaches a constant) with increase in the pipe diameter. However, on further visual analysis, the three sets of coefficients used from the results have different pipe diameters with different  $R_c$  values gave just three points for analysis. This created a gap in the understanding of the influence of the last two components with fixed pipe diameter and interchangeably the  $R_c$  on the 90° bend for analysis.

Despite this gap, the behaviour of the friction coefficient with fixed pipe diameter was obtained from the published results from literature though with smaller bend length shown in Appendix B and shown graphically in Figure 3.7 for the Standard and Long radius bends.

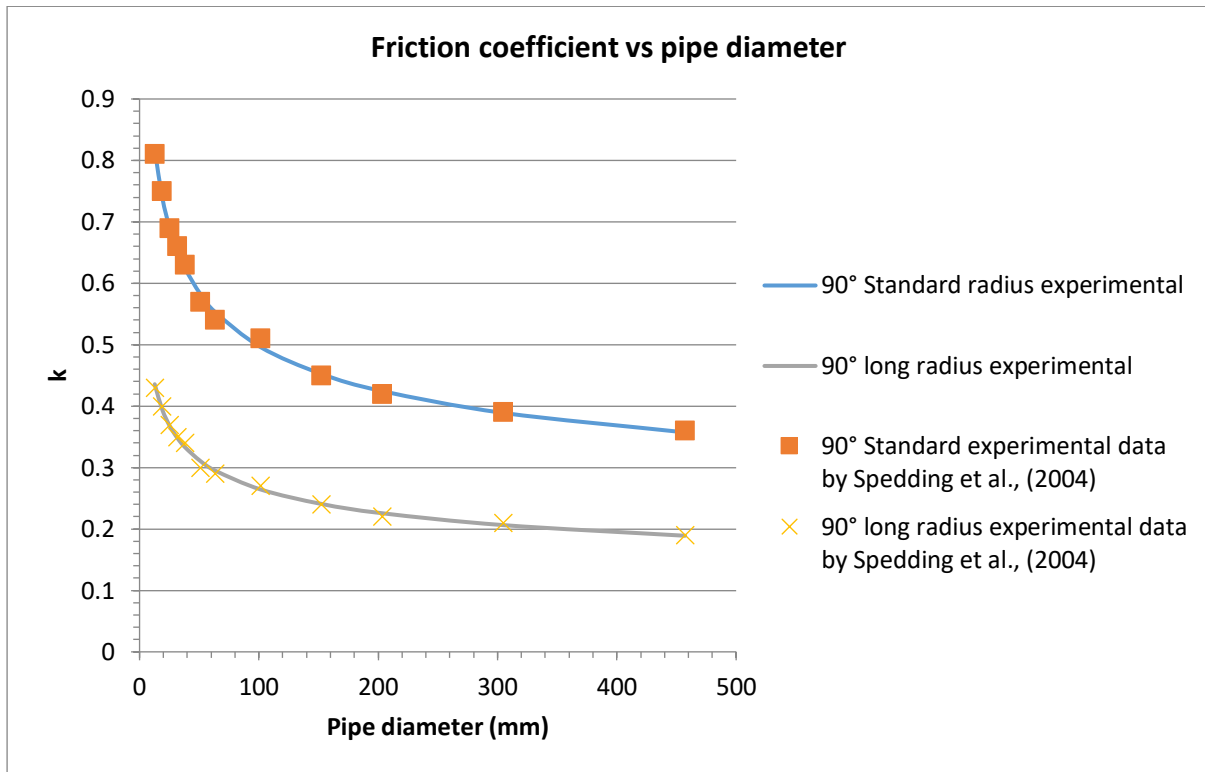


**Figure 3.7 Friction coefficient,  $k$ , with change in pipe diameter for fixed  $R_c$  at 90° bend (Spedding *et al.*, 2004).**

As seen graphically the fitted relationship for the different pipe diameters with a fixed  $R_c$ , a friction coefficient relationship is found for the effect of change in pipe diameter only with more data points. The two 90° bends, Standard and Long radius bend (two different  $R_c$ ) are seen to be related with a multiplier or scaling. The difference in the two (Figure 3.6 and 3.7) also show the influence on the increase in the bend length. As bend length increases the curve flattens. This is because we approach the straight pipe condition with increase in bend length.

The fitted relationship for the 90° bends with each fixed  $R_c$  (Figure 3.7), were then used for the development of the Empirical Equation, again defining the best or closest reference for its basis on the Standard radius bend. Using MATLAB R2014a curve fitting tool, this fitted pipe diameter and friction coefficient relation was then expressed for the theoretical Standard radius bend as a function  $g(D)$  for a General Model Power2 equation:

$$g(D) = a * D^b + c \quad (3.6)$$

Wherein  $D$  = respective pipe diameter with coefficients (with 95% confidence bounds):

$a = 1.487, b = -0.2862, c = 0.09968$ .

$$g(D) = 1.487D^{-0.2862} + 0.09968 \quad (3.7)$$

*Goodness of fit: SSE: 0.0008363; Adjusted R-square: 0.9956; RMSE: 0.009639*

$g(D)$  defines the departure of the friction coefficient from the standard to the desired pipe diameter. The Empirical Equation was then formulated from a convention from the change in the theoretical friction coefficient (0.7394), emanating firstly from a friction coefficient of the theoretical 19.05 mm Standard radius, with  $R_c = 1$  which was comparable to the experimental tests done as cited by ARC (2003) and Spedding *et al.* (2004).

The choice of convention could equally work with using any known friction coefficient and chosen pipe diameter available for comparison. Though the outside diameter was considered in the published friction coefficients, the choice of using the internal diameter was used in deriving the Empirical Equation. This is due to the fact that the frictional influence is mainly due to the cross-sectional area or hydraulic diameter of the bend despite the pipe wall thickness. In other words when considering the ratio of the pipe diameter to wall thickness for most bends, the wall thickness is normally small for most pipes used in irrigation design.

#### **3.4.6. Friction Coefficient with changing $R_c$ and Bend Angle**

With the above understanding (the translation of the friction coefficient,  $k$ , with change in pipe diameter for fixed  $R_c$ , Figure 3.7), this meant that to get to any unknown friction coefficient including the experimental friction coefficient, translation of the friction coefficient through the behaviour of  $R_c$  was only need which also entails the influence of changing bend length. The behaviour of the friction coefficient with fixed  $R_c$  was obtained also from the several published results, from literature, as shown in Figure 3.8 and was aligned with the experimental data.

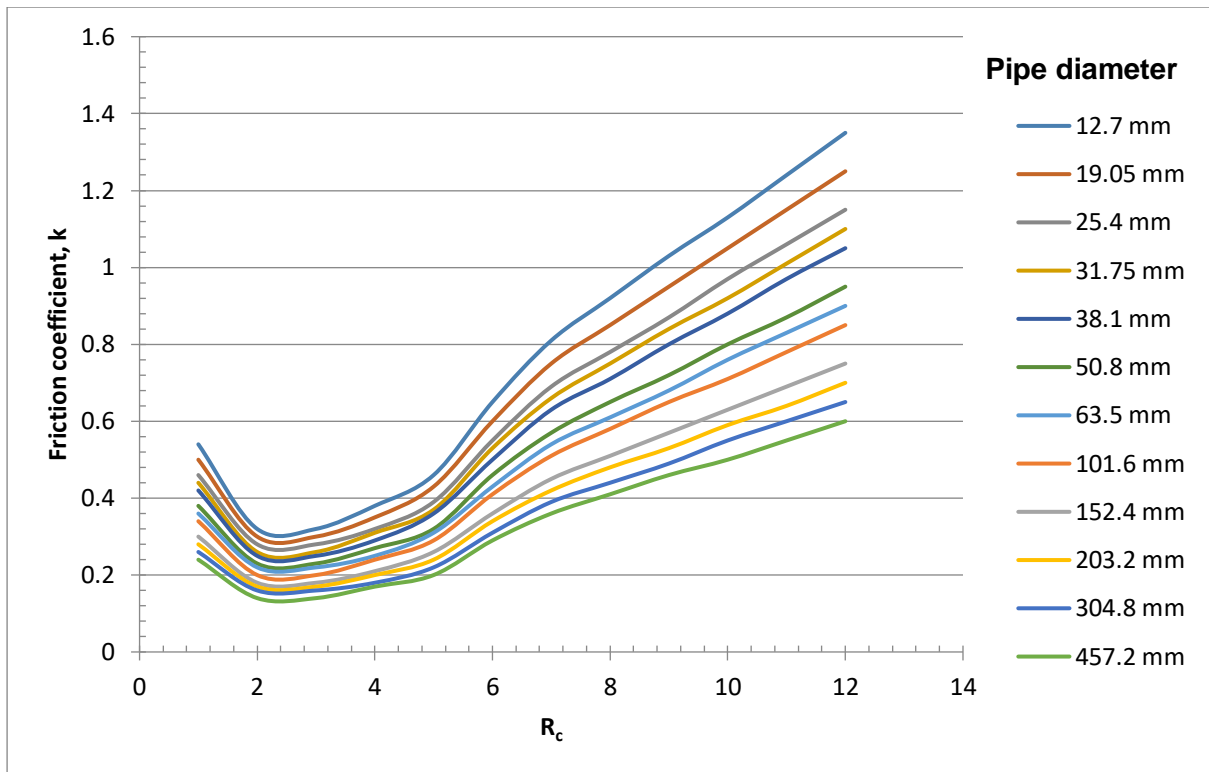


**Figure 3.8 Friction coefficient with change in  $R_c$  for fixed pipe diameters for the  $90^\circ$  bend (Data from Spedding *et al.* (2004) and Neutrium (2016)).**

Initially the friction coefficient decreases only to increase as  $R_c$  increases. This is because a friction coefficient exists for both the straight pipe conditions and the scenario of any bend, giving the two extremes of the friction coefficient (on the left or lower values of  $R_c$  and the right or larger values of  $R_c$  graphically) and eventually intercept giving the depression seen in Figure 3.8.

The relationship of the friction coefficient with  $R_c$  is seen to be similar for all pipe diameters as seen graphically (see Figure 3.8). Clearly a multiplier is seen to relate all the different friction coefficients for the changing pipe diameter with fixed  $R_c$ . From the analyses of the experimental data patterns and those of the published data (see Figure 3.8), a fitted relationship was then derived which best explained the translation of the friction coefficient with reference to the chosen theoretical Standard Radius 19.05 mm bend (convention adopted). This was best expressed by a General Model Rational Function (Equation 3.9) with respect to the theoretical Standard Radius 19.05mm  $90^\circ$  bend with a function  $h(R_c)$ :

$$h(R_c) = \frac{(p4*R_c^2 + p5*R_c + p6)}{(R_c^2 + q1*R_c + q2)} \quad (3.8)$$

Wherein  $R_c$  is based on the derived theoretical Standard Radius 19.05 mm pipe aligned to the experimental data and used as the convention or point of translation or base for determining friction coefficient and is  $> 0$  always (with 95% confidence bounds):  $p4 = 4.02$ ,  $p5 = -11.07$ ,  $p6 = 29.93$ ,  $q1 = 18.53$ ,  $q2 = 11.41$ .

Then

$$h(R_c) = \frac{(4.02R_c^2 - 11.07R_c + 29.93)}{(R_c^2 + 18.53R_c + 11.41)} \quad (3.9)$$

*Goodness of fit: SSE:  $2.184e^{-13}$ ; Adjusted R-square: 1; RMSE:  $2.165e^{-08}$*

Due to the nature of the rational function derived from the MATLAB R2014a curve fitting tool, it can safely be agreed that the friction coefficient approaches a constant with the inclusion of the experimental data in the fitting (see Table 3.3), confirming the hypothesis, friction coefficient approaches saturation or a constant as the  $R_c$  increases. Generally, the fitted friction coefficients from the measured (average friction coefficients) three experimental results and the published friction coefficients (Short, Standard and Long radius bends) were used for the validation of the derived Empirical Equation (see Table 3.4 and 3.5).

### **3.4.7. Composition of the Empirical Equation**

On analysis and amalgamation of the various relations found in the experimental data and the published data from literature, the main components to the mathematical build-up of the Empirical Equation were best be described as three main components stated earlier. These were made up of the main components from  $\theta$ ; and  $D, L$  and  $r$  ( $R_c$  and the  $L/D$  ratio) derived from the relationships observed. The Empirical Equation for the determination of the theoretical dynamic frictional loss coefficient  $k$ , that is from  $0^\circ$  to  $90^\circ$ , was then expressed as a single equation with these components:

1.  $\frac{p(\theta)_{wrt \theta}}{p(\theta)_{wrt 90^\circ}}$  – which gives the spread of the friction coefficients over the extent of bending  $0^\circ$  to  $90^\circ$  as mathematically determined.
2.  $\frac{g(D)_{new \text{ pipe diameter}}}{g(D)_{wrt 19.05mm, R_c=1, 90^\circ}}$  – which institutes the multiplier required for the translating of the theoretical friction coefficient of the 19.05 mm diameter pipe (convention or adopted) to that of the new pipe diameter chosen during the design process, and lastly
3.  $h(R_c)_{wrt R_c=new, 90^\circ} * g(D)_{wrt 19.05mm, R_c=1, 90^\circ}$  – which gives the theoretical friction coefficient for the chosen diameter that is the resulting or new  $R_c$  for a  $90^\circ$  bend founded on the Standard theoretical 19.05 mm diameter pipe friction coefficient.

The combined mathematical relationship for the homogenous equation for the association of the measured parameters gave the theoretical friction coefficient,  $k$  of the pressure drop due to each bend parameter. The Empirical Equation is finally shown with the inclusion of the velocity head component (finally the minor or secondary loss required during the design process) and expressed as Equation 3.12.

$$\Delta P = k * \frac{V^2}{2g} \quad (3.10)$$

Wherein

$$k = f(\theta, D, L, r)$$

Then

$$k = \frac{g(D)_{new \text{ pipe diameter}}}{g(D)_{wrt 19.05mm, R_c=1, 90^\circ}} * h(R_c)_{wrt R_c=new, 90^\circ} * g(D)_{wrt 19.05mm, R_c=1, 90^\circ} * \frac{p(\theta)_{wrt \theta}}{p(\theta)_{wrt 90^\circ}} \quad (3.11)$$

And finally

$$\Delta P = \left( \frac{g(D)_{new \text{ pipe diameter}}}{g(D)_{wrt 19.05mm, R_c=1, 90^\circ}} * h(R_c)_{wrt R_c=new, 90^\circ} * g(D)_{wrt 19.05mm, R_c=1, 90^\circ} * \frac{p(\theta)_{wrt \theta}}{p(\theta)_{wrt 90^\circ}} \right) \frac{V^2}{2g} \quad (3.12)$$

With condition

$$g(D)_{wrt 19.05mm, R_c=1, 90^\circ} = 1 \text{ and } \frac{g(D)_{new \text{ pipe diameter}}}{g(D)_{wrt 19.05mm, R_c=1, 90^\circ}} \text{ remains applicable only when } D = 19.05 \text{ mm and } R_c \text{ remains 1}$$

Development of the Empirical Equation, named the Dayton Equation, enabled the determination of the theoretical friction coefficient,  $k$  value of any bend ( $0^\circ$  to  $90^\circ$ ) with respect to  $\theta, D, L$  and  $r$  for use in the design of irrigation systems as anticipated by Equation 3.3. This gave a close approximation of the frictional loss due to bending in the comparisons done hereafter (Table 3.4 and 3.5). As postulated, saturation was seen as  $R_c$  increased beyond all experimental values.

### 3.4.8. Validation of the Empirical Equation

The theoretical friction coefficients ( $k$  values) relationship derived from the experimental data and published (friction coefficients) on development (fitting coefficients) and validation of the developed Empirical Equation are expressed and tabulated in Table 3.3. Comparison of the specific friction coefficients (experimental and published) is further shown in Table 3.4 and Table 3.5.

**Table 3.3 Theoretical friction coefficients  $k$ , from the developed Empirical Equation (In bold are the published values available from Spedding *et al.* (2004) and those adopted in the Irrigation Design Manual by ARC (2003) and experimental values available from experimental data for comparison and linkage)**

$R_c$ D	0.5	1	1.5	2.6409 (minima)	13.545	27.679	79.578	Scaling
8	1.1165	0.9198	0.4964	0.3926	1.2740	1.9983	<b>2.8948</b>	<b>1.2439</b>
<b>19.05</b>	<b>0.8976</b>	<b>0.7395</b>	<b>0.3990</b>	0.3156	1.0242	1.6065	2.3273	<b>1.0000</b>
<b>23</b>	0.8569	0.7059	0.3809	0.3013	0.9777	<b>1.5335</b>	2.2216	<b>0.9546</b>
<b>47</b>	0.7208	0.5938	0.3204	0.2534	<b>0.8224</b>	1.2899	1.8687	<b>0.8029</b>

From the theoretical friction coefficients above and the analysis done, multipliers exist due to changes in the pipe bends as seen on analysis, which involves a horizontal translation of  $k$  with changing  $R_c$  and vertical translation with changing diameter. Initially the  $R_c$  is seen to decrease but it then increases until constant or saturation creeps in with large  $R_c$  values, a concept cited by Blanckaert (2009).

The levels of accuracy of these theoretical friction coefficients determined by the Empirical Equation are much better understood when shown with the comparison of the  $k$  values found in the published and experimental data as tabulated in Table 3.4 and Table 3.5 for validation of the Empirical Equation from the fitting and derivation.

**Table 3.4 Comparison of friction coefficients,  $k$ , produced by the Empirical Equation with the published friction coefficients**

	$R_c = 0.5$					$R_c = 1$					$R_c = 1.5$				
	0°	22.5°	45°	67.5°	90°	0°	22.5°	45°	67.5°	90°	0°	22.5°	45°	67.5°	90°
<b>Adopted by ARC (2003)</b>	-	-	-	-	0.90	-	0.15	0.30	-	0.75	-	-	-	-	0.40
<b>Spedding <i>et al.</i> (2004) for the 19.05mm pipe</b>	-	-	-	-	-	-	-	0.40	-	0.75	-	-	-	-	0.40
<b>(Neutrium, 2016)</b>	-	-	-	-	0.90	-	-	0.35	-	0.75	-	-	0.20	-	0.45
<b>Theoretical coefficients for 19.05mm pipe</b>	0.060	0.180	0.359	0.598	0.898	0.049	0.148	0.296	0.493	0.739	0.027	0.080	0.160	0.266	0.399

**Table 3.5 Comparison of friction coefficients produced by the Empirical Equation with the experimental data friction coefficients**

	<b>Diameter 0.047 m, <math>R_c = 13.545</math></b>					<b>Diameter 0.023 m, <math>R_c = 27.679</math></b>					<b>Diameter 0.008 m, <math>R_c = 79.578</math></b>				
	0°	22.5°	45°	67.5°	90°	0°	22.5°	45°	67.5°	90°	0°	22.5°	45°	67.5°	90°
<b>Experimental coefficients</b>	0.00	0.09	0.22	0.40	0.66	0.09	0.29	0.60	1.01	1.51	0.25	0.75	1.50	2.50	3.74
<b>Theoretical coefficients for 19.05mm pipe</b>	0.05	0.16	0.33	0.55	0.82	0.10	0.31	0.61	1.02	1.53	0.19	0.58	1.16	1.93	2.89
<b>Difference (%)</b>	-100	- 48.06	- 33.27	- 27.02	- 20.26	-9.77	-3.84	-2.15	-1.46	-1.24	30.09	29.46	29.43	29.31	29.29

From the comparisons in the two tables (Table 3.4 and 3.5), the derived Empirical Equation has a fairly good estimate of the friction coefficient,  $k$  value with the changing bend parameters. Accuracy is seen to be more with the published data due to the multiple testing by many authors. This shows that more testing can be done on the experimental data for the fixed  $R_c$  and pipe diameters chosen to reduce the level of error. However, it can be agreed

that the  $k$  values obtained by the Empirical Equation have a reduced level of error due to the fitting of all experimental data (published and tested) in its derived form, giving the closest approximation of pressure drop or head loss as desired for irrigation systems design.

On derivation of the formula, clearly the Short radius was found to be  $R = 0.5D$  that is  $R_c = 0.5$  with the confirmed theoretical  $k$  value of 0.898 which is approximately 0.9 as adopted in the Irrigation Design Manual by ARC (2003). No values were given by Spedding *et al.* (2004) with the accompanied confusion in the use of the Short radius when referring to the bend  $R = D$  that is  $R_c = 1$  which is a Standard radius bend. Generally, the derivation of the Empirical Equation also bridged the gap between the friction coefficients published with the absence of specific bend information and the approximation of coefficients that were not pragmatically found or tested (experimental and published).

### **3.5. Conclusions**

The flow about any bend follows a very similar flow pattern for all smooth circular pipes relative to the extent of bending or curvature. In all cases there exist multipliers relative to the bend curvature ratio ( $L/D$ ) and  $R_c$  with the change in pipe diameter for the associated bend angles, that is a multiplier due to each changing bend parameter. Due to this phenomenon observed in the flow about the bend, the frictional loss or pressure drop component (minor losses or secondary losses) can thus be easily calculated with the use of the correct multipliers with reference to a convention adopted or a reference theoretical friction coefficient as seen with the derived Empirical Equation.

Derivation of the Dayton Equation Empirical Equation, allowed for finding the correct friction coefficient with the use of the multipliers mathematically for specific bend parameters, coupled with the velocity head component which can readily be determined. The Empirical Equation bridged the gap between the uncertainties in the use of the various methods and friction coefficients often requiring a thorough knowledge of their development, eliminating error. It allowed for the easy, quick, accurate and precise determination of frictional losses due to bending dynamically from  $0^\circ$  to  $90^\circ$  for use in the design of irrigation systems (Standard bends and most importantly specialised bends and bends due to bending schedules). Of significant importance, it allowed this through the modification of the friction

coefficient with the respective changing bend parameters as postulated, catering for the changes in the bend parameters as seen in the design processes.

A new correlation can safely be said to have been developed in relation to the curvature multiplier and the momentum change due to bending. This is essential with the current and future introduction of low operating pressure emitters and the use of special bends in irrigation systems. The developed Empirical Equation can suitably be used in a MS Excel sheet or input into irrigation design software for better approximation of minor or secondary loss in the irrigation design process.

**APPENDIX A: EXPERIMENTAL DATA FOR PRESSURE DROP DUE TO SUCCESSIVE PIPE BENDING WITH FIXED  $R_c$**

Bend angle	0°	22.5°	45°	67.5°	90°	0°	22.5°	45°	67.5°	90°	0°	22.5°	45°	67.5°	90°					
Velocity (ms <sup>-1</sup> )	Diameter 0.047 m					Diameter 0.023 m					Diameter 0.008 m									
0.033	Too low flow relative to the pipe size, pipe not full					0.0000	0.0000	0.0001	0.0002	0.0004	Flow below tested range									
0.039	0.0000	0.0000	0.0001	0.0001	0.0002															
0.047	0.0000	0.0000	0.0001	0.0002	0.0004															
0.055	0.0000	0.0001	0.0002	0.0003	0.0005															
0.063	0.0000	0.0001	0.0002	0.0004	0.0007															
0.066						0.0001	0.0003	0.0007	0.0011	0.0017										
0.071	0.0000	0.0001	0.0003	0.0006	0.0009															
0.079	0.0000	0.0002	0.0004	0.0007	0.0011															
0.086	0.0000	0.0002	0.0005	0.0009	0.0013															
0.098	Too high flow, relative to the pump size					0.0002	0.0007	0.0015	0.0026	0.0039										
0.131						0.0004	0.0014	0.0028	0.0046	0.0070										
0.164						0.0007	0.0021	0.0043	0.0073	0.0109										
0.197						0.0010	0.0031	0.0063	0.0105	0.0158										
0.230						0.0014	0.0043	0.0086	0.0143	0.0215										
0.263						0.0018	0.0056	0.0112	0.0187	0.0280										
0.271																0.0050	0.0148	0.0296	0.0492	0.0738
0.543											0.0197	0.0591	0.1181	0.1968	0.2951					
0.814											0.0443	0.1328	0.2656	0.4427	0.6640					

**APPENDIX B: AVAILABLE PUBLISHED BEND LOSSES COEFFICIENTS FOR VARIOUS PIPE DIAMETRES TESTED**

Short Radius (R = 0.5D)					Standard Radius (R = 1D)					Long Radius (R = 1.5D)					Reference	mm	inch
0°	22.5°	45°	67.5°	90°	0°	22.5°	45°	67.5°	90°	0°	22.5°	45°	67.5°	90°			
-	-	-	-	0.90	-	0.15	0.30	-	0.75	-	-	-	-	0.40	(ARC, 2003)	Not given	Not given
-	-	-	-	-	-	-	0.43	-	0.81	-	-	-	-	0.43	(Spedding <i>et al.</i> , 2004)	12.70	0.50
-	-	-	-	-	-	-	0.40	-	0.75	-	-	-	-	0.40		19.05	0.75
-	-	-	-	-	-	-	0.37	-	0.69	-	-	-	-	0.37		25.40	1.00
-	-	-	-	-	-	-	0.35	-	0.66	-	-	-	-	0.35		31.75	1.25
-	-	-	-	-	-	-	0.34	-	0.63	-	-	-	-	0.34		38.10	1.50
-	-	-	-	-	-	-	0.30	-	0.57	-	-	-	-	0.30		50.80	2.00
-	-	-	-	-	-	-	0.29	-	0.54	-	-	-	-	0.29		63.50	2.50 to 3
-	-	-	-	-	-	-	0.27	-	0.51	-	-	-	-	0.27		101.60	4.00
-	-	-	-	-	-	-	0.24	-	0.45	-	-	-	-	0.24		152.40	6.00
-	-	-	-	-	-	-	0.22	-	0.42	-	-	-	-	0.22		203.20	8.0 to 10
-	-	-	-	-	-	-	0.21	-	0.39	-	-	-	-	0.21		304.80	12.0 to 16
-	-	-	-	-	-	-	0.19	-	0.36	-	-	-	-	0.19	457.20	18.0 to 24	
-	-	-	-	0.90	-	-	0.35	-	0.75	-	-	0.20	-	0.45	(Neutrium, 2016)	Not given	Not given
R <sub>b</sub> = R = Radius; D = Outside Diameters																	

**APPENDIX C: FITTED COEFFICIENT MULTIPLIER FOR THE “FRICTION COEFFICIENT vs. PIPE DIAMETER CURVE”  
WITH CHANGING  $R_c$**

<b>Pipe dia. mm</b>	<b>r/d=1</b>	<b>r/d=2</b>	<b>r/d=3</b>	<b>r/d=4</b>	<b>r/d=6</b>	<b>r/d=8</b>	<b>r/d=10</b>	<b>r/d=12</b>	<b>r/d=14</b>	<b>r/d=16</b>	<b>r/d=18</b>	<b>r/d=20</b>
<b>12.7</b>	0.54	0.32	0.32	0.38	0.46	0.65	0.81	0.92	1.03	1.13	1.24	1.35
<b>19.05</b>	0.50	0.3	0.3	0.35	0.43	0.6	0.75	0.85	0.95	1.05	1.15	1.25
<b>25.4</b>	0.46	0.28	0.28	0.32	0.39	0.55	0.69	0.78	0.87	0.97	1.06	1.15
<b>31.75</b>	0.44	0.26	0.26	0.31	0.37	0.53	0.66	0.75	0.84	0.92	1.01	1.1
<b>38.1</b>	0.42	0.25	0.25	0.29	0.36	0.5	0.63	0.71	0.8	0.88	0.97	1.05
<b>50.8</b>	0.38	0.23	0.23	0.27	0.32	0.46	0.57	0.65	0.72	0.8	0.87	0.95
<b>63.5</b>	0.36	0.22	0.22	0.25	0.31	0.43	0.54	0.61	0.68	0.76	0.83	0.9
<b>101.6</b>	0.34	0.2	0.2	0.24	0.29	0.41	0.51	0.58	0.65	0.71	0.78	0.85
<b>152.4</b>	0.3	0.18	0.18	0.21	0.26	0.36	0.45	0.51	0.57	0.63	0.69	0.75
<b>203.2</b>	0.28	0.17	0.17	0.2	0.24	0.34	0.42	0.48	0.53	0.59	0.64	0.7
<b>304.8</b>	0.26	0.16	0.16	0.18	0.22	0.31	0.39	0.44	0.49	0.55	0.6	0.65
<b>457.2</b>	0.24	0.14	0.14	0.17	0.2	0.29	0.36	0.41	0.46	0.5	0.55	0.6
<b>Fitted multiplier</b>	<b>1.0000</b>	<b>0.5963</b>	<b>0.5963</b>	<b>0.7069</b>	<b>0.8456</b>	<b>1.2074</b>	<b>1.4997</b>	<b>1.7068</b>	<b>1.9042</b>	<b>2.0960</b>	<b>2.2929</b>	<b>1.0897</b>

## **CHAPTER 4: DEVELOPMENT OF THE DYNAMIC HYDRAULIC GRADIENT WITHIN THE PIPE BEND DUE TO SUCCESSIVE PIPE BENDING**

### **Abstract**

Development of the successive dynamic hydraulic gradient (change in main pressure head) due to successive pipe bending is necessary to give understanding of and influence of the pressure differentials developed due to pipe bending, resulting in the pressure drop across a bend section and peripherals (influence region around bend) in irrigation systems. Introduction of bends in irrigation systems has a problem of causing unbalanced thrust forces in pressurised pipelines, often resulting in leakage and separation of joints. Development of the successive dynamic hydraulic gradient will assist with knowledge required in designing of thrust blocks, pipe erosion, generation of secondary flow and swirl due to bending.

Measurement of pressure differentials on the outer side and inner side of a straight pipe sections successively bent to form different bend angles  $0^\circ$ ,  $22.5^\circ$ ,  $45^\circ$ ,  $67.5^\circ$  and finally  $90^\circ$ , as the case with irrigation systems when using the normal and specialised bends was done. The inner and outer pressures were measured on two opposite axes of a one meter pipe bend at 5 cm intervals within  $\pm 15$  cm peripherals. This gave minimum and maximum pressures along the bent pipe section due to curvature introduced. The resultant of the two smooth splines of pressure differentials along the pipe bend section and peripherals from experimental data, were associated with the change of the main pressure head over the bend section and peripherals. Extrapolation of the smooth spline pressure differentials and normalisation was then undertaken to describe the behaviour of the main pressure head just before (upstream), within and after (downstream of) the bend section.

Analysis, smoothing and association of the inner and outer pressures differentials lead to the development of a normalised chart for manually determining the successive dynamic hydraulic gradient for sections before, after and within the bend for pressure drop of -1 bar due to bend angles  $0^\circ$ ,  $22.5^\circ$ ,  $45^\circ$ ,  $67.5^\circ$  and finally  $90^\circ$ . This was also expressed mathematically for use in a MS Excel spread sheet tool for varying curvature and flow velocities. The two extremes (constant pressure drop) of the dynamic hydraulic gradient line

outside of the bend due to the straight pipe sections could then be linked. Perturbation (partial backward or resistance to flow due to bend) was also seen to occur upstream and downstream of pipe bends, also contributing to pressure drop. The main restraining forces in the design of thrust blocks must be targeted more at forces due to fluid entering the bend (larger force) and less the exit stream (lesser force).

**Keywords:** *Pressure differential, Resultant, Bend angle, Radius of curvature, Perturbation.*

#### **4.1. Introduction**

The dynamic hydraulic gradient is the slope of the water pressure along an irrigation pipe or potentiometric surface of the pressure drop over the pipe. This simply put is the free water level at any given position (drop in water head per unit of distance) of the pipe along the maximum head path (Cheremisinoff, 1998; ARC, 2003). Development of the successive dynamic hydraulic gradient due to successive pipe bending giving different bend angles, curvature, specific pipe diameter and flow velocity, will enable one to link the two constant pressure drop extremes of the dynamic hydraulic gradient line due to the straight pipe sections outside of the bend, to that of the bend.

The existence of the dynamic hydraulic gradient is quite indicative of the differential resultant external thrust due to the existence of a bend (Ono *et al.*, 2018). A good knowledge of the potential thrust direction due to a bend can also assist in the design of thrust blocks in the irrigation design and installation process (Thorley, 1994). Efficient design of thrust blocks can be performed with sufficient knowledge of the forces involved due to the extent of bending, which will result in the saving of material used in the constructing of thrust blocks.

With a good understanding of the dynamic hydraulic gradient line over the respective bending and peripheral sections, points of potential erosion of the pipe bend can also be more easily identified (Lin *et al.*, 2015; Liang *et al.*, 2017). This can help advance the design of bulk irrigation main lines supplying large schemes, increasing their life span and pipe designs for other applications.

Generally, pressure drop occurs due to bending (over the bend section), in the peripherals of the bend (upstream and more on the down steam side due to the bend influence regions) as seen in irrigation systems. Determination of the dynamic hydraulic gradient with the extrapolation of the dynamic hydraulic gradient lines will give a clearer understanding of pressure drop as shown by Padilla *et al.* (2012) considerably at sections before, after and within the bend sections for better understanding of the influence of pipe bending.

To join the measured pressure differentials due to the formation of the bend and the straight pipe sections, extrapolation of the dynamic hydraulic gradient line is necessary (Ito, 1960; Padilla *et al.*, 2012). Extrapolation of the dynamic hydraulic gradient lines will also give a more understanding of the resulting generation of two secondary helical vortex flows of the fluid column, oscillating downstream of the pipe when the irrigation system is in operation which contributes in part to the secondary pressure losses (Ghobadi and Muzychka, 2016).

Due to the existence of bends in pipe systems, the concept of swirl or vortex formation has been discovered to occur relative to the curvature and flow velocities (Dutta *et al.*, 2016). An understanding of the concept of swirl intensity as identified by Kim *et al.* (2014) can also be linked to the extent of bending and flow velocities involved when designing irrigation systems. Concept of swirl intensity can also be used to understand the influence or resulting minor losses in instances where one bend is following another bend in an irrigation system (Zardin *et al.*, 2017).

In the analysis of the pressure about the bend, it was apparent from the literature reviewed that the maximum and minimum pressure differentials (on the outside and inside of the bend respectively) are likely to occur close to the walls of the pipe bends due to successive pipe bending (Röhrig *et al.*, 2015). With the measurement of the inner (inside bend) and outer (outside bend) pressures within the pipe bend, the resultant pressure or force due to the curvature introduced would help in the understanding and knowledge required in the efficient design of thrust blocks, pipe erosion and generation of secondary flow and swirl due to successive pipe bending.

The complexity of the pressure differential measurement is largely due to the multidimensional nature of the flowing fluid observed at the bend (Azzi and Friedel, 2005).

Analysis of the inner and outer differential pressure due to bending has mainly been focused on the 90° bend but they are also 45° bends and specialised bends (unique bends made specifically for an irrigation system or cases of applying the bending schedule according to the pipe manufacturing bend limits) which are less than 90°, in use in irrigation systems wherein there is no information on the resulting differential pressures.

The development of the successive dynamic hydraulic gradient due to the successive pipe bending and the peripherals (surroundings) will help shed light on the behaviour of the spread of pressure drop due to all bending (from 0° to 90° to include specialised bends) as used in the irrigation systems. The main pressure head over the pipe bend and the surroundings was considered since the existence of bends brings about the problem of unbalanced thrust forces in pressure pipelines, often resulting in leakage and separation of the joints, erosion, and generation of secondary flow responsible for pressure drop due to bending. This research aims at expressing the successive dynamic hydraulic gradient due to pipe bending as a chart for manually determining the change in the main pressure head or pressure drop across the bend section(s) and the peripheral(s) and also expresses this as a MS Excel spread sheet tool.

In this research, it is hypothesised that the nature or shape of the hydraulic gradient line due the bend angle is the same for different pressure drop owing to varied curvature and flow velocity.

## **4.2. Materials and Methods**

The experimental study laboratory for the standard of quality, experimental methodology and equipment on how the tests were undertaken and experimental data analysis of the experimental results are looked at in the following subsections.

### **4.2.1. Study Laboratory**

Experimental work was carried out in the HydroLab of the Agricultural Research Council – Institute for Agricultural Engineering (ARC-IAE) one of the accredited laboratory in South Africa.

#### **4.2.2. Experimental Methodology and Equipment**

For the measurement of the pressure differentials, the use of a single pressure gauge on consideration of the cost of using more than one gauge was done. Consideration was also for ease of handling and reduced unwanted frictional losses that would have otherwise occurred in the experiment due to multiple perforations of the pipe while placing multiple gauges, and the need to calibrate each gauge on initiating measurements. Revolving the gauge at the end of measuring on axis allowed for measurement on the two different axes separately.

The behavioural change or pressure differentials of the fluid within the pipe bends was measured at intervals just before, within and just after the bend influence regions at 5 cm intervals over 26 points along the two opposite sides of the bends individually. Figure 4.1 shows the schematic diagram of the test apparatus and the positions of the measuring gauge points explained.

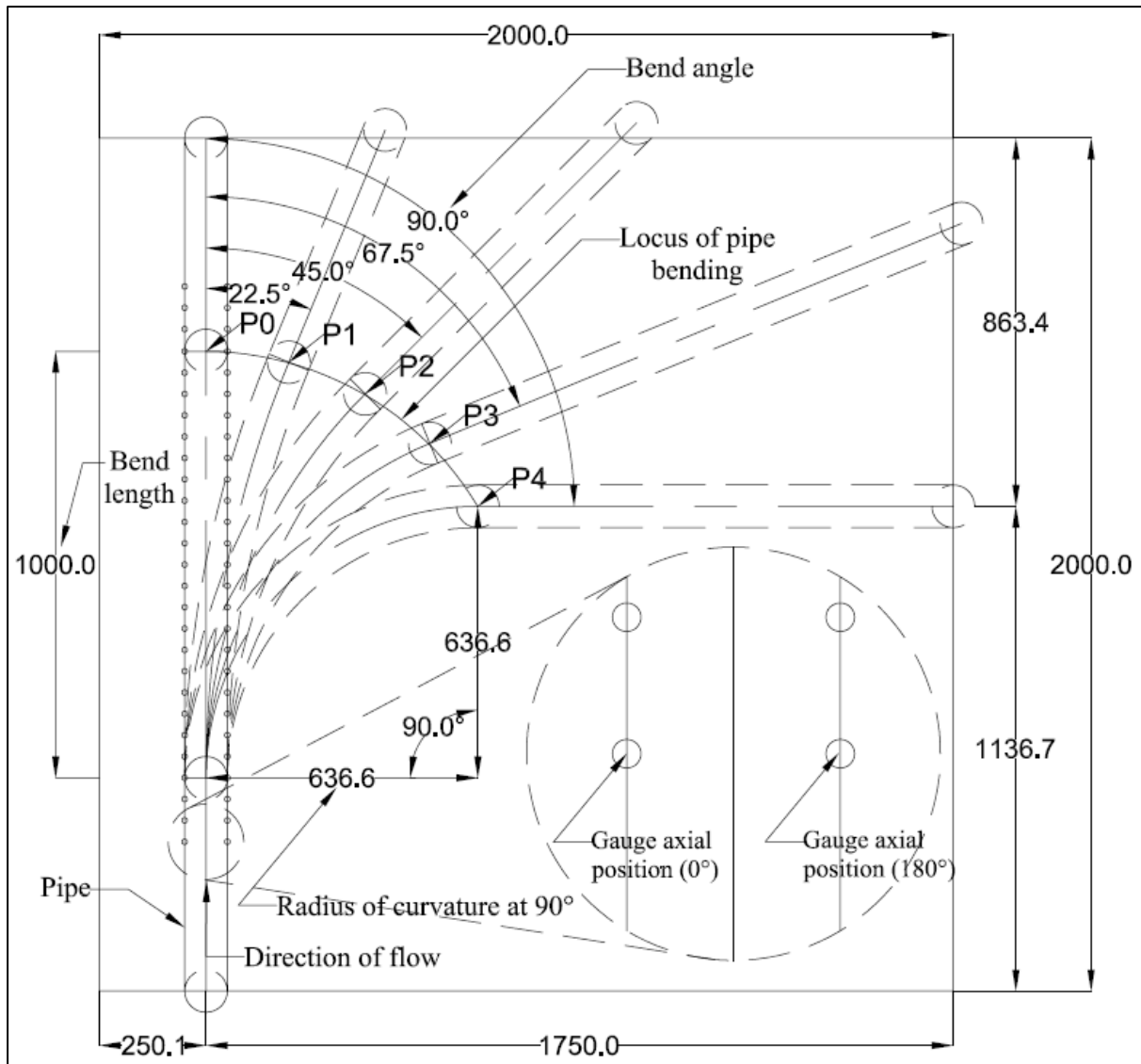


**Figure 4.1 Schematic diagram of the test apparatus showing the successive pipe bending angles and successive gauge positions for the inner and outer pressures measured.**

The two sides, the outer side of the bend,  $0^\circ$  axial position and the inner side,  $180^\circ$  axial positions as illustrated in Figure 4.1 were chosen as they gave the maximum and minimum pressure changes, respectively, with the formation of the bends and successive pressure measurements. Measurements were also taken  $\pm 15$  cm outside of the 100 cm bend section to get more understanding for linking of the straight pipe section dynamic hydraulic gradient lines with the bends formed. Pressure measurements were done on the internal walls of the pipe tested.

Two pipe diameters, 25 mm (23 mm ID) and 50 mm (47 mm ID), were fed water from a 100 mm (97 mm ID) pipe individually through a flow meter (ZJ-LCD-M Digital Display Water Flow Sensor Meter 0.01 LPM, 1% accuracy), while the supply flow was varied from  $0.0000136 \text{ m}^3\text{s}^{-1}$  to  $0.0001500 \text{ m}^3\text{s}^{-1}$  to achieve the varied flow velocities and resulting measured pressure differentials. Bending was allowed to form over the one meter pipe section (mid-section of each pipe length) as it was successively bent about a locus, points P0 to P4, giving rise to bend angles  $0^\circ$ ,  $22.5^\circ$ ,  $45^\circ$ ,  $67.5^\circ$  and  $90^\circ$  (see Figure 4.1). This allowed for less disturbance in and easy measurement of the variables while undertaking the tests.

Pressure variation was measured with the WIKA CPG1500 series precision digital pneumatic pressure gauge ( $-1$  to  $+5 \times 10^2$  kPa 0.1% accuracy). The fluid was not monitored as it exited the open-ended test apparatus at atmospheric pressure conditions. Since water is relatively incompressible, the test setup was based on atmospheric pressure also allowing for a low operating pressure catering for the limitation in the gauge sensitivity range. The pressure sensor measuring section was made flush on the inside of the pipe, measuring the test pressures across the length of the straight pipe section as it was successively bent in the two axes tested (inside and outside of the bend).

Pressure differentials were measured for the successive pipe bending for incremental intervals of  $0.0000136 \text{ m}^3\text{s}^{-1}$  of the supply, until some trends could be seen. Five flows were tested following some trends observed on measuring the pressure differentials and tabulated in Table 4.1 for the successive bending.

**Table 4.1 Single phase supply pipe line flow rate ( $\text{m}^3\text{s}^{-1}$ ) tested and individual test pipe diameter flow velocities ( $\text{ms}^{-1}$ )**

Main supply line flow rate with flow meter Outside pipe diameter, 100 mm (OD) Internal pipe diameter, 97 mm (ID)		Actual flow velocity in each pipe ( $\text{ms}^{-1}$ )	
		25mm (OD) 23 mm (ID)	50mm (OD) 47mm (ID)
( $\text{m}^3\text{s}^{-1}$ )	(LPM)		
0.0000136	0.82	0.033 (No clear trend)	Too low flow relative to the pipe size (open channel flow)
0.0000273	1.64	0.066 (No clear trend)	
0.0000409	2.45	0.0985	
0.0000545	3.27	0.1313	
0.0000682	4.09	0.1641	0.039 (No clear trend)
0.0000818	4.91	0.1969	0.047 (No clear trend)
0.0000955	5.73	(tests not done)	0.055 (No clear trend)
0.0001091	6.55	(tests not done)	0.063 (No clear trend)
0.0001227	7.36	Too high flow, relative to the pipe size (tests not done)	0.071 (No clear trend)
0.0001364	8.18		0.079 (No clear trend)
0.0001500	9.00		0.086

#### 4.2.3. Experimental Data Analysis

After all measurements were taken, a general pattern of the differential pressures was observed within and outside the pipe bend as the gauge was moved and measured along the sides of the continuously bending pipes. Experimental data from the tests was then fitted into smooth splines to give a picture (estimating functional relationship) of the behaviour of the flow about the bend for the two axes by interpolation and approximation of sampled data. The best smooth splines were obtained mainly in the case where the experimental data showed a marked or fairly clear pattern and were used for predicting behaviour in the cases where there was much randomness of the measured experimental data. The use of smooth splines for digital filtering and interpretation as used by Enting (1987) was considered principally applicable since flow about the bend is similar.

The smooth splines (inner and outer pressures) developed from the experimental data were then combined to give the resultant of the main pressure head at each point (interval

measured) over the bend section and peripherals. This resultant was then associated with the change of the main pressured head over the bend and peripherals by having the cumulative of this resultant. Finally, the extrapolated smooth splines associated with the change of the main pressure head were then normalised to give the successive dynamic hydraulic gradient lines about the bend and the peripherals. Normalising the data as done by Röhrig *et al.* (2015), was done by making the overall pressure drop in the main pressure head due to the bend section to a magnitude of -1 bar with extrapolation of the theoretical data. Scaling of the cumulative resultant of the smooth spline pressure of the measured data, made a standard pattern or picture of the behaviour of the main pressure head or successive hydraulic gradients due to successive bending involved, would then be used to achieve the dynamic hydraulic gradient of any level of bending  $0^\circ$  to  $90^\circ$  for different extents of pressure drop and flow.

#### **4.3. Theoretical Approach to the Development of the Dynamic Hydraulic Gradient.**

The pressure measurements taken before, within and after the bend were indicative of the behavioural pattern of the inner and outer differential pressures at different points axial to the pipe on intervals, as the different bend angles were successively introduced. Applying the Newton's third law, at equilibrium conditions the resultant of the inner and outer pressures is supposed to cancel out. This means that the resultant of the two positive (outer) and negative (inner) pressures acting about the confined space in the bend in this case gives the resultant or restrain needed by the thrust block or erosive force of water due to the bend in this case. Different pressure contours seen, as illustrated by Sun *et al.* (2012) were the result of gradual changes in pressure due to pipe bend.

Adding or superimposing the measured pressure differentials as justified by Kalpakli and Örlü (2013) on the inner and outer wall of the bends gave the resultant pressures due to the adjacent points observed, indicative of the thrust due to the bend, owing to the inflowing fluid and accompanying curvature. The resultant at points along the bend gave the intermittent pressure drop at the points observed over the pipe sections (bend length in question). This resultant pressure was then associated to the change in the main pressure head along the bent pipe section and peripherals by having the cumulative resultant pressures of the measured data, deducing the change in pressure over the bend section and peripherals, the hydraulic gradient line.

Smooth splines of the experimental data were used to develop the pattern of the change in the differential pressures over the different bend angles ( $0^\circ$ ,  $22.5^\circ$ ,  $45^\circ$ ,  $67.5^\circ$  and  $90^\circ$ ) tested with corresponding curvature. Extrapolation of the pressure gradients following the superimposing, cumulation (cumulative of the resultant) and normalisation helped assess the concept of perturbation (partial backward or resistance to flow due to bend) just before and just after the bend. The overall pressure drop due to the bending with the respective flow and curvature in each case formed the magnitude of the general main pressure head considered due to the extent of bending. This in essence is the difference between the two constant gradient lines due to the straight pipe sections before and after each bend in question.

#### **4.4. Results and Discussion**

The observed pressures differential trends due to successive pipe bending, outer and inner pressures due to successive pipe bending, superimposing of the inner and outer pressures measured over the successive pipe bend(s), change of the hydraulic gradient along bend due to successive pipe bending, normalisation of the change of hydraulic gradient over bend section and peripherals on a chart and a MS Excel sheet tool are presented and discussed in the following sections.

##### **4.4.1. Pressures differential trends due to Successive Pipe Bending**

With the highest flow tested on the 25 mm (OD) pipe, some clearer trends were picked up as seen in Figure 4.2. These trends became more distorted as flow velocities decreased for the pipes tested in Figures 4.3 to 4.6.

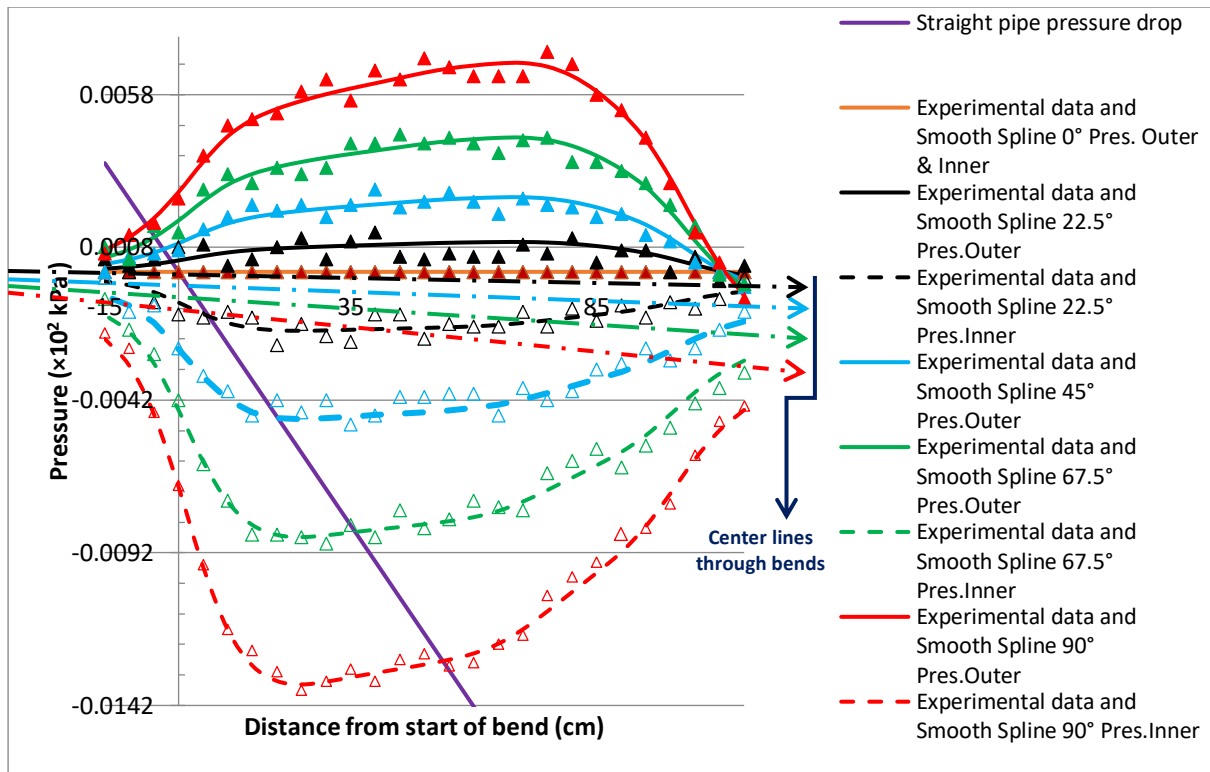


**Figure 4.2 Behaviour of pressure along the outer and inner axis of the pipe bend for the 25 mm (OD) pipe at  $0.197 \text{ ms}^{-1}$  with smoothed spline expected trend**

The behaviour of the differential pressures due to the successive pipe bending introduced were seen to show similar trends for all the tests undertaken despite the anomalies observed in the experimental data. Despite these anomalies, smooth splines for the outer and inner pressure differentials were generated using the MATLAB R2014a curve fitting tool from fairly clear trends observed in experimental results of the 25 mm pipe at  $0.197 \text{ ms}^{-1}$  (see Figure 4.2). These were then scaled to give the estimates or expected of the behaviour (trends) of the other pressure differentials at lower flows tested.

Based on the fitted smooth splines, a better understanding and analysis of the inner and outer pressures was derived. These smooth splines were applied to all other experimental results with scaling of the smooth splines relative to the individual test flow velocities. The smooth splines were in essence used to give the perceived ideal pattern (trend) relative to the experimental results obtained for better visual analysis and the development of the successive dynamic hydraulic gradient. Trends for other tests captured are shown in Figures 4.3, 4.4, 4.5 and 4.6.

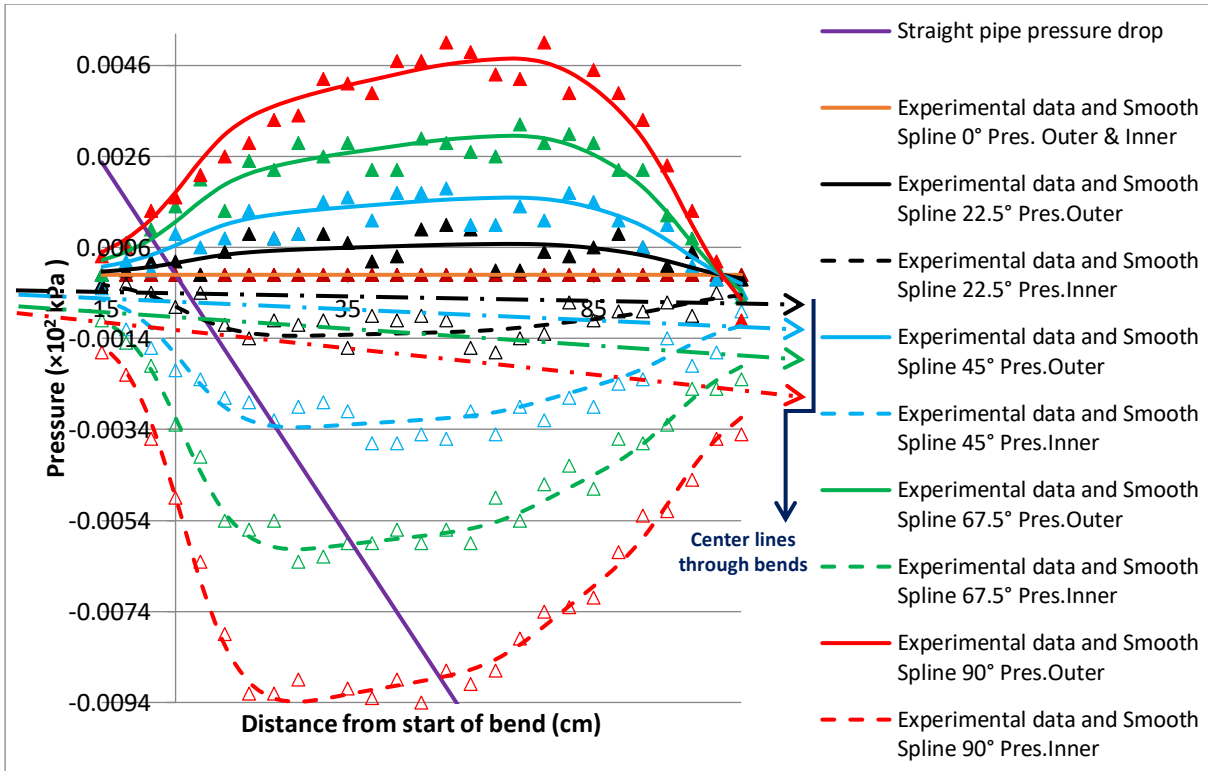


**Figure 4.3 Behaviour of pressure along the outer and inner axis of the pipe bend for the 25 mm (OD) pipe at  $0.164 \text{ ms}^{-1}$  with smoothed spline expected trend**

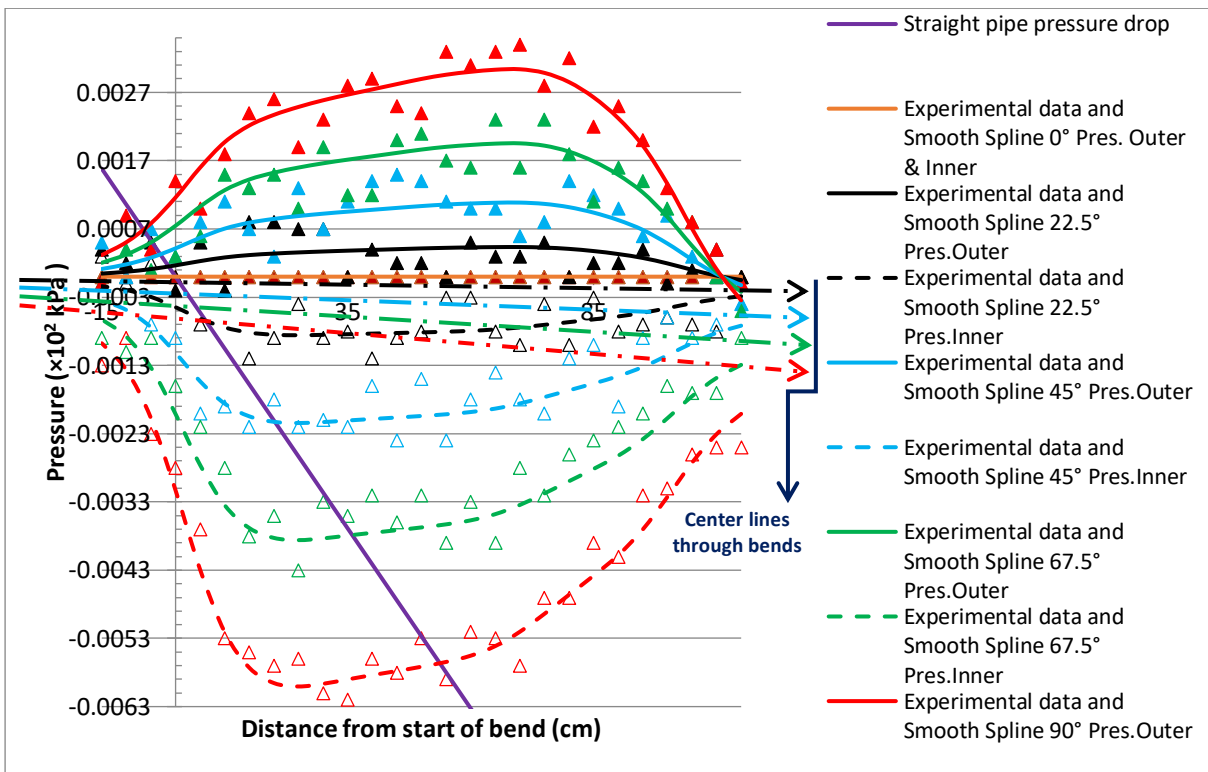


**Figure 4.4 Behaviour of pressure along the outer and inner axis of the pipe bend for the 25 mm (OD) pipe at  $0.131 \text{ ms}^{-1}$  with smoothed spline expected trend**

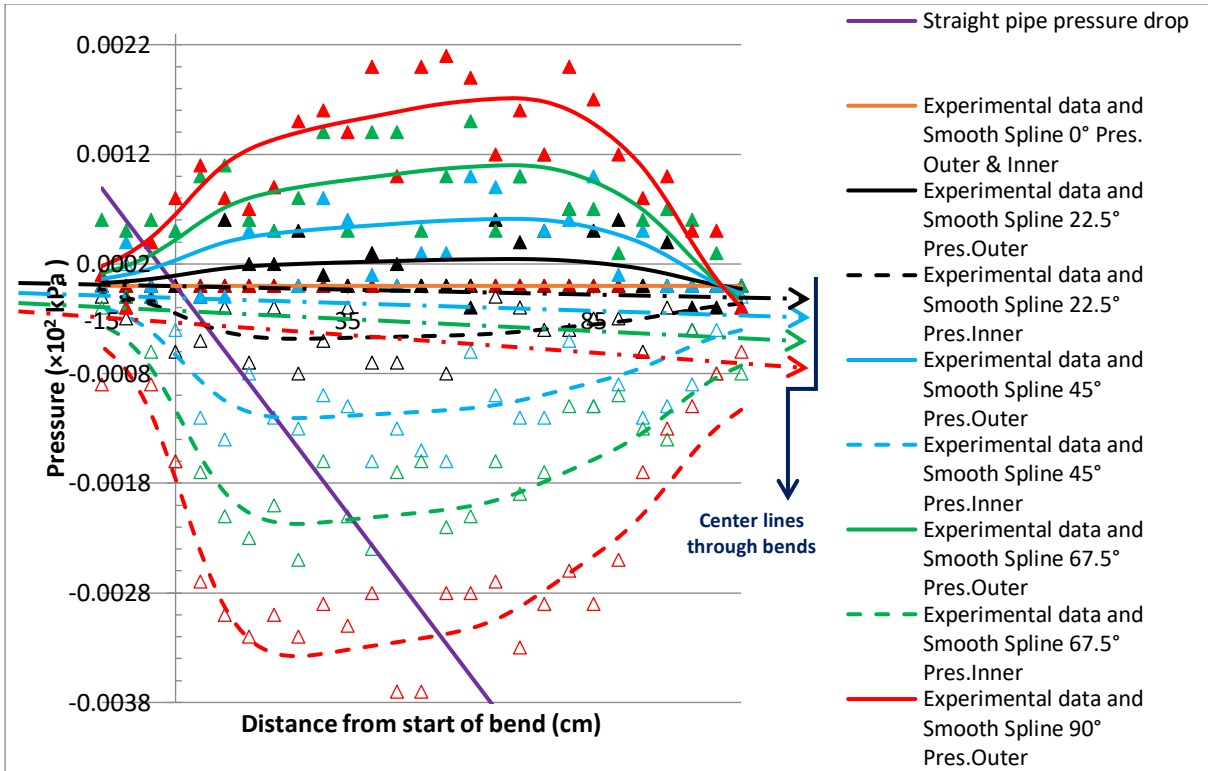


Figure 4.5 Behaviour of pressure along the outer and inner axis of the pipe bend for the 25 mm (OD) pipe at  $0.0985 \text{ ms}^{-1}$  with smoothed spline expected trend

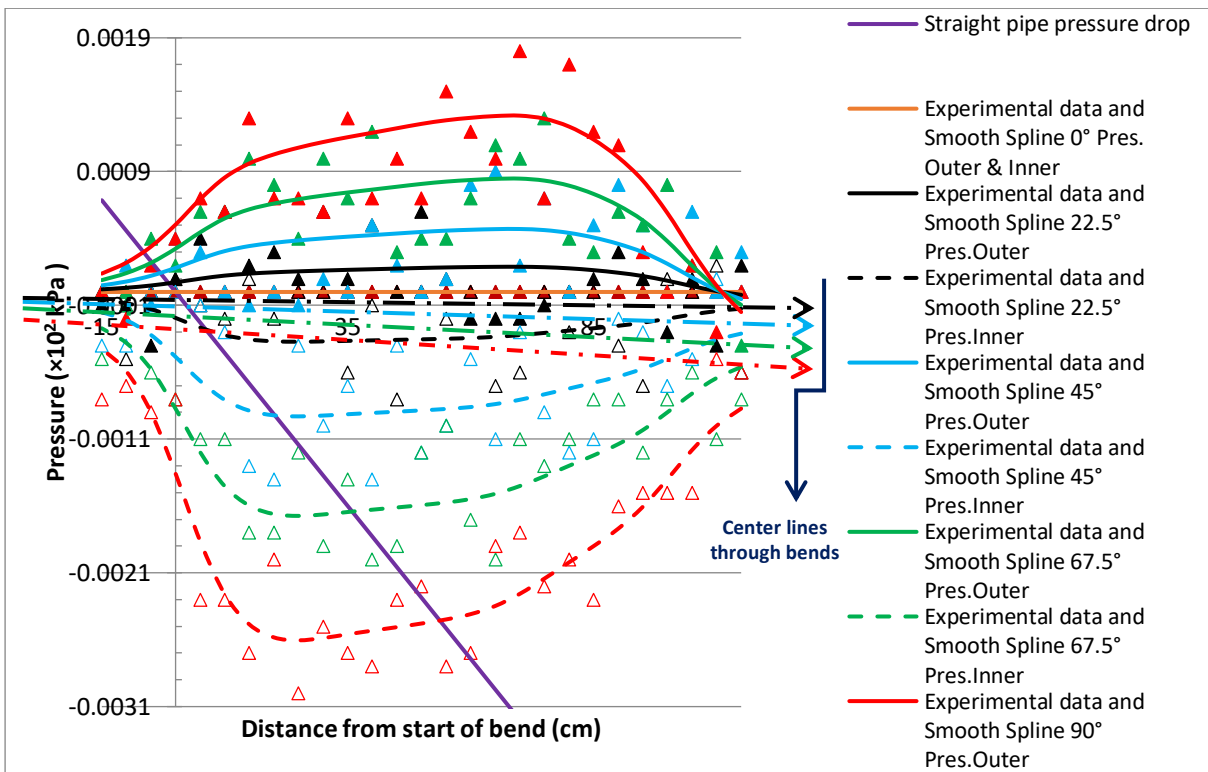


Figure 4.6 Behaviour of pressure along the outer and inner axis of the pipe bend for the 50 mm (OD) pipe at  $0.0865 \text{ ms}^{-1}$  with smoothed spline expected trend

For the last two tests (see Figure 4.5 and 4.6) there seemed to be almost no clear pressures trends shown on the outer side and inner side of the pipes tested considering the smooth spline trends as the expected pattern. There, however, seemed to be somewhat trends exhibited on the 90° bends. The absence of trends was mainly due to the low flows relative to the pipe diameter tested coupled with vibrations due to the pipe movement during the testing.

Despite the observed trends, results showed that trends were marked as the bend angles increased. With the observed trends, it was fairly clear that the patterns exhibited due to the successive pipe bending were common to all pipes tested, with the exception of the more varied pressure differential readings at lower flows and lower bend angles.

#### **4.4.1.1. Outer Pressures due to Successive Pipe Bending**

For the measured pressure differentials on the outer side of the bend lengths tested and the peripherals ( $\pm 15$  cm outside of the bend), generally the pressure gradually rose and eventually decreased (Figures 4.2, 4.3 and 4.4). Generally, in all cases of the different bend angles tested, there was a first instance of a sharp rise in pressure moving into the first quarter of the bend, followed by a decrease in the rate of increase in pressure until it reached a peak from wherein it sharply started dropping in the last quarter of the bend. The first instance of the rise in pressure was due to the collision of the first half of the fluid column, to the outer half cylinder wall of the bend as flow entered the respective bend. As the first half of the fluid collided and was redirected with the bend wall, the straight flowing streamlines of the fluid column gave rise to the first sharp rise in pressure as initially observed.

The flowing fluid streamlines in the process was split sideways giving rise to the formation of the Dean-vortices as it cleared spiralling sideways as described by Kim *et al.* (2014). This process then allowed for the opposite fluid column on the inner half cylinder of the pipe bend to commence the fluid wall collision on the outside of the bend, following the decreased rate of increase in pressure until the peak observed. As the remaining inner half of the fluid column finished collision on the outside wall of the bend within the pipe, the sharp decrease in pressure commenced with the completion of and the start of formation of the vortex flow describe the Dean number.

As water continued into the bend, energy was lost, and this was mainly due to the collision of the fluid with the wall and itself. However, as collision occurred, there was a simultaneous pull on the fluid column due to curvature, which also contributed to the energy loss. The effect of coupling of forces, together with the influence of the pipe geometry, gave the fluid elements angular direction and energy to start the generation of the Dean vortices and eddies. In the process of flow, dynamic and kinematic energy losses also occurred in the fluid medium.

The above phenomenon occurred at different magnitudes throughout all the successive bend angles for the pipes tested, guided by the centre line of the entering flow as it touched the outer wall of the pipe due to the formation of the bend. Generally, as the radius of curvature decreased, there was a movement of the peak pressure towards the inside of the bend as the bend angle increased also seen by Lin and Pauley (1996).

#### **4.4.1.2. Inner Pressures due to Successive Pipe Bending**

In the case of the inner pressure as seen above (Figures 4.2, 4.3 and 4.4), the converse occurred. The pressure decreased to a minimum in the first quarter of the bend as the vacuum was created due to the formation of the bend with the accompanied detachment and replacement of the fluid in the mid-section as explained by Lin and Pauley (1996) for a 90° bend. Pressure decreased until such a time when the rate of decrease in pressure stopped, forming the lower peak (minimum) on the inner pressure measured. Again, this was due to the influence of the phenomenon explained earlier, due to the collision of, and simultaneous detachment of the half cylinders adjacent to the inside of the bend. Detachment of fluid adjacent to the inner wall on the inner side of bend caused the sharp rise in the pressure drop first observed, followed by the replacement of fluid from the opposite collision and swirl.

The replacement of the detached fluid from the inner wall of the bend generated swirl for each bend in question, starting the vortices and eddies also seen by dos Santos *et al.* (2014), which add to pressure drop. As flow continued past the bend(s), there was more rapid decrease in the rate of rise of pressure as a result of the complete formation of the Dean vortices explained by Dutta *et al.* (2016), followed by the oscillation of the fluid column.

#### 4.4.2. Superimposing of the Inner and Outer Pressures measured over the Successive Pipe Bend

For further analysis of the measured pressure differentials (focused only on Figure 4.2), adding or combining of the inner and outer measured pressures differentials as supported by Kalpakli and Örlü (2013) made better understanding, giving the resultant of the two extremes of the pressure differentials (Figure 4.7). However, due to the scatter of the measured experimental values, the smoothed splines of the experimental data were best used to describe the behaviour of the main pressure head about the bend. Figure 4.7 shows the resulting smooth spline resultant pressure differentials plot due to the successive bending, again with reference to the 25 mm (OD) pipe at  $0.1969 \text{ ms}^{-1}$ .

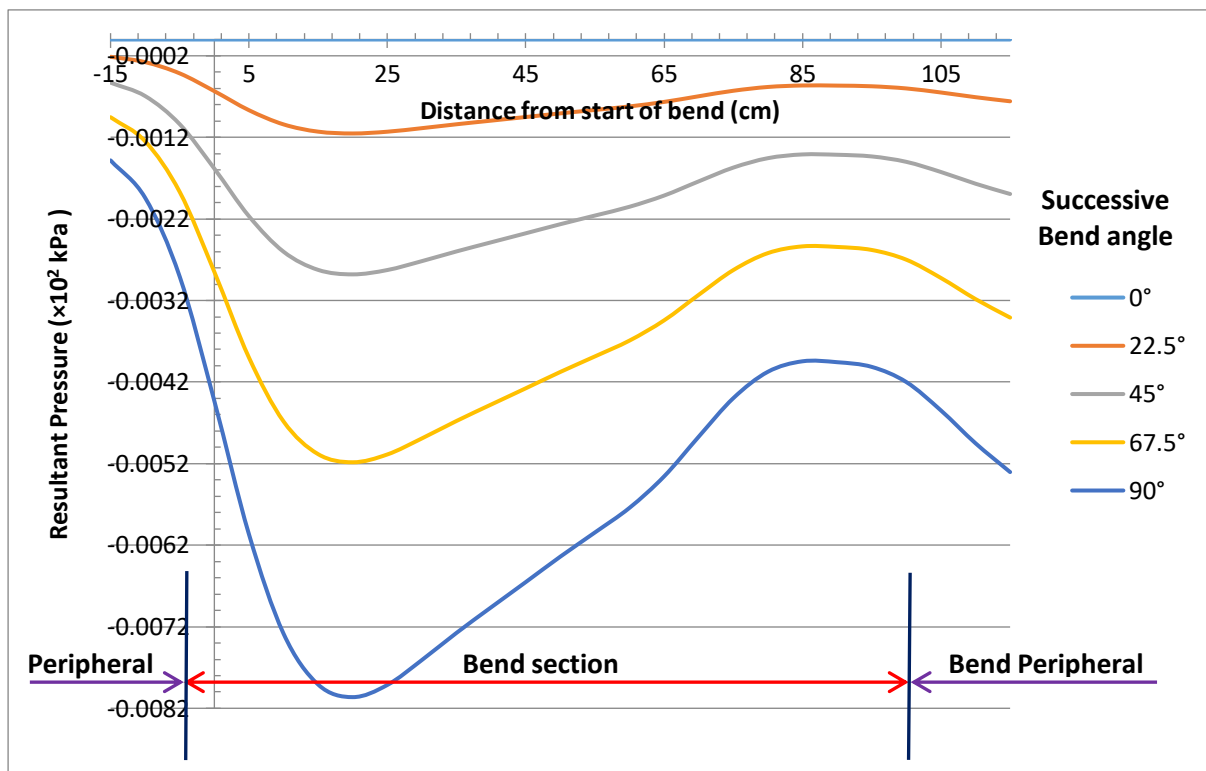


**Figure 4.7 Smooth spline resultant pressure differentials for the 25 mm (OD) pipe at  $0.1969 \text{ ms}^{-1}$**

Clearly as the bend angle increased oscillation of the fluid column starts within the bend as seen with the rise and fall of the resultant pressure differentials and seen largely for the  $90^\circ$  bend. Oscillation is also seen to increase with increase in curvature as confirmed by Röhrig *et*

*al.* (2015). The resultant pressure is seen to drop at first as the geometry of the bend introduces pressured drop. The resultant pressure recovers somewhat as vortex and eddy generation starts, and then seems to repeat the drop with the oscillation (a phenomenon also explained by Kim *et al.* (2014)) of the fluid, which is also seen to decay as we move away from the bend.

From the similarities in the behaviour of the resultant pressure head (seen in Figure 4.7) of the experimental findings for varied curvature and flow, the fluid oscillation or swirl intensity (as defined by Kim *et al.* (2014)) depended very much on the radius of curvature. This is seen by the decrease in the oscillation of the main pressure head as the bend angle decreases. The area-averaged flux of angular momentum, swirl number, in general represents the intensity of a swirl on a cut plane normal to the axial flow direction as defined by Putnam (1964). This swirl intensity produced by the successive bending was in general seen to reduce exponentially along the downstream of the bends from the experiment findings (see following Figure 4.8).

#### **4.4.3. Change of the Hydraulic Gradient along Bend due to Successive Pipe Bending**

From the two pipes diameters tested, it can be agreed that there exists a similar pattern for the behaviour of the fluid about the bend, with the magnitude of the resultant differential pressure drop confined to the overall pressure drop due to an extent of bending (curvature) with the respective flow. The change of the successive dynamic hydraulic gradient (main pressure head), which describes the pressure drop over the section about the bend and peripherals (due to the bend), can be better expressed by the successive change or cumulative resultant pressure differentials, as shown in Figures 4.8. The use of the cumulative resultant of the pressure best simulates the successive change of the main pressured head over the bend length.

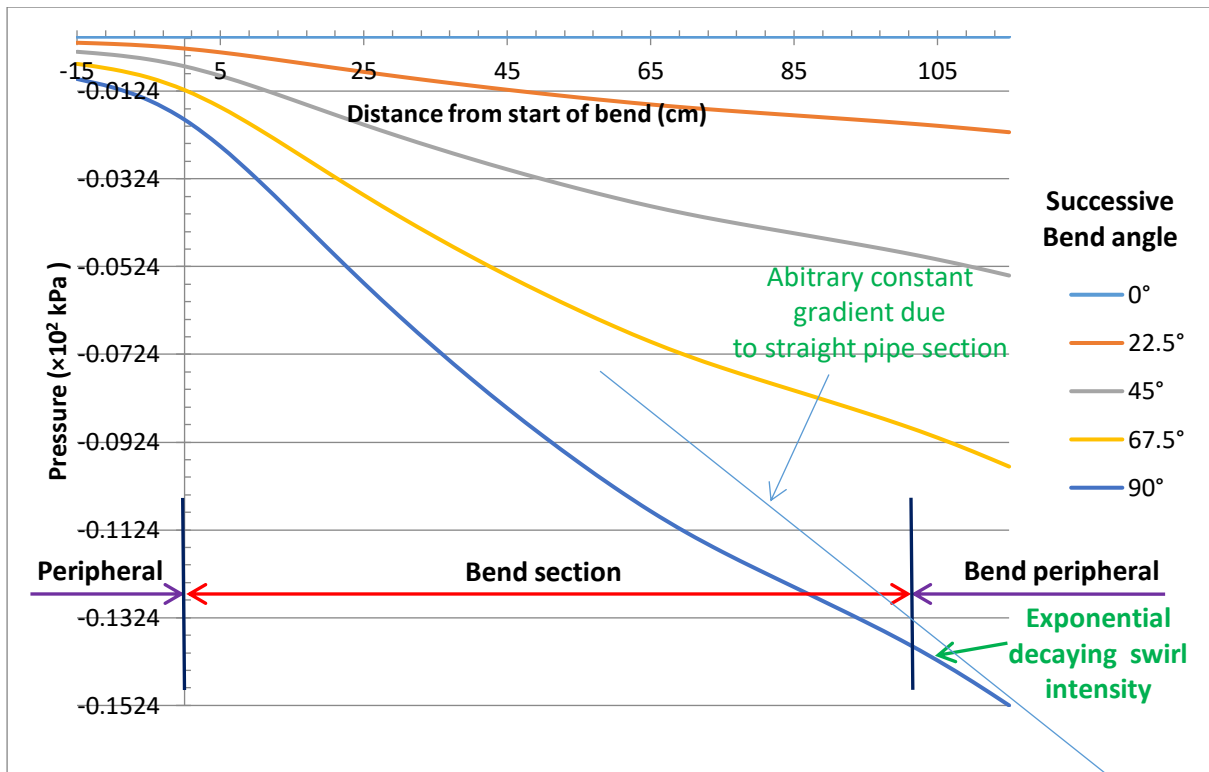


**Figure 4.8 Cumulative smooth spline resultant pressure differentials for the 25 mm (OD) pipe at  $0.1969 \text{ ms}^{-1}$  over the bend section and peripherals**

The change or drop in the main pressure head as seen in the cumulation (cumulative resultant smooth spline) can then be linked to the two extremes of the main pressure head or hydraulic gradient (constant gradient or drop) due to the straight pipe sections before and after the bend. The two extremes of the main pressure head due to the straight pipe sections confine or constitute the magnitude of the pressure drop due to the bend in question or successive bending.

In all the pipe diameters tested, the change in the pipe diameter was catered for with the change in flow velocity as described by Neutrium (2016) due to the flow coefficient  $L/D$  ratio, for bend length “L” and respective diameter “D”. Since the flow about the bend is similar, there exist multipliers due to curvature for the change in the main pressure head which align with respective flow, while joining to the pressure gradient to the straight pipe sections.

Considering the method of analyses in literature reviewed by Röhrig *et al.* (2015) and Wang *et al.* (2015) the patterns observed can be normalised by expressing the observed behaviour

over a magnitude of one for the bend section pressure drop in preparation of scaling when in use. With the normalising, the different experimental pressure gradients found with the successive introduction of a bend can then be used or associated for any (varied) curvature and flow for different pipe diameters and bend length simply by scaling.

#### 4.4.4. Normalisation of the Change of Hydraulic gradient over Bend Section and Peripherals on a Chart

In pursuit of the aim of the study, the extrapolated normalised smooth splines derived from the experimental data best describe the differential flow patterns or graphical picture of the main pressure head for the successive bending finally achieved. The presentation of the normalised extrapolated smooth splines derived from the experimental results gave a chart for manually determining the successive dynamic hydraulic gradient or the main pressure head as shown in Figure 4.9.

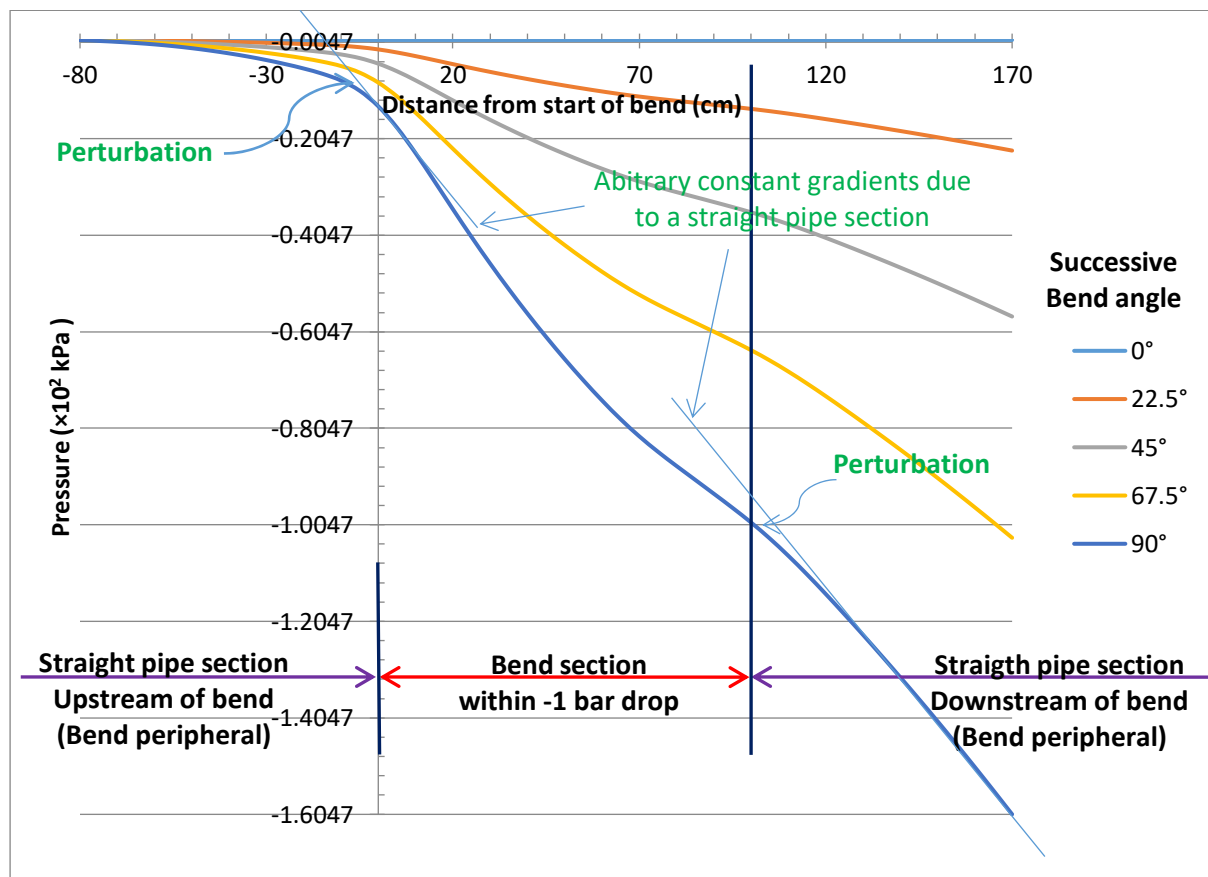


Figure 4.9 Normalised extrapolated change of the successive dynamic hydraulic gradient (main pressure head) for the successive pipe bending for a one meter bend

Pressure drop is initially constant for the straight pipe section before the bend. From the extrapolation of the cumulative smooth spline resultant pressure head, clearly perturbation occurred before and after the bend relative to the flow velocities and bend parameters tested. This is shown by the continued negative pressure or change in the hydraulic gradient (which should be a constant drop) before the zero mark (the start of the bend) and the asymptotic behaviour after the 100 cm mark (the end of the bend). Given the magnitude of the pressure drop in each of the bending involved, estimated at 30 to 50 pipe diameters as cited Spedding *et al.* (2004), can be used to actually get the asymptotic tolerance or difference in arriving at the actual perturbation downstream of bend.

Due to the change in the fluid elements' flow velocities in the circular motion of the vortices formed, pressure drop continued after the bend mainly because of the two generated oscillating secondary flows. These attenuated some pipe diameters downstream of the bend, until eventually the pressure gradient became a constant drop as the case with the straight pipe section before the bend.

#### **4.4.5. Normalisation of the Change of Hydraulic gradient over Bend Section and Peripherals on a MS Excel Tool**

In each case of the bending, the individual graphical normalised extrapolated change or drop of the main pressure head can be expressed as a mathematical function for the bend angles tested. This can then be expressed as change of the hydraulic gradient (main pressure head) on an Excel spread sheet in pursuit of the research objective. A Microsoft Excel spread sheet tool for determining the dynamic hydraulic gradient can thus be realised and can be used by scaling up the change of the main pressure head for a given pipe diameter with bend length with respect to the magnitude of the pressure drop for particular curvature and flow.

Using the Gaussian function for the extents of the experimental data and theoretical extrapolation in the MATLAB R2014a curve fitting tool, a function, General model Gauss3: can be generated with respect to each bend angle tests except the  $0^\circ$  which is a straight pipe section. Then the above the change in the hydraulic gradient (Figure 4.9) can be expressed mathematically as functions;

For a 22.5° bend:

$$J(x) = 0.008934 \exp^{-\left(\frac{x+2.061}{20.17}\right)^2} - 0.06263 \exp^{-\left(\frac{x-61.49}{58.85}\right)^2} - 0.2436 \exp^{-\left(\frac{x-199.7}{107}\right)^2} \quad 4.1$$

For a 45° bend:

$$K(x) = 0.02312 \exp^{-\left(\frac{x+2.906}{21.75}\right)^2} - 0.1563 \exp^{-\left(\frac{x-61.8}{59.68}\right)^2} - 0.6134 \exp^{-\left(\frac{x-201.4}{108.1}\right)^2} \quad 4.2$$

For a 67.5° bend:

$$L(x) = 0.04199 \exp^{-\left(\frac{x+2.961}{22.11}\right)^2} - 0.283 \exp^{-\left(\frac{x-61.9}{59.94}\right)^2} - 1.105 \exp^{-\left(\frac{x-201.5}{107.9}\right)^2} \quad 4.3$$

And for a 90° bend:

$$M(x) = 0.06532 \exp^{-\left(\frac{x+2.961}{22.11}\right)^2} - 0.4403 \exp^{-\left(\frac{x-61.9}{59.94}\right)^2} - 1.718 \exp^{-\left(\frac{x-201.5}{107.9}\right)^2} \quad 4.4$$

Interpolation can then be used for the bend angles in between and these equations can be put in a MS excel spread sheet tool for use. Again, scale factor will be defined by the pressure drop (magnitude or confines of the derived smooth splines) due to the extent of bending involved with the respective bend parameters and flow velocity.

#### 4.5. Conclusions

Due to curvature and bend angle, the momentum balance of the fluid was maintained by the centrifugal and centripetal forces acting on the flowing fluid. The resultant pressure gradient was then developed as the slower moving fluid was pulled towards the inside of the bend with simultaneous collision of the fluid column. This gave rise to pressure drop on the inside of the bend and pressure on the outside of the bend, confirming the generation of secondary flow also adding to the pressure drop within the bend region, shaping the main pressure head. In this research case, the resultant of the two extremes of the differential pressures were used to give the intermittent pressure drop over the bend and the peripherals and associated (cumulative resultant) with the change of the hydraulic gradient (main pressure head) over the bend section and peripherals.

Since the behaviour of flow about the bend was found to be similar, the derived smoothed splines could be scaled up to cater for the change in bend length,  $L$ , per diameter,  $D$ , ( $L/D$  ratio) with various flows when in use. As postulated, the nature or shape of the hydraulic gradient line due the bend angle is the same for different pressure drop owing to varied curvature and flow velocity. The resultant of the inner and outer pressures was successfully associated with drop of the main pressure head and connected to the straight pipe sections as desired by the research giving a graphical and mathematical solution.

## APPENDIX D: NORMALISED SMOOTH SPLINE OF EXPERIMENTAL AND THEORETICAL DATA (25mm Ø, 0.1969 ms<sup>-1</sup>)

		Outer And Inner Pressure Differential Smooth Splines For Respective Bend Angles										Resultant Smooth Spline Pressures					Cumulative Resultant Smooth Spline Pressures					
		0° Pres.Outer	0° Pres.Inner	22.5° Pres.Outer	22.5° Pres.Inner	45° Pres.Outer	45° Pres.Inner	67.5° Pres.Outer	67.5° Pres.Inner	90° Pres.Outer	90° Pres.Inner	0°	22.5°	45°	67.5°	90°	0°	22.5°	45°	67.5°	90°	
Downstream Of Bend (Bend Peripheral)	170	0.0000	0.0000	-0.0035	-0.0035	-0.0088	-0.0088	-0.0159	-0.0159	-0.0247	-0.0247	0.0000	-0.0071	-0.0176	-0.0317	-0.0494	0.0000	-0.2292	-0.5731	-1.0316	-1.6047	Normalised Smoothed Theoretical Data
	165	0.0000	0.0000	-0.0035	-0.0035	-0.0087	-0.0087	-0.0156	-0.0156	-0.0243	-0.0243	0.0000	-0.0069	-0.0174	-0.0312	-0.0486	0.0000	-0.2222	-0.5555	-0.9998	-1.5553	
	160	0.0000	0.0000	-0.0034	-0.0034	-0.0085	-0.0085	-0.0154	-0.0154	-0.0239	-0.0239	0.0000	-0.0068	-0.0171	-0.0308	-0.0478	0.0000	-0.2153	-0.5381	-0.9686	-1.5067	
	155	0.0000	0.0000	-0.0034	-0.0034	-0.0084	-0.0084	-0.0151	-0.0151	-0.0236	-0.0236	0.0000	-0.0067	-0.0168	-0.0302	-0.0471	0.0000	-0.2084	-0.5210	-0.9378	-1.4589	
	150	0.0000	0.0000	-0.0033	-0.0033	-0.0083	-0.0082	-0.0149	-0.0148	-0.0231	-0.0230	0.0000	-0.0066	-0.0165	-0.0296	-0.0461	0.0000	-0.2017	-0.5042	-0.9076	-1.4118	
	145	0.0000	0.0000	-0.0032	-0.0032	-0.0081	-0.0081	-0.0145	-0.0145	-0.0225	-0.0226	0.0000	-0.0064	-0.0161	-0.0290	-0.0451	0.0000	-0.1951	-0.4878	-0.8780	-1.3657	
	140	0.0000	0.0000	-0.0031	-0.0032	-0.0077	-0.0081	-0.0139	-0.0146	-0.0216	-0.0227	0.0000	-0.0063	-0.0158	-0.0285	-0.0443	0.0000	-0.1887	-0.4716	-0.8489	-1.3206	
	135	0.0000	0.0000	-0.0029	-0.0033	-0.0072	-0.0084	-0.0129	-0.0151	-0.0201	-0.0234	0.0000	-0.0062	-0.0156	-0.0280	-0.0436	0.0000	-0.1823	-0.4558	-0.8204	-1.2762	
	130	0.0000	0.0000	-0.0026	-0.0036	-0.0064	-0.0089	-0.0115	-0.0160	-0.0179	-0.0249	0.0000	-0.0061	-0.0153	-0.0275	-0.0428	0.0000	-0.1761	-0.4402	-0.7924	-1.2327	
	125	0.0000	0.0000	-0.0021	-0.0038	-0.0053	-0.0096	-0.0096	-0.0173	-0.0149	-0.0269	0.0000	-0.0060	-0.0149	-0.0269	-0.0418	0.0000	-0.1700	-0.4250	-0.7649	-1.1899	
	120	0.0000	0.0000	-0.0016	-0.0042	-0.0039	-0.0105	-0.0071	-0.0190	-0.0110	-0.0295	0.0000	-0.0058	-0.0145	-0.0260	-0.0405	0.0000	-0.1640	-0.4100	-0.7380	-1.1481	
	115	0.0000	0.0000	-0.0008	-0.0047	-0.0020	-0.0117	-0.0036	-0.0211	-0.0057	-0.0329	0.0000	-0.0055	-0.0138	-0.0248	-0.0385	0.0000	-0.1582	-0.3956	-0.7120	-1.1076	
	110	0.0000	0.0000	0.0003	-0.0054	0.0006	-0.0135	0.0011	-0.0243	0.0018	-0.0377	0.0000	-0.0051	-0.0129	-0.0231	-0.0360	0.0000	-0.1527	-0.3818	-0.6872	-1.0690	
	105	0.0000	0.0000	0.0016	-0.0064	0.0041	-0.0159	0.0074	-0.0287	0.0115	-0.0446	0.0000	-0.0047	-0.0118	-0.0212	-0.0331	0.0000	-0.1476	-0.3690	-0.6641	-1.0331	
Bend Section	<b>100</b>	<b>0.0000</b>	<b>0.0000</b>	<b>0.0032</b>	<b>-0.0075</b>	<b>0.0079</b>	<b>-0.0188</b>	<b>0.0143</b>	<b>-0.0339</b>	<b>0.0222</b>	<b>-0.0528</b>	<b>0.0000</b>	<b>-0.0044</b>	<b>-0.0109</b>	<b>-0.0196</b>	<b>-0.0305</b>	<b>0.0000</b>	<b>-0.1429</b>	<b>-0.3572</b>	<b>-0.6429</b>	<b>-1.0000</b>	Normalised Smoothed Experimental Data
	95	0.0000	0.0000	0.0045	-0.0087	0.0112	-0.0216	0.0202	-0.0389	0.0314	-0.0606	0.0000	-0.0042	-0.0104	-0.0188	-0.0292	0.0000	-0.1385	-0.3462	-0.6232	-0.9695	
	90	0.0000	0.0000	0.0054	-0.0095	0.0136	-0.0238	0.0244	-0.0429	0.0380	-0.0667	0.0000	-0.0041	-0.0103	-0.0185	-0.0288	0.0000	-0.1343	-0.3358	-0.6045	-0.9403	
	85	0.0000	0.0000	0.0061	-0.0102	0.0153	-0.0256	0.0276	-0.0461	0.0430	-0.0716	0.0000	-0.0041	-0.0102	-0.0184	-0.0287	0.0000	-0.1302	-0.3256	-0.5860	-0.9115	
	80	0.0000	0.0000	0.0067	-0.0109	0.0167	-0.0272	0.0300	-0.0490	0.0466	-0.0762	0.0000	-0.0042	-0.0106	-0.0190	-0.0296	0.0000	-0.1261	-0.3153	-0.5676	-0.8829	
	75	0.0000	0.0000	0.0070	-0.0115	0.0174	-0.0289	0.0314	-0.0519	0.0488	-0.0808	0.0000	-0.0046	-0.0114	-0.0205	-0.0320	0.0000	-0.1219	-0.3047	-0.5485	-0.8533	
	70	0.0000	0.0000	0.0071	-0.0122	0.0178	-0.0304	0.0320	-0.0547	0.0497	-0.0851	0.0000	-0.0051	-0.0126	-0.0228	-0.0354	0.0000	-0.1173	-0.2933	-0.5280	-0.8213	
	65	0.0000	0.0000	0.0071	-0.0126	0.0177	-0.0316	0.0319	-0.0569	0.0496	-0.0885	0.0000	-0.0056	-0.0139	-0.0250	-0.0389	0.0000	-0.1123	-0.2807	-0.5052	-0.7859	
	60	0.0000	0.0000	0.0070	-0.0130	0.0175	-0.0324	0.0316	-0.0584	0.0491	-0.0908	0.0000	-0.0060	-0.0149	-0.0268	-0.0417	0.0000	-0.1067	-0.2668	-0.4802	-0.7470	
	55	0.0000	0.0000	0.0069	-0.0132	0.0173	-0.0330	0.0311	-0.0594	0.0484	-0.0923	0.0000	-0.0063	-0.0157	-0.0282	-0.0439	0.0000	-0.1008	-0.2519	-0.4534	-0.7052	
	50	0.0000	0.0000	0.0068	-0.0134	0.0169	-0.0334	0.0305	-0.0601	0.0474	-0.0935	0.0000	-0.0066	-0.0165	-0.0296	-0.0461	0.0000	-0.0945	-0.2362	-0.4251	-0.6613	
	45	0.0000	0.0000	0.0066	-0.0135	0.0165	-0.0337	0.0297	-0.0607	0.0461	-0.0945	0.0000	-0.0069	-0.0173	-0.0311	-0.0484	0.0000	-0.0879	-0.2197	-0.3955	-0.6152	
	40	0.0000	0.0000	0.0064	-0.0136	0.0160	-0.0341	0.0288	-0.0614	0.0449	-0.0955	0.0000	-0.0072	-0.0181	-0.0325	-0.0506	0.0000	-0.0810	-0.2025	-0.3644	-0.5669	
	35	0.0000	0.0000	0.0062	-0.0138	0.0156	-0.0345	0.0280	-0.0620	0.0436	-0.0965	0.0000	-0.0076	-0.0189	-0.0340	-0.0529	0.0000	-0.0738	-0.1844	-0.3319	-0.5163	
	30	0.0000	0.0000	0.0060	-0.0139	0.0151	-0.0348	0.0272	-0.0627	0.0423	-0.0976	0.0000	-0.0079	-0.0197	-0.0355	-0.0553	0.0000	-0.0662	-0.1655	-0.2979	-0.4634	
	25	0.0000	0.0000	0.0058	-0.0140	0.0145	-0.0351	0.0262	-0.0631	0.0407	-0.0982	0.0000	-0.0082	-0.0205	-0.0370	-0.0575	0.0000	-0.0583	-0.1458	-0.2624	-0.4081	
	20	0.0000	0.0000	0.0055	-0.0139	0.0138	-0.0348	0.0249	-0.0626	0.0388	-0.0974	0.0000	-0.0084	-0.0209	-0.0377	-0.0586	0.0000	-0.0501	-0.1252	-0.2254	-0.3506	
15	0.0000	0.0000	0.0052	-0.0134	0.0129	-0.0335	0.0233	-0.0602	0.0362	-0.0937	0.0000	-0.0082	-0.0205	-0.0370	-0.0575	0.0000	-0.0417	-0.1043	-0.1877	-0.2920		
10	0.0000	0.0000	0.0046	-0.0122	0.0115	-0.0304	0.0207	-0.0548	0.0323	-0.0852	0.0000	-0.0076	-0.0189	-0.0340	-0.0529	0.0000	-0.0335	-0.0838	-0.1508	-0.2345		
5	0.0000	0.0000	0.0037	-0.0100	0.0093	-0.0251	0.0168	-0.0452	0.0262	-0.0702	0.0000	-0.0063	-0.0157	-0.0283	-0.0441	0.0000	-0.0259	-0.0648	-0.1167	-0.1816		
<b>0</b>	<b>0.0000</b>	<b>0.0000</b>	<b>0.0027</b>	<b>-0.0073</b>	<b>0.0068</b>	<b>-0.0183</b>	<b>0.0122</b>	<b>-0.0329</b>	<b>0.0190</b>	<b>-0.0512</b>	<b>0.0000</b>	<b>-0.0046</b>	<b>-0.0115</b>	<b>-0.0207</b>	<b>-0.0322</b>	<b>0.0000</b>	<b>-0.0196</b>	<b>-0.0491</b>	<b>-0.0884</b>	<b>-0.1375</b>		

		Outer And Inner Pressure Differential Smooth Splines For Respective Bend Angles										Resultant Smooth Spline Pressures					Cumulative Resultant Smooth Spline Pressures				
x	0°	0°	22.5°	22.5°	45°	45°	67.5°	67.5°	90°	90°	0°	22.5°	45°	67.5°	90°	0°	22.5°	45°	67.5°	90°	
	Pres.Outer	Pres.Inner	Pres.Outer	Pres.Inner	Pres.Outer	Pres.Inner	Pres.Outer	Pres.Inner	Pres.Outer	Pres.Inner											
Upstream Of Bend (Bend Peripheral)	-5	0.0000	0.0000	0.0018	-0.0048	0.0046	-0.0121	0.0082	-0.0218	0.0128	-0.0339	0.0000	-0.0030	-0.0076	-0.0136	-0.0211	0.0000	-0.0150	-0.0376	-0.0677	-0.1052
	-10	0.0000	0.0000	0.0012	-0.0032	0.0030	-0.0080	0.0053	-0.0144	0.0083	-0.0224	0.0000	-0.0020	-0.0050	-0.0091	-0.0141	0.0000	-0.0120	-0.0300	-0.0541	-0.0841
	-15	0.0000	0.0000	0.0007	-0.0023	0.0018	-0.0057	0.0033	-0.0103	0.0052	-0.0160	0.0000	-0.0015	-0.0038	-0.0069	-0.0108	0.0000	-0.0100	-0.0250	-0.0450	-0.0700
	-20	0.0000	0.0000	0.0004	-0.0017	0.0011	-0.0044	0.0019	-0.0079	0.0030	-0.0122	0.0000	-0.0013	-0.0033	-0.0059	-0.0092	0.0000	-0.0085	-0.0211	-0.0381	-0.0592
	-25	0.0000	0.0000	0.0002	-0.0014	0.0005	-0.0035	0.0009	-0.0062	0.0014	-0.0097	0.0000	-0.0012	-0.0029	-0.0053	-0.0083	0.0000	-0.0071	-0.0178	-0.0321	-0.0500
	-30	0.0000	0.0000	0.0000	-0.0011	0.0001	-0.0027	0.0002	-0.0049	0.0003	-0.0076	0.0000	-0.0011	-0.0026	-0.0047	-0.0074	0.0000	-0.0060	-0.0149	-0.0268	-0.0417
	-35	0.0000	0.0000	-0.0001	-0.0009	-0.0002	-0.0022	-0.0003	-0.0039	-0.0004	-0.0060	0.0000	-0.0009	-0.0023	-0.0042	-0.0065	0.0000	-0.0049	-0.0123	-0.0221	-0.0344
	-40	0.0000	0.0000	-0.0001	-0.0007	-0.0003	-0.0017	-0.0005	-0.0031	-0.0009	-0.0049	0.0000	-0.0008	-0.0020	-0.0037	-0.0057	0.0000	-0.0040	-0.0100	-0.0179	-0.0279
	-45	0.0000	0.0000	-0.0002	-0.0006	-0.0004	-0.0014	-0.0007	-0.0026	-0.0011	-0.0040	0.0000	-0.0007	-0.0018	-0.0032	-0.0050	0.0000	-0.0032	-0.0079	-0.0142	-0.0221
	-50	0.0000	0.0000	-0.0002	-0.0005	-0.0004	-0.0011	-0.0007	-0.0020	-0.0011	-0.0032	0.0000	-0.0006	-0.0015	-0.0028	-0.0043	0.0000	-0.0024	-0.0061	-0.0110	-0.0171
	-55	0.0000	0.0000	-0.0002	-0.0003	-0.0004	-0.0009	-0.0007	-0.0016	-0.0012	-0.0024	0.0000	-0.0005	-0.0013	-0.0023	-0.0036	0.0000	-0.0018	-0.0046	-0.0082	-0.0128
	-60	0.0000	0.0000	-0.0002	-0.0003	-0.0004	-0.0006	-0.0007	-0.0011	-0.0011	-0.0018	0.0000	-0.0004	-0.0010	-0.0019	-0.0029	0.0000	-0.0013	-0.0033	-0.0059	-0.0092
	-65	0.0000	0.0000	-0.0002	-0.0002	-0.0004	-0.0005	-0.0007	-0.0008	-0.0011	-0.0013	0.0000	-0.0003	-0.0008	-0.0015	-0.0024	0.0000	-0.0009	-0.0023	-0.0041	-0.0063
	-70	0.0000	0.0000	-0.0001	-0.0001	-0.0003	-0.0003	-0.0006	-0.0006	-0.0009	-0.0010	0.0000	-0.0003	-0.0007	-0.0012	-0.0019	0.0000	-0.0006	-0.0014	-0.0025	-0.0040
	-75	0.0000	0.0000	-0.0001	-0.0001	-0.0002	-0.0002	-0.0004	-0.0004	-0.0007	-0.0007	0.0000	-0.0002	-0.0005	-0.0009	-0.0014	0.0000	-0.0003	-0.0007	-0.0013	-0.0021
-80	0.0000	0.0000	-0.0001	0.0000	-0.0001	-0.0001	-0.0002	-0.0002	-0.0004	-0.0003	0.0000	-0.0001	-0.0002	-0.0004	-0.0007	0.0000	-0.0001	-0.0002	-0.0004	-0.0007	

Normalised Smoothed Theoretical Data

## **CHAPTER 5: COMPARISON OF TRADITIONAL METHODS WITH THE DEVELOPED EMPIRICAL EQUATION IN DETERMINATION OF MINOR LOSSES**

### **Abstract**

Traditional methods principally used for determination of secondary or minor losses are the Equivalent Length, Resistance Coefficient and Valve Flow Coefficient method. The problem of the use of these methods during irrigation design is the uncertainty of their accuracies considering the shortfalls identified in each method. These are fixed flow coefficient (L/D ratio), thorough knowledge of development of coefficient required for application and reliance on conversion parameters, respectively. This research aims at comparison of traditional methods, considering their shortfalls, for the extent of error involved in their estimation of minor losses with reference to a developed Empirical Equation, deemed most accurate as it caters for all the shortfalls identified in the traditional methods.

The degree of accuracy or error involved in the use of each traditional method was achieved by comparison (% difference) of the frictional losses as determined by the 19.05 mm diameter pipe published and adopted for each traditional method to the theoretical 19.05 mm pipe (Empirical Equation, as reference). This was also expanded to different friction coefficients on the same pipe diameter. Choice of pipe diameter was mainly due to availability of data points (friction coefficients) for comparison compared to other pipe diameters.

The Equivalent Length method was found to be fairly accurate for determining the secondary losses during the irrigation design stage, provided the bend length to pipe diameter (L/D) ratio relative to the flow velocity was considered in the determination of the equivalent lengths. The Resistance Coefficient method was confirmed to be the best method due to the closeness of the published friction coefficients to the theoretical 19.05 mm values. The Valve Flow Coefficient method, largely dependent on the values from the Equivalent Length and the Resistance Coefficient on for conversion if not found with respect to the changing pipe bend curvature and flow velocity. Frictional loss estimation with nearly all traditional methods was generally poor with bend angles less than 90°.

**Keywords:** *Equivalent Length, Resistance Coefficient, Valve Flow Coefficient, Minor, Secondary Loss.*

## **5.1 Introduction**

In the design of irrigation systems, there are two main components of frictional losses. These are mainly due to the fluid interactions with the straight pipe lengths and secondly the fittings, major (primary) and minor (secondary) losses, respectively (Berger *et al.*, 1983). In the determination of primary losses, there are many methods that can be used depending on the straight pipe parameters and field of application for the designer and these methods give generally the same measure of frictional losses (ARC, 2003). These methods for example the Darcy-Weisbach developed in 1845, Hazen-Williams developed in 1906, Newton-Raphson developed in 1911 or Colebrook-White developed in 1939, Moody chart developed in 1944, Wood developed in 1966, Swamee - Jain developed in 1976, Barr developed in 1981, Haaland developed in 1983, Lamont and General Exponential equation developed in 1998, on comparison give reasonably similar results and cater for different fields of application.

When determining the secondary losses there are however three traditional methods, the Equivalent Length, Resistance Coefficient and the Valve Flow Coefficient method in use for similar fields of application but there is a lot of variability in the frictional loss determined (Wilson, 2012; Neutrium, 2016). The Equivalent Length and Resistance Coefficient methods are used mainly for calculating the minor losses while the Valve Flow Coefficient method is mainly used for used determining frictional losses in valves. Conversion is often done between the Resistance and Valve Flow Coefficient method. Experimental data from these methods is often used to eliminate the cost involved in testing of all valves and fittings for use. Equivalent lengths and coefficients are available from published tables, diagrams and online from various writers as well as valve manufacturers and are associated with pipe diameters. Despite the variability in the frictional loss values as determined by the different traditional methods, they all aim to determine the best approximate of the velocity head multiplier (equivalent length or friction coefficient) for determining secondary losses (Wilson, 2012).

The Equivalent Length method is based on observations made on the determination of the primary losses, in that the frictional loss component is proportional to the velocity head. As a result an equivalent straight pipe length's pressure drop is used to represent frictional loss due to pipe bending or curvature, hence its name (Wilson, 2012). Determination of this equivalent length to be used for an extent of bending is often determined experimentally for close approximation of length. However, when using the Equivalent Length method, the approach assumes that the relative proportions of the fitting size remains constant as the pipe size varies (Neutrium, 2016). This is rarely the case in irrigation systems and as a result, there is some error in the estimation of the frictional loss due to bending or curvature. Since the flow coefficient (bend length,  $L$  / pipe diameter  $D$  ratio) decreases as the fitting size increases, the pressure drop would be overestimated at pipe sizes greater than those for which the fittings Equivalent Length was calculated. The pressure drop would also be underestimated at smaller pipe sizes than those for which the Equivalent Length was measured and this simply means the resistance coefficient (equivalent length) is constant (Neutrium, 2016). Despite these shortfalls, the Equivalent Length method has the advantage of being very easy to apply.

The Resistance Coefficient method is characterised against quite a number of varying pipe diameters, making it more reliable compared to the Equivalent Length method for use in irrigation systems design (ARC, 2003). It is, however, less reliable because it lacks the different or changing pipe geometries for fittings with various sizes (Neutrium, 2016). The Resistance Coefficient method sums up the resistance coefficients and has the objective of using a resistance coefficient as though it were the same for different diameters again, introducing inaccuracies (Perry, 1950). It was found generally that though the resistance coefficient decreased as the fitting size increased, the  $K$  value was used in the fully turbulent flow conditions and not on laminar flow by Perry (1950) to date (Wilson, 2012). In a bid to improve the friction factor  $K$ , the Crane 2 friction factor was introduced with a range of  $K$  factors for each fitting, with the provision of adjusting the  $K$  values per fitting (Wilson, 2012; Neutrium, 2016). This further complicated the use of the Resistance Coefficient method since thorough knowledge of how the  $K$  value was developed was needed for use with each change in pipe diameter. It was also discovered that at Reynolds numbers less than 2 000, there was an express increase in the  $K$  values (Silverberg, 2001).

Despite the efforts to correctly quantify the secondary losses, friction factors smaller than those obtained by the Moody, Prandtl, White-Colebrook, or Nikuradse smooth pipe rule (or Blasius law) have been calculated in large diameter pipes, according to findings in literature (Berlamont, 2014). It was shown that a small amount of rotation or swirl, such as that induced by curvature, continued downstream of the straight pipe, decreasing the apparent friction factor premeditated or predicted using the nominal Reynolds number. The Blasius rule can also hold true if the friction factor is measured using the real Reynolds number and rotation of fluid downstream of a 90° bend is taken into account. For rotation numbers less than 1 to 2, the reduction in friction factor is usually in the 5 to 10% range. Only big diameter pipes and/or high Reynolds numbers are prone to experience the phenomena.

The Valve Flow Coefficient method, though mainly used for valves  $C_v$  ( $A_v$  in the S.I. units) values can be easily converted to  $K$  values. The methods outlined earlier uses the multiplier with the velocity head term giving a likelihood of the same results with the Valve Flow Coefficient method (Wilson, 2012). The Equivalent Length and the Resistance Coefficient methods use the same or similar velocity head multiplier when predicting the frictional losses, allowing conversion between the two, considering the fitting dimensions are known in either case.

The  $C_v$  and  $K_v$  methods are used to characterize all kinds of fittings and are the most general for control valves (Neutrium, 2016). The  $C_v$ , which is provided in US gallons per minute, is equivalent to the value of the  $K_v$ , which is expressed in cubic meters per hour. Both equations are both dependent on one flow rate and apply to the same properties, which enable one to estimate the characteristics of flow at other flow rates.  $C_v = 1.157 * K_v$  and  $K_v = 0.8646 * C_v$ . For calculating the head loss using  $k$  value;  $h_L = 0.0295 * k * (Q^2/d^4)$  and  $k = f(L/D)$  (Crane, 1957).

The argument however, pertaining to the Equivalent Length and the Resistance Coefficient methods is how the equivalent length  $L_e$  for a pipe diameter  $D$ , ( $L_e/D$ ) and the resistance coefficient ( $k$ ) are compared with different Reynolds numbers and pipe roughness (Wilson, 2012). When determining the secondary losses with the above three methods, there is a lot of variability in the determined frictional losses when considering the published results (Spedding *et al.*, 2004). The resulting problem in the use of the traditional methods during the

irrigation design process is this variability, leading to the uncertainty of the accuracies or approximation of the methods, considering the shortfalls identified in each method. This research aims at comparison of the three traditional methods for specific curvature (0° to 90°) to determine their accuracy, repeatability, and reliability in the estimation of secondary losses with reference to the theoretical method developed (Empirical Equation) when using smooth pipes for irrigation design. This will allow for an appreciation of the extent of error due to the shortfalls identified in each case in the use of the traditional methods.

It is hypothesised that frictional loss estimation is generally poor for bend angles less than 90°.

## 5.2 Method of Comparison of the Frictional Loss by Traditional Methods

An Empirical Equation for determining the dynamic frictional loss coefficient,  $k$  which was expressed as a single equation for bend angles over 0° to 90° in smooth pipes for irrigation (refer to Chapter 3 for development). This was to allow irrigation system designers to calculate the  $k$  value of any bend angle with changing pipe diameter, curvature, bend length and flow. The combined mathematical relationship for the homogenous equation for the pressure loss due or frictional losses due to a bend was then expressed as follows:

$$\Delta P = k * \frac{v^2}{2g} \quad (5.1)$$

Wherein (refer to Chapter 3 for derivation).

$$k = f(\theta, D, L, r) \quad (5.2)$$

With

$$k = \frac{g(D)_{new\ pipe\ diameter}}{g(D)_{wrt\ 19.05mm, R_c=1, 90^\circ}} * h(R_c)_{wrt\ R_c=new, 90^\circ} * g(D)_{wrt\ 19.05mm, R_c=1, 90^\circ} * \frac{p(\theta)_{wrt\ \theta}}{p(\theta)_{wrt\ 90^\circ}} \quad (5.3)$$

Then

$$\Delta P = \left( \frac{g(D)_{new\ pipe\ diameter}}{g(D)_{wrt\ 19.05mm, R_c=1, 90^\circ}} * h(R_c)_{wrt\ R_c=new, 90^\circ} * g(D)_{wrt\ 19.05mm, R_c=1, 90^\circ} * \frac{p(\theta)_{wrt\ \theta}}{p(\theta)_{wrt\ 90^\circ}} \right) \frac{V^2}{2g} \quad (5.4)$$

Wherein (refer to Chapter 3 for derivation)

$$p(\theta) = 4.869e^{-05}\theta^2 + 0.003287\theta + 0.0493 \quad (5.5)$$

*Goodness of fit: SSE: 1.676e<sup>-31</sup>; Adjusted R-square: 1; RMSE: 2.895e<sup>-16</sup>*

$$g(D) = 1.487D^{-0.2862} + 0.09968 \quad (5.6)$$

*Goodness of fit: SSE: 0.0008363; Adjusted R-square: 0.9956; RMSE: 0.009639*

$$h(R_c) = \frac{(4.02R_c^2 - 11.07R_c + 29.93)}{(R_c^2 + 18.53R_c + 11.41)} \quad (5.7)$$

*Goodness of fit: SSE: 2.184e<sup>-13</sup>; Adjusted R-square: 1; RMSE: 2.165e<sup>-08</sup>*

With condition

$g(D)_{wrt\ 19.05mm, R_c=1, 90^\circ} = 1$  and  $\frac{g(D)_{new\ pipe\ diameter}}{g(D)_{wrt\ 19.05mm, R_c=1, 90^\circ}}$  remains applicable only when  $D = 19.05\ mm$  and  $R_c$  remains 1.

Derivation of the Empirical Equation was based on experimental data and the published data on the Resistance Coefficient method, validating it, and deemed most accurate method. The Empirical Equation catered for the change in the bend length per diameter ratio and ease of application, which was found to be missing in the traditional methods. The Equation also took in to account the changes in the relative radius of curvature and thus all the shortfalls in the traditional methods. It was then made the reference or point of departure in determining secondary losses during the comparison to correctly bring about the error involved in the use of each of the traditional methods as well as the possible conversion between the three methods.

The use of the Empirical Equation allowed for determination of frictional losses due to bending within ranges outside and between the pragmatic tests done, and those of the published literature. This allowed for comparison of the different equivalent lengths and coefficients published. Comparison of the traditional methods was however done using the

same pipe diameter and curvature for the published data since the friction coefficient was found to be constant for a fixed pipe diameter and relative radius of curvature,  $R_c$ . The 19.05 mm pipe diameter was chosen since it had the most data sets from published literature on all traditional methods, giving more information on the comparisons made. Table 5.1 shows the friction coefficients with the Empirical Equation in the determination of frictional losses within and above the allowable flow velocities in irrigation systems for comparison.

**Table 5.1 Empirical Equation friction coefficients for the 19.05 mm diameter pipe used for comparison of the frictional losses**

Short radius						Standard radius					Long radius				
0°	22.0°	22.5°	45°	67.5°	90°	0°	22.5°	45°	67.5°	90°	0°	22.5°	45°	67.5°	90°
0.060	0.176	0.180	0.359	0.598	0.898	0.049	0.148	0.296	0.493	0.739	0.027	0.080	0.160	0.266	0.399

Comparison with the Empirical Equation was done individually for each of the traditional method to give the percentage error or difference (for smooth pipes with roughness of 0.03) in the frictional losses determined for the chosen 19.05 mm diameter. This was then expanded to the different published equivalent lengths or coefficients for the same pipe diameter. Based on these differences, it could then be found to what extent correction of the traditional method would need and the error in the derivation of the equivalent lengths and coefficients in the absence of experimental data and conversion as and when required. Tables 5.2 to 5.4 show the published equivalent lengths and friction coefficients used in the comparisons of the traditional methods.

**Table 5.2 Equivalent lengths (L/D values) for the 19.05 mm diameter pipe used for comparison of the frictional losses wherein  $h_f = f (L/D)V^2/2g$**

Short radius						Standard radius						Long radius						Source
0°	22.0°	22.5°	45°	67.5°	90°	0°	22°	22.5°	45°	67.5°	90°	0°	22°	22.5°	45°	67.5°	90°	
-	9	-	18	-	45	-	7	-	14	-	34	-	5	-	9	-	18	(ARC, 2003)
-	-	-	-	-	-	-	-	-	16	-	30	-	-	-	-	-	16	Spedding <i>et al.</i> , 2004)
-	-	-	-	-	-	-	-	-	16	-	30	-	-	-	-	-	16	(Neutrium, 2016)

**Table 5.3 Resistance coefficients ( $k$  values) for the 19.05 mm diameter pipe used for comparison of the frictional losses wherein  $h_f = kV^2/2g$**

Short radius					Standard radius					Long radius					Source
0°	22.5°	45°	67.5°	90°	0°	22.5°	45°	67.5°	90°	0°	22.5°	45°	67.5°	90°	
-	-	-	-	0.90	-	0.15	0.30	-	0.75	-	-	-	-	0.40	(ARC, 2003)
-	-	-	-	-	-	-	0.40	-	0.75	-	-	-	-	0.40	Spedding <i>et al.</i> , 2004)
-	-	-	-	0.90	-	-	0.35	-	0.75	-	-	0.2	-	0.45	(Neutrium, 2016)

**Table 5.4 Valve flow coefficients ( $k$  values) for the 19.05 mm diameter pipe used for comparison of frictional losses wherein  $C_v = 1.157K_v$ ,  $K_v = 0.8646C_v$ ;  $h_L = 0.0295 k Q^2/d^4$**

Short radius					Standard radius					Long radius					Source
0°	22.5°	45°	67.5°	90°	0°	22.5°	45°	67.5°	90°	0°	22.5°	45°	67.5°	90°	
-	-	-	-	-	-	-	-	-	-	-	-	-	-	-	(ARC, 2003)
-	-	-	-	-	-	-	-	-	-	-	-	-	-	-	Spedding <i>et al.</i> , 2004)
-	-	-	-	-	-	-	1.1	-	2.06	-	-	-	-	1.1	(Neutrium, 2016)

### 5.3 Results and Discussion

The variances found for the Equivalent Length, Resistance Coefficient, and the Valve Flow Coefficient Method in the determination of minor or secondary losses is presented and discussed in the following subsections.

#### 5.3.1 Equivalent Length Method

Looking at the comparisons made on the minor loss as generated by the Empirical Equation and the Equivalent Length method as summarised in Table 5.5 for the available published experimental data, there are generally large differences in the estimation of the frictional loss looking at the 90° bends. Clearly there were over estimations when coming up with the equivalent length as derived from the principle of pressure loss as in the straight pipe.

**Table 5.5 Comparison of head losses as determined by the Empirical Equation and the Equivalent Length method for the 19.05 mm diameter pipe**

Short radius						Standard radius						Long radius						
0°	22.0°	22.5°	45°	67.5°	90°	0°	22°	22.5°	45°	67.5°	90°	0°	22°	22.5°	45°	67.5°	90°	
-	9	-	18	-	45	-	7	-	14	-	34	-	5	-	9	-	18	<b>(ARC, 2003)</b>
-	53.231%	-	50.406%	-	50.409%	-	41.986%	-	41.986%	-	37.932%	-	-6.018%	-	-32.332%	-	35.336%	Accuracy / Difference
-	-	-	-	-	-	-	-	-	16	-	30	-	-	-	-	-	16	<b>(Spedding et al., 2004)</b>
-	-	-	-	-	-	-	-	-	62.270%	-	-35.091%	-	-	-	-	-	20.298%	Accuracy / Difference
-	-	-	-	-	-	-	-	-	16	-	30	-	-	-	-	-	16	<b>(Neutrium, 2016)</b>
-	-	-	-	-	-	-	-	-	62.270%	-	-35.091%	-	-	-	-	-	20.298%	Accuracy / Difference
$h_f = f \cdot L/D \cdot V^2/2g,$ <b>(L/D) values following corresponding accuracies on comparison with the Empirical Equation</b>																		

Since the flow coefficient ( $L/D$  ratio) decreases as the fittings size increases, the pressure drop was generally overestimated at pipe sizes greater than those for which the pipe equivalent length was calculated (Table 5.5). This was the case since most pipes tested for the published results were limited to the small sizes (less than 19.05 mm) that could be handled. This left the bigger pipe (larger than 19.05 mm) subject to scaling up to get the equivalent lengths. As pipes become too small, testing also becomes less accurate again leaving users and others to scale down the equivalent lengths again. This generally results in the underestimating of the equivalent length at smaller pipe sizes than those for which the equivalent length was calculated.

From the results (Table 5.5), more deviation or error is seen with the Standard radius bend. Accuracy or approximation of the minor losses is much poorer as we reduce the bend angle (from the  $90^\circ$  to the  $45^\circ$  bends shown). This is the case coupled with the uncertainties involved in finding the equivalent length. The converse is seen on the long radius, giving the lesser or least error of the three sets of data available for comparison. It is clear there was no consideration of the change in the  $L/D$  ratio, introducing significant inaccuracies with the use of the Equivalent length method.

From the  $90^\circ$  Standard and Long radius results, though scaled without the consideration of the  $L/D$  ratio (seen to introduce the inaccuracies in the traditional method ) but using only roughness and Reynolds number (likely to vary from the conditions used to characterize the fitting), the approach can be considered fairly reliable as deemed by Spedding *et al.* (2004) and Neutrium (2016). This is particularly in the case when the  $L/D$  ratio is nearly the same for a pipe diameter in question as that for which the equivalent length would have been derived.

The Equivalent Length method however has the advantage of being very easy to calculate the minor loss component, provided the pragmatic values (equivalent lengths) are available. Both pipe runs (straight pipe sections) and fittings (bends) can be added together to form a single total length, from which the overall pressure loss can be determined. Unfortunately, despite this advantage, inaccurate determination of the equivalent length due to the constant  $L/D$  ratio as seen in the comparison renders the method erroneous. Iterations or goal seeking in MS Excel can however be done with reference to the Empirical Equation to deduce the correct

equivalent length for use in the event that there is need to use the equivalent length repeatedly elsewhere (See Appendix F).

The uncertainty in the Equivalent Length method to date has left irrigation designers to apply the general rule of thumb which states that for 90° bends, pressure drop due to a pipe bend is equal to a pipe length of 30 to 50 diameters in excess of the length of the straight pipe as given by Spedding *et al.* (2004). This however introduces gross inaccuracies as seen by the results of the comparison.

### 5.3.2 Resistance Coefficient Method

On comparison, there was nearly insignificant variation of the frictional losses determined by the Resistance Coefficient method when compared with the Empirical Equation. Results for the comparison are tabulated in Table 5.6.

**Table 5.6 Comparison of head losses as determined by the Empirical Equation Empirical Equation and the Resistance Coefficient method for the 19.05 mm diameter pipe**

Short radius					Standard radius					Long radius					
0°	22.5°	45°	67.5°	90°	0°	22.5°	45°	67.5°	90°	0°	22.5°	45°	67.5°	90°	
-	-	-	-	0.90	-	0.15	0.30	-	0.75	-	-	-	-	0.40	<b>(ARC, 2003)</b>
-	-	-	-	0.272%	-	1.418%	1.419%	-	1.420%	-	-	-	-	0.249%	Accuracy / Difference
-	-	-	-	-	-	-	0.40	-	0.75	-	-	-	-	0.40	<b>(Spedding et al., 2004)</b>
-	-	-	-	-	-	-	35.225%	-	1.420%	-	-	-	-	0.249%	Accuracy / Difference
-	-	-	-	0.90	-	-	0.35	-	0.75	-	-	0.2	-	0.45	<b>(Neutrium, 2016)</b>
-	-	-	-	0.272%	-	-	18.322%	-	1.420%	-	-	25.309%	-	12.780%	Accuracy / Difference
<b><math>h_f = kv^2/2g,</math></b>															
<b><math>k</math> values following corresponding accuracies on comparison with the Empirical Equation</b>															

With the exception of the Standard and Long radius 45° bends as deemed by Spedding *et al.* (2004) and Neutrium (2016), the closeness of the theoretical Empirical Equation frictional loss to the published Resistance Coefficient method results reaffirms the accuracy of the Resistance Coefficient methods compared to all the other methods, also making it a good reference for comparison. It can also be seen that there was consideration of the changing bend parameters on the published coefficients that is the changing curvature as considered by the Empirical Equation (the reference deem most accurate estimate).

Using the published resistance coefficients would give good close estimates of the frictional losses due to bending when designing irrigation systems. The only limitation would be the availability of the correct published coefficients with changing pipe diameters as well as curvature. This is however catered for in the use of the Empirical Equation.

### 5.3.3 Valve Flow Coefficient

Considering the Standard and Long radius 90° bends compared, it can be agreed from the comparisons made that the method is fairly accurate but underestimates the losses. Results are tabulated Table 5.7.

**Table 5.7 Comparison of head losses as determined by the Empirical Equation Empirical Equation and the Valve Flow Coefficient Method for the 19.05 mm diameter pipe**

Short radius					Standard radius					Long radius					
0°	22.5°	45°	67.5°	90°	0°	22.5°	45°	67.5°	90°	0°	22.5°	45°	67.5°	90°	
-	-	-	-	-	-	-	1.1	-	2.06	-	-	-	-	1.1	(Neutrium, 2016)
-	-	-	-	-	-	-	32.767%	-	-0.544%	-	-	-	-	-1.574%	Accuracy / Difference
$C_v = 1.157K_v$ and $K_v = 0.8646C_v$ ; $h_L = 0.0295 K Q^2/d^4$ , <b>K values following corresponding accuracies on comparison with the Empirical Equation</b>															

Accuracy of the method is seen to continue to underestimate as we continue to increase the relative radius of curvature from the Standard to the Long Radius bend.

Clearly from the 45° Standard radius bend, over estimation is seen for lower levels of bending (smaller bend angle). This again is largely due to the uncertainties with the reduced size of

the fittings. The Valve Flow Coefficient methods' poor estimates when applied to the bends can again simply be corrected using iterations from values obtained from the Empirical Equation for use in instances wherein it may be required repeatedly (See Appendix F).

Much of the comparison with all the traditional methods was achieved for the Standard bend despite the limited data. Fairly good comparison was achieved to check the accuracy of the tradition methods on the Long and Short radius bend only for the 90° bends though the absence of equivalent lengths and coefficients for bend angles less than 90°.

Despite the complexity of using the  $k$  values published for the Resistance Coefficient method compared to the findings of the Empirical Equation, the reliance of the Valve Flow method for the conversion of the Resistance Coefficient shows that moving to the Valve Flow method slightly under predicts the determination of minor losses. This leaves room for error but reasonably acceptable and better corrected using the Empirical Equation. This further justifies the use of the Empirical equation and derivation of coefficients for use in the Valve Flow Coefficient method for repeated use (Equation 5.4 or Appendix F again).

In the comparisons made with reference to the Empirical Equation, generally there were significant differences for the frictional losses estimated with the Equivalent Length method. Losses were nearly the same with the Resistance Coefficient method, accenting the accuracy of the method. For the Valve Flow Coefficient method frictional losses were nearly the same but quite varied in some instances. Frictional loss estimations were some somewhat poor for the Equivalent Length and the Valve Flow Coefficient method for bend angles less than 90° as postulated.

## **5.4 Conclusions**

The use of the Empirical Equation as a reference allowed for the comparison of all the traditional methods even with the absence of the corresponding equivalent lengths and coefficients from different sources published since the Empirical Equation catered for determination of values within and outside the published. The equivalent lengths and coefficients for the 90° bend were much close for the published experimental results compared to the Empirical Equation for the lower angles. This showed that the traditional

methods are fairly accurate for the 90° bend with limitation for use when there are changing flow coefficients or bend parameters.

Comparison of the three traditional methods for different curvature determined their accuracy or extent of error, repeatability, and reliability in estimation of secondary losses with reference to the theoretical method developed when using smooth pipes for irrigation design. This allowed for an appreciation of the extent of the shortfalls identified in each case of the traditional methods.

With the chosen reference of the Empirical Equation, generally the Resistance Coefficient method proved to be the most accurate. This is followed by the Valve Flow Coefficient method and lastly the Equivalent Length method. In all the traditional methods, significant error was picked when estimation of the bend angles was anything less than the 90° as postulated. This gap in essences is filled by the developed Empirical Equation.

**APPENDIX E: FRICTIONAL LOSSES AS DETERMINED BY EMPIRICAL EQUATION FOR THE 19.05 mm DIAMETER PIPE**

	Velocity (ms <sup>-1</sup> )	Short radius						Standard radius					Long radius							
		0°	22.0°	22.5°	45°	67.5°	90°	0°	22.5°	45°	67.5°	90°	0°	22.5°	45°	67.5°	90°			
Allowable flow for irrigation ↑	0.0328	3.29E-06	9.67E-06	9.86E-06	1.97E-05	3.29E-05	4.93E-05	2.71E-06	8.12E-06	1.62E-05	2.71E-05	4.06E-05	1.46E-06	4.38E-06	8.76E-06	1.46E-05	2.19E-05			
	0.0393	4.71E-06	1.39E-05	1.41E-05	2.83E-05	4.71E-05	7.07E-05	3.88E-06	1.16E-05	2.33E-05	3.88E-05	5.82E-05	2.09E-06	6.28E-06	1.26E-05	2.09E-05	3.14E-05			
	0.0472	6.78E-06	2.00E-05	2.03E-05	4.07E-05	6.78E-05	1.02E-04	5.59E-06	1.68E-05	3.35E-05	5.59E-05	8.38E-05	3.02E-06	9.05E-06	1.81E-05	3.02E-05	4.52E-05			
	0.0550	9.23E-06	2.72E-05	2.77E-05	5.54E-05	9.23E-05	1.38E-04	7.61E-06	2.28E-05	4.56E-05	7.61E-05	1.14E-04	4.10E-06	1.23E-05	2.46E-05	4.10E-05	6.16E-05			
	0.0629	1.21E-05	3.55E-05	3.62E-05	7.23E-05	1.21E-04	1.81E-04	9.93E-06	2.98E-05	5.96E-05	9.93E-05	1.49E-04	5.36E-06	1.61E-05	3.22E-05	5.36E-05	8.04E-05			
	0.0656	1.31E-05	3.87E-05	3.94E-05	7.88E-05	1.31E-04	1.97E-04	1.08E-05	3.25E-05	6.50E-05	1.08E-04	1.62E-04	5.84E-06	1.75E-05	3.51E-05	5.84E-05	8.76E-05			
	0.0707	1.53E-05	4.49E-05	4.58E-05	9.16E-05	1.53E-04	2.29E-04	1.26E-05	3.77E-05	7.54E-05	1.26E-04	1.89E-04	6.78E-06	2.04E-05	4.07E-05	6.78E-05	1.02E-04			
	0.0786	1.88E-05	5.55E-05	5.65E-05	1.13E-04	1.88E-04	2.83E-04	1.55E-05	4.66E-05	9.31E-05	1.55E-04	2.33E-04	8.38E-06	2.51E-05	5.03E-05	8.38E-05	1.26E-04			
	0.0865	2.28E-05	6.71E-05	6.84E-05	1.37E-04	2.28E-04	3.42E-04	1.88E-05	5.63E-05	1.13E-04	1.88E-04	2.82E-04	1.01E-05	3.04E-05	6.08E-05	1.01E-04	1.52E-04			
	0.0985	2.96E-05	8.71E-05	8.87E-05	1.77E-04	2.96E-04	4.44E-04	2.44E-05	7.31E-05	1.46E-04	2.44E-04	3.65E-04	1.31E-05	3.94E-05	7.89E-05	1.31E-04	1.97E-04			
	0.1313	5.26E-05	1.55E-04	1.58E-04	3.15E-04	5.26E-04	7.88E-04	4.33E-05	1.30E-04	2.60E-04	4.33E-04	6.50E-04	2.34E-05	7.01E-05	1.40E-04	2.34E-04	3.51E-04			
	0.1641	8.21E-05	2.42E-04	2.46E-04	4.93E-04	8.21E-04	1.23E-03	6.77E-05	2.03E-04	4.06E-04	6.77E-04	1.02E-03	3.65E-05	1.10E-04	2.19E-04	3.65E-04	5.48E-04			
	0.1969	1.18E-04	3.48E-04	3.55E-04	7.10E-04	1.18E-03	1.77E-03	9.74E-05	2.92E-04	5.85E-04	9.74E-04	1.46E-03	5.26E-05	1.58E-04	3.15E-04	5.26E-04	7.89E-04			
	0.2297	1.61E-04	4.74E-04	4.83E-04	9.66E-04	1.61E-03	2.41E-03	1.33E-04	3.98E-04	7.96E-04	1.33E-03	1.99E-03	7.16E-05	2.15E-04	4.29E-04	7.16E-04	1.07E-03			
	0.2626	2.10E-04	6.19E-04	6.31E-04	1.26E-03	2.10E-03	3.15E-03	1.73E-04	5.20E-04	1.04E-03	1.73E-03	2.60E-03	9.35E-05	2.80E-04	5.61E-04	9.35E-04	1.40E-03			
	0.2713	2.24E-04	6.61E-04	6.73E-04	1.35E-03	2.24E-03	3.37E-03	1.85E-04	5.55E-04	1.11E-03	1.85E-03	2.77E-03	9.98E-05	2.99E-04	5.99E-04	9.98E-04	1.50E-03			
	0.5426	8.98E-04	2.64E-03	2.69E-03	5.39E-03	8.98E-03	1.35E-02	7.40E-04	2.22E-03	4.44E-03	7.40E-03	1.11E-02	3.99E-04	1.20E-03	2.39E-03	3.99E-03	5.99E-03			
	0.8139	2.02E-03	5.95E-03	6.06E-03	1.21E-02	2.02E-02	3.03E-02	1.66E-03	4.99E-03	9.99E-03	1.66E-02	2.50E-02	8.98E-04	2.69E-03	5.39E-03	8.98E-03	1.35E-02			
	1	3.05E-03	8.98E-03	9.15E-03	1.83E-02	3.05E-02	4.57E-02	2.51E-03	7.54E-03	1.51E-02	2.51E-02	3.77E-02	1.36E-03	4.07E-03	8.13E-03	1.36E-02	2.03E-02			
2	1.22E-02	3.59E-02	3.66E-02	7.32E-02	1.22E-01	1.83E-01	1.01E-02	3.02E-02	6.03E-02	1.01E-01	1.51E-01	5.42E-03	1.63E-02	3.25E-02	5.42E-02	8.13E-02				
3	2.74E-02	8.08E-02	8.23E-02	1.65E-01	2.74E-01	4.12E-01	2.26E-02	6.78E-02	1.36E-01	2.26E-01	3.39E-01	1.22E-02	3.66E-02	7.32E-02	1.22E-01	1.83E-01				
Above allowable flow ↓	4	4.88E-02	1.44E-01	1.46E-01	2.93E-01	4.88E-01	7.32E-01	4.02E-02	1.21E-01	2.41E-01	4.02E-01	6.03E-01	2.17E-02	6.51E-02	1.30E-01	2.17E-01	3.25E-01			
	5	7.62E-02	2.25E-01	2.29E-01	4.57E-01	7.62E-01	1.14E+00	6.28E-02	1.88E-01	3.77E-01	6.28E-01	9.42E-01	3.39E-02	1.02E-01	2.03E-01	3.39E-01	5.08E-01			
		R <sub>c</sub> at 90°						0.5	R <sub>c</sub> at 90°					1	R <sub>c</sub> at 90°					1.5
		Pipe diameter (mm)						19.05	Pipe diameter (mm)					19.05	Pipe diameter (mm)					19.05
	<b>Theoretical friction coefficients for 19.05mm pipe</b>	<b>0.060</b>	<b>0.176</b>	<b>0.180</b>	<b>0.359</b>	<b>0.598</b>	<b>0.898</b>	<b>0.049</b>	<b>0.148</b>	<b>0.296</b>	<b>0.493</b>	<b>0.739</b>	<b>0.027</b>	<b>0.080</b>	<b>0.160</b>	<b>0.266</b>	<b>0.399</b>			

**APPENDIX F: EMPIRICAL EQUATION CALCULATOR BASED ON THE THEORETICAL 19.05 mm DIAMETER PIPE**



Empirical Equation  
Calculator.xlsx

## CHAPTER 6: EFFECT OF TWO PHASE FLOW, SLOPE AND PLANE ON THE BEND PRESSURE LOSS

### Abstract

Irrigation systems normally operate using single phase flow for efficient hydraulic conveyance of water. This however is not always the case as the introduction of air into the system results in two phase flow. Two phase flow also has the potential of flow reversal and increased pressure drop with further complexities on introduction of slope and plane of the bend. This research aims at determination of pressure losses due to the change from single to two phase flow and the effect of slope and plane on bends as they are essential in the design of irrigation systems and installation of air relief valves.

Experimental tests were conducted to check the influence of two phase flow (air and water) and the influence of slope and plane on pressure drop with successive pipe bending,  $0^\circ$ ,  $22.5^\circ$ ,  $45^\circ$  and to  $90^\circ$ , with different pipe sizes as the case with irrigation systems. Three pipe diameters 10 mm (8 mm ID), 25 mm (23 mm ID), and 50 mm (47 mm ID) were fed from a 100 mm (97 mm ID) pipe to assess pressure drop due to two phase flow and single phase flow for change in slope and plane of the bend(s).

Experimental results showed that pressure drop increased on introduction of two phase flow. Pressure drop was more with lower levels of bending than at higher levels of bending that is more pressure drop at  $0^\circ$  (straight pipe) than at  $90^\circ$  bending. Despite the different pipe sizes used, at low flow velocities the effect of pressure drop due to bending is superseded by the influence of two phase flow. With higher flows, the pressure loss due to two phase flow was less significant for the same extent of bending. For the bend angles tested, the change in the slope and the change in plane was found to have no effect on the pressure drop. Pressure drop was seen to change relative to the liquid depth or level to hydrostatic pressure relative to the bend position. Considering design of irrigation systems, air should be eliminated in the normal operation of an irrigation system to reduce the increase in minor losses and potential water hammer. The effect of change in slope and plane on bends in an irrigation system can be considered catered for in the rise and fall from natural ground of the straight pipe sections as considered during the design process calculations.

**Keywords:** *Single phase flow, Bend angle, Pressure drop, Bend angle, Irrigation system.*

## 6.1 Introduction

In the normal operation of an irrigation system, air can potentially be introduced into the system from the suction side, fall in the supply line level with air leaking into pipe line, due to build-up of air in the irrigation water chemically and at times due to cavitation at pump. These conditions inevitably change the fluid flow state from single phase to two phase flow. To prevent pipe splits due to the enormous pressures that very rapid air compression can produce due to two phase flow, close attention to this problem is needed (Izquierdo *et al.*, 1999). However the use of air valves in irrigation systems strives to keep it in the single phase state to avoid air pockets from being trapped in pipes, reducing the efficient pipe cross-section and increasing energy loss (Pozos *et al.*, 2010).

In the event of two phase flow in an irrigation system the key variables in the flow are the same as in single phase flow, with the exception of the mass and void fraction. Mass is conserved when irrigation water runs into the bend or fitting, and the mechanism is adiabatic (Azzi and Friedel, 2005). Two phase flow around a bend is synonymous with a centrifugal-force-induced stratification of the two phases, as well as a mechanism of bubble migration in the internal side of the bend (Jayanti, 2011).

The heavier phase of the flow migrates to the outside of the bend due to the dynamic interaction of the fluid, centrifugal forces, viscous, surface tension, adhesion and gravitational forces, a phenomenon known as film inversion (Azzi and Friedel, 2005). In the case of bubble or slug flow in a vertical curve, gas was observed flowing on the inner side of the bend due to the balance of centrifugal forces pushing the liquid to the outside and gravity pulling it back. In the experiment conducted, it was assumed that the flow was well formed because of the usage of large inlet and outlet pipes (Azzi and Friedel, 2005).

Single phase pressure drop and flow pattern were tested in an upward, lateral, and downward arrangement with a 90° bend. The friction effect due to the 90° bend was found to be greater than that of a straight pipe length for the same Reynolds number in single phase flow

(Buscher, 2019). The friction factor for a bend with a smaller curvature ratio ( $2R_b/D$ ) was found to be higher than for a bend with a larger curvature ratio. Owing to the swirled motion and liquid flow reversal in the bent pipe, the pressure decrease in the upward structure of the  $90^\circ$  bend was greater than that in the horizontal setup for two phase pressure drop (Hsu *et al.*, 2015). However, only basic flow patterns (Reynolds number) and pressure gradients occurred in the upward configuration, whereas none occurred in the downward configuration.

Because of the rising flow inertia, the gap in pressure decreases for all three scenarios became negligible as the mass flux and efficiency rose (two phase to single phase). The larger pipe diameter used in the test caused further liquid flow reversal, but there were maximum velocities in each situation after which no more liquid flow reversal occurred. For a 5.5 mm diameter bent pipe, the threshold flow velocities were found to be  $2 \text{ ms}^{-1}$  and for a 5.9 mm diameter pipe bend,  $4 \text{ ms}^{-1}$  (Ghajar and Bhagwat, 2013).

In some experiments conducted on the  $90^\circ$  bend with a horizontal inlet and upward outlet, the frictional losses were equivalent to those in the reverse flow, that is, a vertical inlet and a horizontal outlet. A 35% reduction in frictional loss was observed at the bend in the case of a horizontal inlet and downward outlet (Deobald, 1962). An inquiry into the plane's impact on the bend was also conducted. Frictional losses were observed to be 30% lower in the vertical plane than in the horizontal plane on a  $90^\circ$  bend (Grant and Cotchin, 1989).

Pressure drop due to the secondary losses contributes significantly to the design of irrigation systems. Uncertainty in the determination of these losses can result in the problem of over and under estimation of the losses in the irrigation design process. Despite the pressure drop often calculated due to single phase flow, it is necessary for the determination of losses due to two phase flow with the introduction of air to understand the extent of possible failure of an irrigation system. This will eliminate the problem of a just failing irrigation system over its useful life. It is also essential that thought flow may remain single phase, the effect of slope and plane on the bend be understood for application in the design of irrigation systems. This research aims at determination of pressure losses due to two phase flow and the effect of slope and plane on bends.

It is hypothesised though two phase flow causes increased pressure drop, at low flow velocities the effect of pressure drop due to bending is supplanted by the influence of two phase flow and at higher flows, the pressure loss due to two phase flow is less significant for the same extent of bending.

## **6.2 Materials and Methods**

The study laboratory, experimental materials, apparatus, and experimental methodology looked at in the following subsections.

### **6.2.1 Study Laboratory**

Experimental work was undertaken at the Agricultural Research Council – Institute for Agricultural Engineering (ARC-IAE) HydroLab, one of the accredited laboratories in South Africa.

### **6.2.2 Experimental Materials and Apparatus**

During each test procedure for single phase flow, water was fed into three pipe diameters 10 mm (8 mm ID), 25 mm (23 mm ID), and 50 mm (47 mm ID) from a 100 mm (97 mm ID) pipe to assess pressure drop due to successive pipe bending  $0^\circ$ ,  $22.5^\circ$ ,  $45^\circ$ ,  $67.5^\circ$ , and up to  $90^\circ$  for a one meter bend section. The flow rate was varied at intervals of  $0.0000136\text{m}^3\text{s}^{-1}$  to  $0.0001500\text{m}^3\text{s}^{-1}$  and measured using a flow meter (ZJ-LCD-M Digital Display Water Flow Sensor Meter, 0.01 LPM, 1% accuracy). Figure 6.1 shows the schematic diagram of the test configuration.

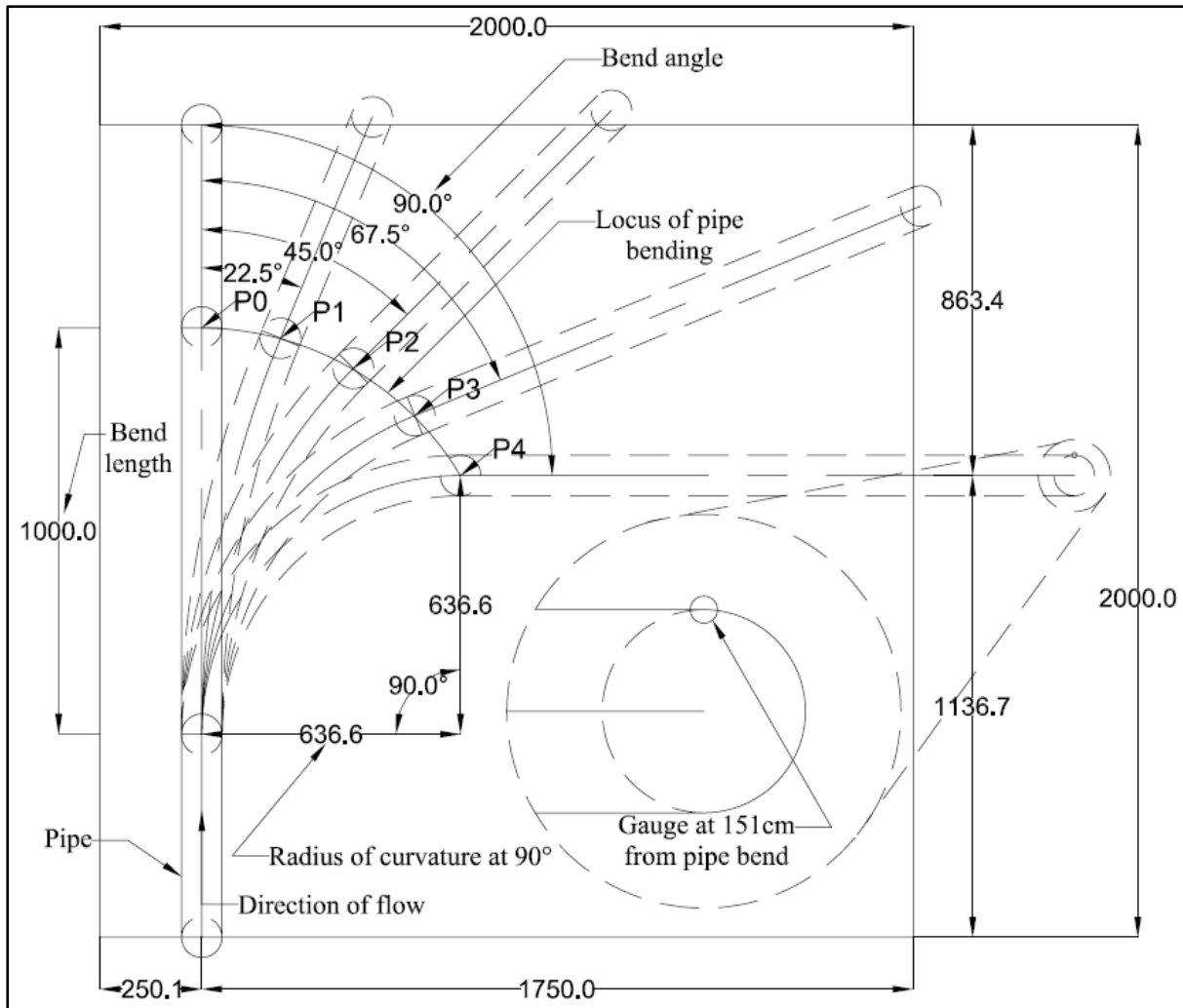


**Figure 6.1 Experimental test configuration for pressure drop due to two phase flow and single phase flow for change in slope and plane with successive pipe bending 0° to 90°**

Bending was applied in stages with the bend angle changing as the pipe moved along the locus of points P0, P1, P2, P3, and P4 with fixed bend length as seen above. Pressure drop was then measured with varying flow velocities for each pipe diameter using the WIKA CPG1500 series precision optical pneumatic pressure gauge (-1 to +5 ×10<sup>2</sup> kPa 0.1 % accuracy). Pressure drop measurements were taken at points 151 cm from each bend in question with the successive pipe bending for single phase and two phase tests conducted.

### 6.2.3 Experimental Methodology

Pressure drop due to bending was done firstly for single phase flow and then done for the two phase flows with apparatus on level ground to achieve a maximum bending of 90° that is

with no slope and no change of plane. In the case of the two phase flow, air was introduced using the Argon flow meter from a compressor unit into the setup before the water supply flow meter at  $0.0004167 \text{ m}^3\text{s}^{-1}$  and the water supply regulated to meet the required varied flow at  $0.0000136 \text{ m}^3\text{s}^{-1}$  intervals up to  $0.0001500 \text{ m}^3\text{s}^{-1}$ .

For testing the effect of slope and the change of plane, flow through the apparatus was restricted to single phase flow for chosen three flows due to the randomness of the pressure readings when air was introduced. Slope was varied from  $0^\circ$  (horizontal) to  $+90^\circ$  (vertical upwards) and  $-90^\circ$  (vertical downward) from the level ground with no change in plane. The plane of the bend was then independently tested again at  $0^\circ$  (horizontal) to  $-90^\circ$  (vertical upwards) and  $+90^\circ$  (vertical downward) from the level ground. The schematic diagram Figure 6.2 shows the slope and plane tested for successive pipe bending with reference to the level ground from the straight pipe conditions.

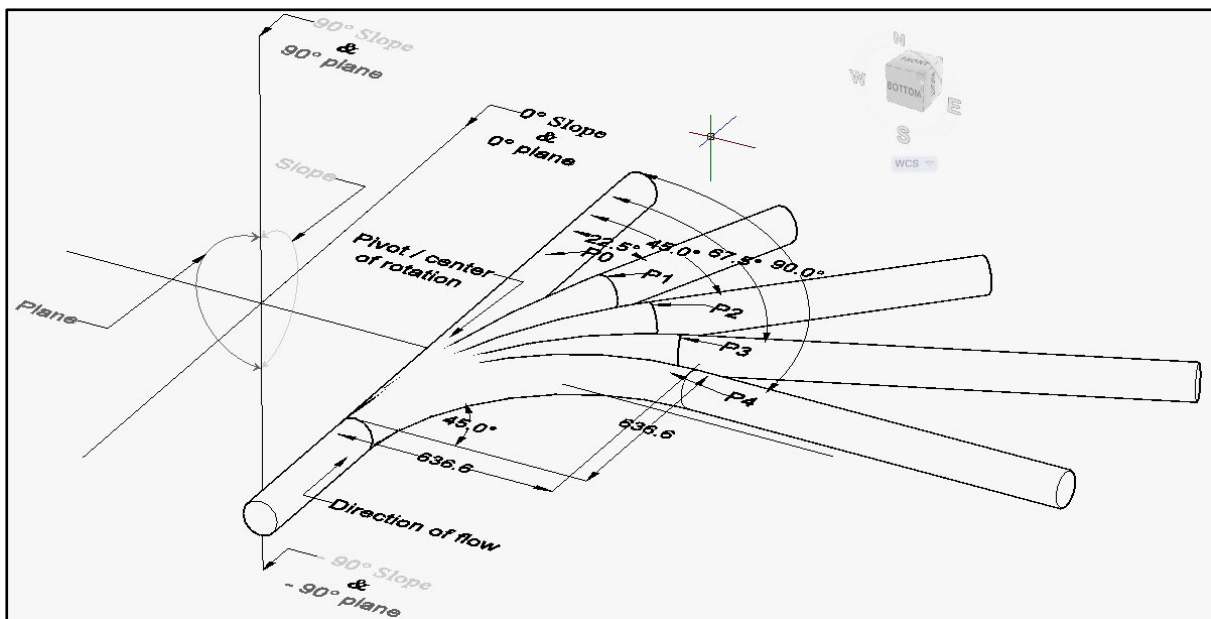


**Figure 6.2 Independent slope and plane tested for pressure drop with single phase flow for successive pipe bending**

The fluid was not monitored as it left the test equipment in either situation (open-ended). The tests were set up at atmospheric pressure, enabling the gauge to function at low pressure gauge ranges within its limits. Since water is relatively incompressible, it was assumed that the test conditions would provide simulate the normal operation of an irrigation system.

### 6.3 Results And Discussion

Experimental findings on the effect of two phase flow on pressure drop and the effect of the change in slope and plane on pressure drop for single phase flow are presented and discussed in the following sections.

#### 6.3.1 Effects of Two Phase Flow on Pressure Drop

From the tests conducted, the introduction of air into the system seemed to flatten or even out the pressure drop due to the bend angles tested; almost bring it to constant state. It was also seen that although pressure drop increased due to two phase flow, two phase flow becomes less of an influence as the flow velocity increased as seen in the smaller pipe diameter (with relatively higher flow) tested. Figures 6.3, 6.4 and 6.5 show the transitional effects of the flow velocity with two phase flow compared to the single phase flow on pressure drop for the three pipes tested at various flow velocities and bend angles.

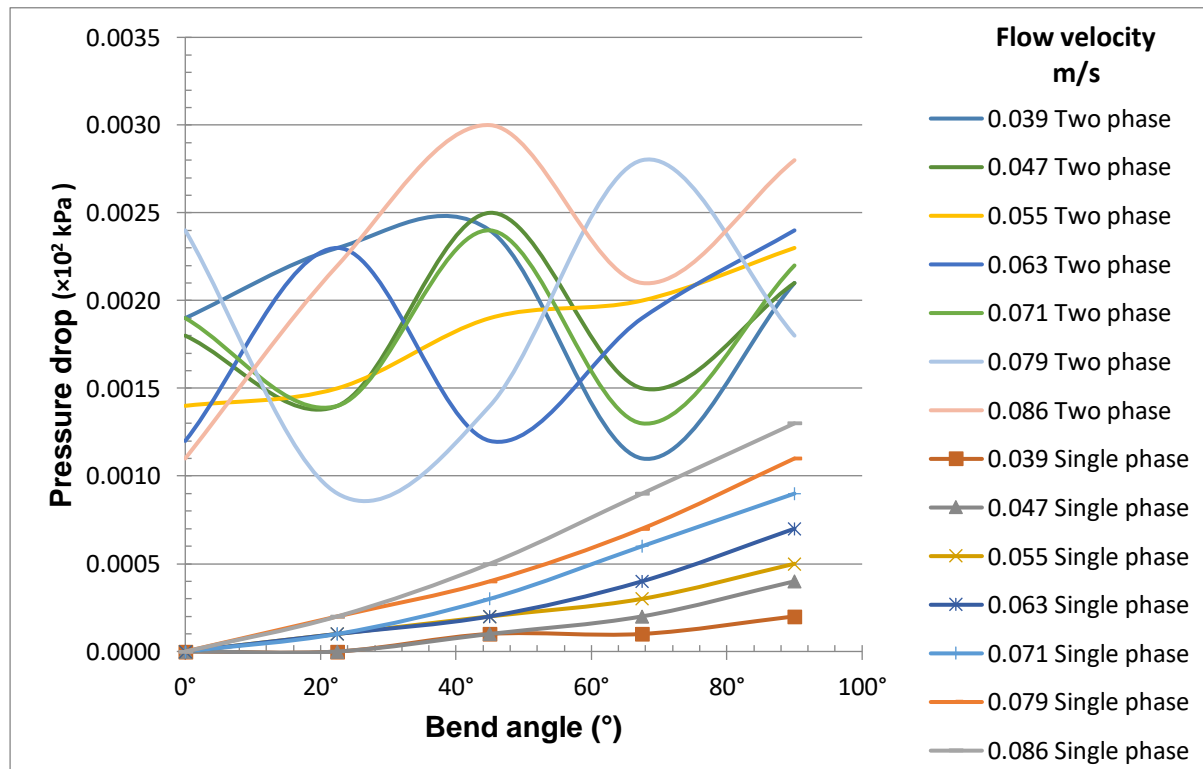
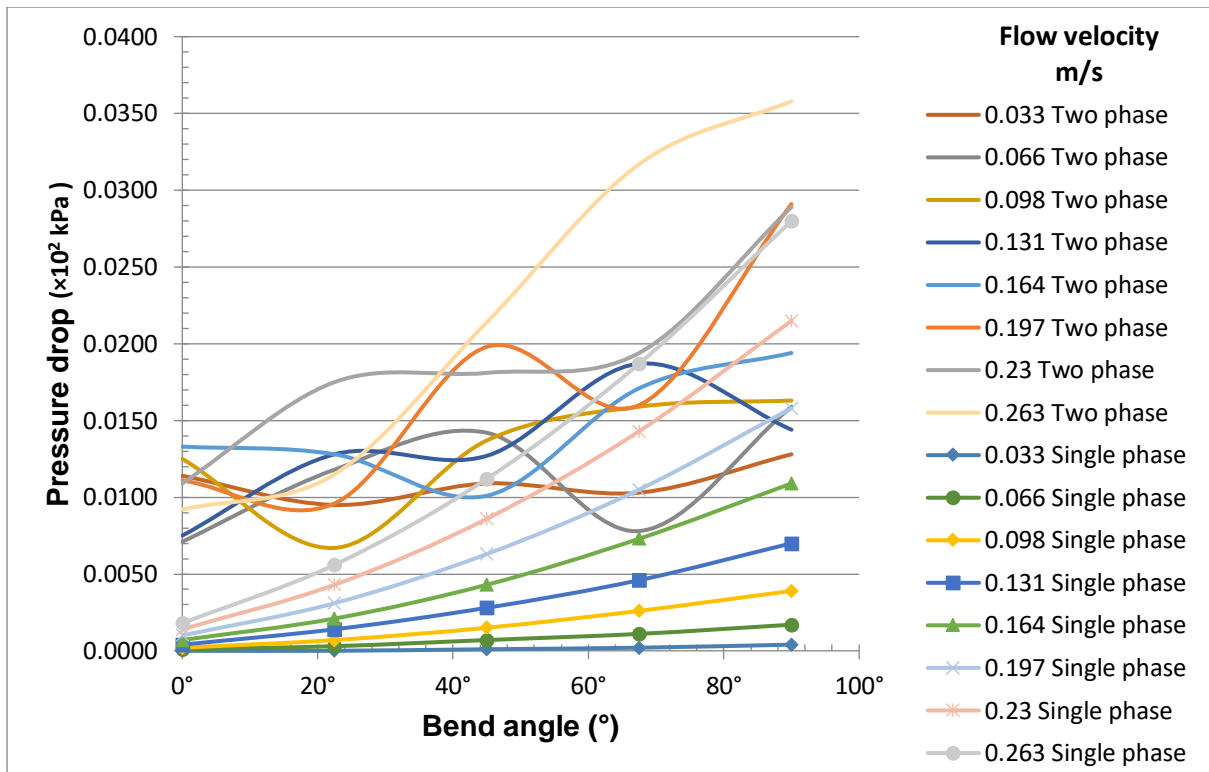
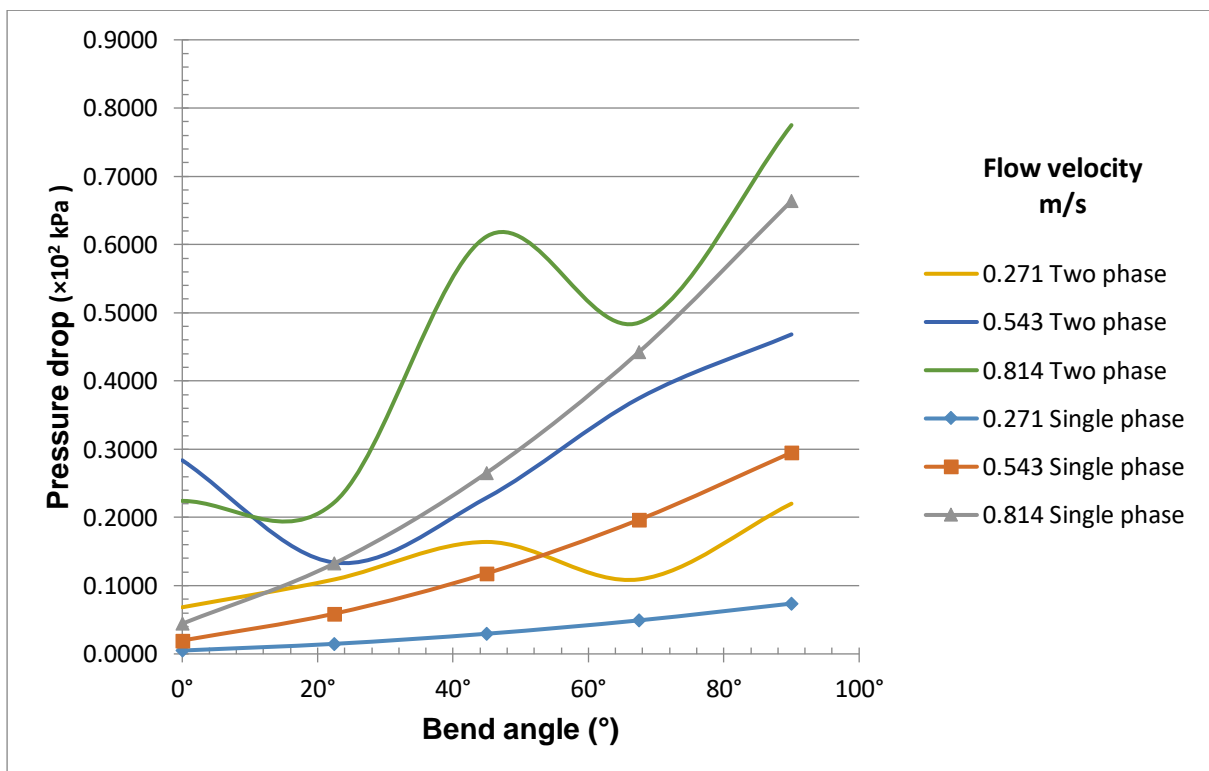


Figure 6.3 Pressure drop due to single and two phase flow for successive pipe bending for the 50 mm (47 ID) diameter pipe



**Figure 6.4 Pressure drop due to single and two phase flow for successive pipe bending for the 25 mm (23 ID) diameter pipe**



**Figure 6.5 Pressure drop due to single and two phase flow for successive pipe bending for the 10 mm (8 ID) diameter pipe**

With introduction of air into the pipe, from single phase to bubbly flow as described by Buscher (2019) or two phase flow, frictional losses increased for all bend angles tested compared to the straight pipe lengths or bends tested under the same flow conditions. As the pipes were burnt to the maximum of  $90^\circ$ , the influence of the bend angle is also seen to have a similar effect on pressure drop. However, the main source or contributor of pressure drop picked at lower levels of bending was more from the two phase flow and this reduced or approached a constant as the bend angle increased to  $90^\circ$ .

The pressure drop in two phase flow was also more than that of single phase flow also due to the reduced hydraulic area. The increase in pressure drop in all cases was a result of the increase in energy dissipation due to the two phase flow from momentum exchange between phases as explained by Azzi and Friedel (2005), as well as separation and mingling of the gas-liquid phase.

Pressure drop is seen to fluctuate generally in all cases since the two phase density estimation is tied to the hydrostatic pressure drop, which is heavily influenced by the void fraction error as proven by Ghajar and Bhagwat (2013).

The behaviour or increased pressure drop due to the introduction of two phase flow shows that an irrigation system are affected by two phase flow at points of low flow velocities. Pressure drop due to two phase flow is less likely to be realised with higher flow velocity systems, but this comes with the challenge of losing more head through primary losses and secondary losses as well. An optimal point is perceived to exist wherein there is a balance of flow velocity and phase, which is likely to be affected by the pipe geometry since flow reversal is prone to occur with large pipe diameters.

### **6.3.2 Effects of the Slope and Plane on Pressure Drop due to Single Phase Flow**

Fixing the plane at  $0^\circ$  and increasing the slope of the bend(s) from  $0^\circ$  to finally at  $+90^\circ$ , the pressure drop generally decreased as the slope increased as tabulated in Table 6.1. In contrast Table 6.2, pressure drop increased with decrease in the slope, from  $0^\circ$  to  $-90^\circ$ .

**Table 6.1 Pressure drop with change in slope from 0° to 90° with fixed plane for flow velocities 0.271, 0.197 and 0.079 ms<sup>-1</sup> for respective pipe diameters**

<b>Slope</b>	<b>0°</b>	<b>0°</b>	<b>0°</b>	<b>0°</b>	<b>0°</b>	<b>22.5°</b>	<b>22.5°</b>	<b>22.5°</b>	<b>22.5°</b>	<b>22.5°</b>	<b>45°</b>	<b>45°</b>	<b>45°</b>
<b>Plane</b>	<b>0°</b>	<b>0°</b>											
<b>Bend angle</b>	<b>0°</b>	<b>22.5°</b>	<b>45°</b>	<b>67.5°</b>	<b>90°</b>	<b>0°</b>	<b>22.5°</b>	<b>45°</b>	<b>67.5°</b>	<b>90°</b>	<b>0°</b>	<b>22.5°</b>	<b>45°</b>
<b>10mm (8 ID)</b>	0.0363	0.0419	0.0499	0.0606	0.0737	-0.0253	-0.0149	0.0048	0.0345	0.0701	-0.0780	-0.0643	-0.0333
<b>25mm (23 ID)</b>	0.0078	0.0094	0.0111	0.0128	0.0157	-0.0537	-0.0481	-0.0340	-0.0136	0.0118	-0.1063	-0.0970	-0.0723
<b>50mm (47 ID)</b>	0.0005	0.0006	0.0007	0.0008	0.0012	-0.0612	-0.0569	-0.0444	-0.0256	-0.0032	-0.1138	-0.1056	-0.0826
<b>Slope</b>	<b>45°</b>	<b>45°</b>	<b>67.5°</b>	<b>67.5°</b>	<b>67.5°</b>	<b>67.5°</b>	<b>67.5°</b>	<b>90°</b>	<b>90°</b>	<b>90°</b>	<b>90°</b>	<b>90°</b>	
<b>Plane</b>	<b>0°</b>												
<b>Bend angle</b>	<b>67.5°</b>	<b>90°</b>	<b>0°</b>	<b>22.5°</b>	<b>45°</b>	<b>67.5°</b>	<b>90°</b>	<b>0°</b>	<b>22.5°</b>	<b>45°</b>	<b>67.5°</b>	<b>90°</b>	
<b>10mm (8 ID)</b>	0.0118	0.0662	-0.1123	-0.0970	-0.0593	-0.0035	0.0634	-0.1249	-0.1081	-0.0684	-0.0087	0.0630	
<b>25mm (23 ID)</b>	-0.0356	0.0079	-0.1418	-0.1299	-0.0986	-0.0512	0.0061	-0.1534	-0.1417	-0.1072	-0.0563	0.0051	
<b>50mm (47 ID)</b>	-0.0482	-0.0066	-0.1487	-0.1382	-0.1084	-0.0632	-0.0091	-0.1610	-0.1498	-0.1172	-0.0685	-0.0098	

**Table 6.2 Pressure drop with change in slope from 0° to -90° with fixed plane for flow velocities 0.271, 0.197 and 0.079 ms<sup>-1</sup> for respective pipe diameters**

<b>Slope</b>	<b>0°</b>	<b>0°</b>	<b>0°</b>	<b>0°</b>	<b>0°</b>	<b>-22.5°</b>	<b>-22.5°</b>	<b>-22.5°</b>	<b>-22.5°</b>	<b>-22.5°</b>	<b>-45°</b>	<b>-45°</b>	<b>-45°</b>
<b>Plane</b>	<b>0°</b>	<b>0°</b>	<b>0°</b>	<b>0°</b>	<b>0°</b>	<b>0°</b>	<b>0°</b>	<b>0°</b>	<b>0°</b>	<b>0°</b>	<b>0°</b>	<b>0°</b>	<b>0°</b>
<b>Bend angle</b>	<b>0°</b>	<b>22.5°</b>	<b>45°</b>	<b>67.5°</b>	<b>90°</b>	<b>0°</b>	<b>22.5°</b>	<b>45°</b>	<b>67.5°</b>	<b>90°</b>	<b>0°</b>	<b>22.5°</b>	<b>45°</b>
<b>10mm (8 ID)</b>	0.0367	0.0420	0.0501	0.0610	0.0734	0.0991	0.0997	0.0959	0.0876	0.0775	0.1507	0.1482	0.1338
<b>25mm (23 ID)</b>	0.0080	0.0088	0.0104	0.0129	0.0160	0.0696	0.0662	0.0558	0.0396	0.0203	0.1224	0.1153	0.0940
<b>50mm (47 ID)</b>	0.0006	0.0007	0.0008	0.0010	0.0010	0.0623	0.0583	0.0460	0.0273	0.0054	0.1149	0.1068	0.0842
<b>Slope</b>	<b>-45°</b>	<b>-45°</b>	<b>-67.5°</b>	<b>-67.5°</b>	<b>-67.5°</b>	<b>-67.5°</b>	<b>-67.5°</b>	<b>-90°</b>	<b>-90°</b>	<b>-90°</b>	<b>-90°</b>	<b>-90°</b>	
<b>Plane</b>	<b>0°</b>	<b>0°</b>	<b>0°</b>	<b>0°</b>	<b>0°</b>	<b>0°</b>	<b>0°</b>	<b>0°</b>	<b>0°</b>	<b>0°</b>	<b>0°</b>	<b>0°</b>	
<b>Bend angle</b>	<b>67.5°</b>	<b>90°</b>	<b>0°</b>	<b>22.5°</b>	<b>45°</b>	<b>67.5°</b>	<b>90°</b>	<b>0°</b>	<b>22.5°</b>	<b>45°</b>	<b>67.5°</b>	<b>90°</b>	
<b>10mm (8 ID)</b>	0.1102	0.0814	0.1863	0.1816	0.1593	0.1245	0.0841	0.1988	0.1927	0.1679	0.1298	0.0848	
<b>25mm (23 ID)</b>	0.0617	0.0240	0.1572	0.1477	0.1195	0.0768	0.0257	0.1694	0.1595	0.1287	0.0820	0.0272	
<b>50mm (47 ID)</b>	0.0499	0.0088	0.1498	0.1395	0.1099	0.0650	0.0112	0.1623	0.1511	0.1187	0.0702	0.0120	

On analysis of the relative change in the pressure drop for the above changes in slope with fixed plane (Table 6.1 and 6.2), it was found that the change in pressure drop was generally close to the change due to elevation difference, that is the calculated liquid depth or hydrostatic pressure relative to the position of the gauge due to the tilt introduced on the pipe or bends.

It was also seen that though they was influence on pressure drop due to elevation and there was no significant influence due to the low and high flow velocities tested. As the flow velocities tested increased, the component of pressure drop also increased relative to the extent of bending. The component of the liquid depth or level to hydrostatic pressure was seen to be the only influence on pressure drop with the successive change in the slope. Table 6.3 shows the approximate calculated liquid depth or level to hydrostatic pressure relative to the pivot.

**Table 6.3 Liquid Depth / Level to Hydrostatic Pressure relative to the change in slope with fixed plane**

<b>Slope</b> <b>Bend angle</b>	<b>0°</b>	<b>22.5°</b>	<b>45°</b>	<b>67.5°</b>	<b>90°</b>	<b>Gauge position relative to pivot (m)</b>
<b>0°</b>	0.0000	0.0619	0.1143	0.1493	0.1616	2.010
<b>22.5°</b>	0.0000	0.0575	0.1063	0.1389	0.1503	1.870
<b>45°</b>	0.0000	0.0452	0.0835	0.1091	0.1181	1.468
<b>67.5°</b>	0.0000	0.0265	0.0490	0.0640	0.0693	0.862
<b>90°</b>	0.0000	0.0042	0.0078	0.0101	0.0110	0.137

As flow through the various bends was tested the Bernoulli's principle applied since the total pressure is the result of the sum of the static pressure and dynamic pressure. The static pressure and the dynamic pressure due to the bending for the accompanied flow with the respective slope and plane gave the resultant of the total pressure observed. It can be concluded that the gravitational force affects the flow form as seen by Barash (2009) though bending is involved due to the close transition values of pressure drop as slope changed.

In the pipe configuration tested (Table 6.1 and 6.2), the effect of curvature is seen to be swallowed up in the changing slope such that the decrease in pressure drop as we move from 0° to 90° is merely due to the bending coupled with the elevation difference. The results of the overall pressure drop for the bend(s) due to the change in the slope are expressed as percentages in Figures 6.6.

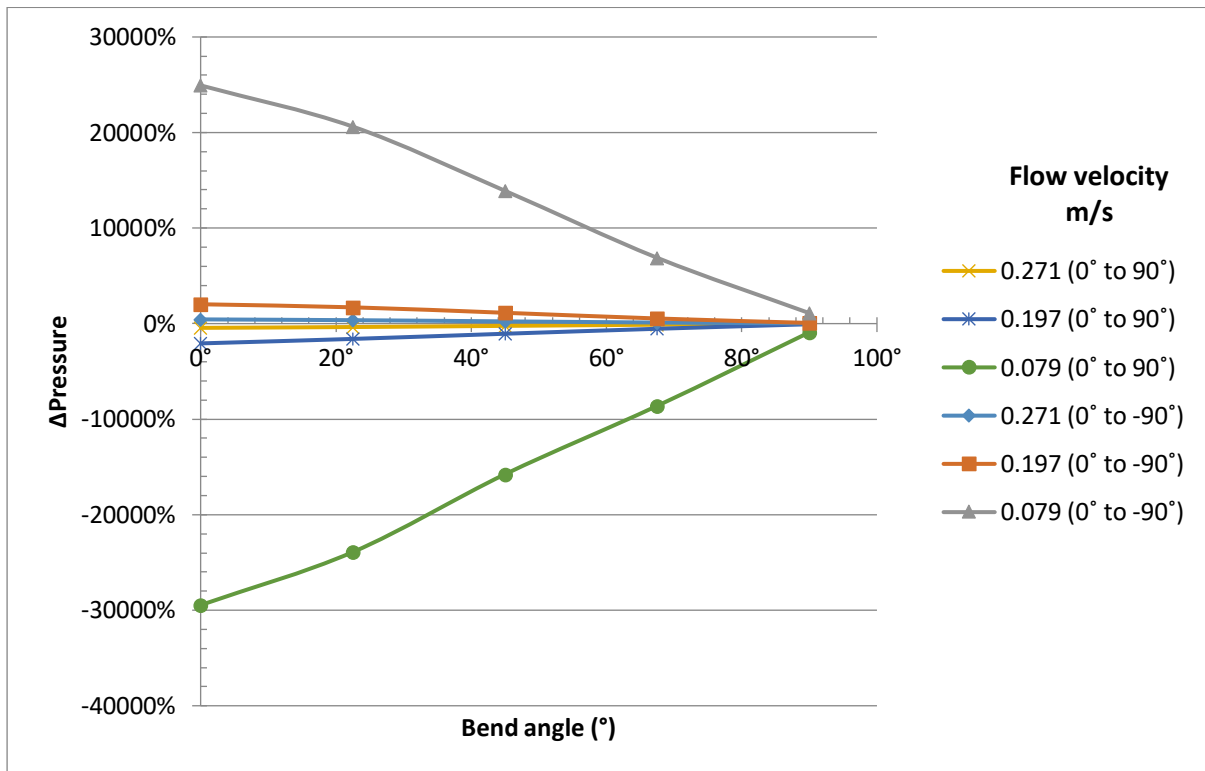


**Figure 6.6 Percentage change in overall pressure drop for slope -90° to 90° and 0° plane with bending**

The pressure change is seen to be due to bend angle and the angular rotation due to the effect of gravity as elevation changed. The slight difference in the positive and negative changes in the slope for the measured results show the inaccuracies involved in the practical measurements done.

To understand the influence of plane on the pressure drop due to the bending, the slope was fixed and the bend(s) moved about the plane - 90°, 0° and 90° (see Figure 6.2). The pressure drop decreased with the increase in the plane from 0° to 90° as seen in Table 6.4. In contrast Table 6.5, pressure drop measured increased with decrease in the plane, from 0° to -90°.

**Table 6. Pressure drop with change in plane from 0° to 90° with fixed slope for flow velocities 0.271, 0.197 and 0.079 ms<sup>-1</sup> for respective pipe diameters**

<b>Slope</b>	<b>0°</b>	<b>0°</b>											
<b>Plane</b>	<b>0°</b>	<b>0°</b>	<b>0°</b>	<b>0°</b>	<b>0°</b>	<b>22.5°</b>	<b>22.5°</b>	<b>22.5°</b>	<b>22.5°</b>	<b>22.5°</b>	<b>45°</b>	<b>45°</b>	<b>45°</b>
<b>Bend angle</b>	<b>0°</b>	<b>22.5°</b>	<b>45°</b>	<b>67.5°</b>	<b>90°</b>	<b>0°</b>	<b>22.5°</b>	<b>45°</b>	<b>67.5°</b>	<b>90°</b>	<b>0°</b>	<b>22.5°</b>	<b>45°</b>
<b>10mm (8 ID)</b>	0.0371	0.0422	0.0505	0.0611	0.0741	0.0369	0.0184	0.0062	0.0019	0.0081	0.0373	-0.0020	-0.0322
<b>25mm (23 ID)</b>	0.0075	0.0094	0.0111	0.0134	0.0157	0.0079	-0.0144	-0.0334	-0.0458	-0.0503	0.0082	-0.0349	-0.0713
<b>50mm (47 ID)</b>	0.0005	0.0007	0.0008	0.0010	0.0011	0.0004	-0.0232	-0.0436	-0.0583	-0.0650	0.0006	-0.0433	-0.0813
<b>Slope</b>	<b>0°</b>												
<b>Plane</b>	<b>45°</b>	<b>45°</b>	<b>67.5°</b>	<b>67.5°</b>	<b>67.5°</b>	<b>67.5°</b>	<b>67.5°</b>	<b>90°</b>	<b>90°</b>	<b>90°</b>	<b>90°</b>	<b>90°</b>	
<b>Bend angle</b>	<b>67.5°</b>	<b>90°</b>	<b>0°</b>	<b>22.5°</b>	<b>45°</b>	<b>67.5°</b>	<b>90°</b>	<b>0°</b>	<b>22.5°</b>	<b>45°</b>	<b>67.5°</b>	<b>90°</b>	
<b>10mm (8 ID)</b>	-0.0479	-0.0483	0.0367	-0.0151	-0.0567	-0.0817	-0.0853	0.0363	-0.0196	-0.0656	-0.0938	-0.0987	
<b>25mm (23 ID)</b>	-0.0957	-0.1065	0.0079	-0.0479	-0.0964	-0.1299	-0.1437	0.0082	-0.0533	-0.1055	-0.1412	-0.1567	
<b>50mm (47 ID)</b>	-0.1081	-0.1210	0.0004	-0.0567	-0.1062	-0.1417	-0.1583	0.0004	-0.0613	-0.1151	-0.1535	-0.1715	

**Table 6.4 Pressure drop with change in plane from 0° to -90° with fixed slope for flow velocities 0.271, 0.197 and 0.079 ms<sup>-1</sup> for respective pipe diameters**

<b>Slope</b>	<b>0°</b>	<b>0°</b>	<b>0°</b>	<b>0°</b>	<b>0°</b>	<b>0°</b>	<b>0°</b>	<b>0°</b>	<b>0°</b>	<b>0°</b>	<b>0°</b>	<b>0°</b>	<b>0°</b>
<b>Plane</b>	<b>0°</b>	<b>0°</b>	<b>0°</b>	<b>0°</b>	<b>0°</b>	<b>-22.5°</b>	<b>-22.5°</b>	<b>-22.5°</b>	<b>-22.5°</b>	<b>-22.5°</b>	<b>-45°</b>	<b>-45°</b>	<b>-45°</b>
<b>Bend angle</b>	<b>0°</b>	<b>22.5°</b>	<b>45°</b>	<b>67.5°</b>	<b>90°</b>	<b>0°</b>	<b>22.5°</b>	<b>45°</b>	<b>67.5°</b>	<b>90°</b>	<b>0°</b>	<b>22.5°</b>	<b>45°</b>
<b>10mm (8 ID)</b>	0.0370	0.0420	0.0501	0.0607	0.0736	0.0369	0.0655	0.0949	0.1198	0.1401	0.0364	0.0860	0.1317
<b>25mm (23 ID)</b>	0.0083	0.0088	0.0108	0.0127	0.0161	0.0080	0.0330	0.0549	0.0723	0.0820	0.0080	0.0533	0.0923
<b>50mm (47 ID)</b>	0.0006	0.0006	0.0008	0.0010	0.0011	0.0005	0.0244	0.0450	0.0599	0.0672	0.0005	0.0446	0.0826
<b>Slope</b>	<b>0°</b>	<b>0°</b>	<b>0°</b>	<b>0°</b>	<b>0°</b>	<b>0°</b>	<b>0°</b>	<b>0°</b>	<b>0°</b>	<b>0°</b>	<b>0°</b>	<b>0°</b>	
<b>Plane</b>	<b>-45°</b>	<b>-45°</b>	<b>-67.5°</b>	<b>-67.5°</b>	<b>-67.5°</b>	<b>-67.5°</b>	<b>-67.5°</b>	<b>-90°</b>	<b>-90°</b>	<b>-90°</b>	<b>-90°</b>	<b>-90°</b>	
<b>Bend angle</b>	<b>67.5°</b>	<b>90°</b>	<b>0°</b>	<b>22.5°</b>	<b>45°</b>	<b>67.5°</b>	<b>90°</b>	<b>0°</b>	<b>22.5°</b>	<b>45°</b>	<b>67.5°</b>	<b>90°</b>	
<b>10mm (8 ID)</b>	0.1703	0.1964	0.0368	0.0994	0.1570	0.2028	0.2338	0.0369	0.1046	0.1659	0.2149	0.2462	
<b>25mm (23 ID)</b>	0.1224	0.1383	0.0075	0.0663	0.1178	0.1552	0.1751	0.0083	0.0707	0.1270	0.1672	0.1888	
<b>50mm (47 ID)</b>	0.1100	0.1233	0.0005	0.0580	0.1077	0.1436	0.1605	0.0006	0.0628	0.1167	0.1551	0.1736	

Again, the transition of the pressure drop with the change in the plane was seen to be mainly due to the bending and the accompanied change in elevation when considering the angular rotation of the gauge due to the effect of gravity. Changes in the pressure drop were found to be close to the calculated liquid depth pressure Table 6.5

**Table 6.5 Liquid Depth / Level to Hydrostatic Pressure relative to the change in plane with fixed slope**

<b>Slope</b> <b>Bend angle</b>	<b>0°</b>	<b>22.5°</b>	<b>45°</b>	<b>67.5°</b>	<b>90°</b>	<b>Gauge position relative to pivot (m)</b>
<b>0°</b>	0.0000	0.0000	0.0000	0.0000	0.0000	0.000
<b>22.5°</b>	0.0000	0.0237	0.0439	0.0573	0.0621	0.772
<b>45°</b>	0.0000	0.0443	0.0819	0.1070	0.1158	1.441
<b>67.5°</b>	0.0000	0.0591	0.1091	0.1426	0.1543	1.919
<b>90°</b>	0.0000	0.0661	0.1221	0.1595	0.1726	2.147

Figure 6.7 expresses the change in the overall pressure for bending with change in plane.

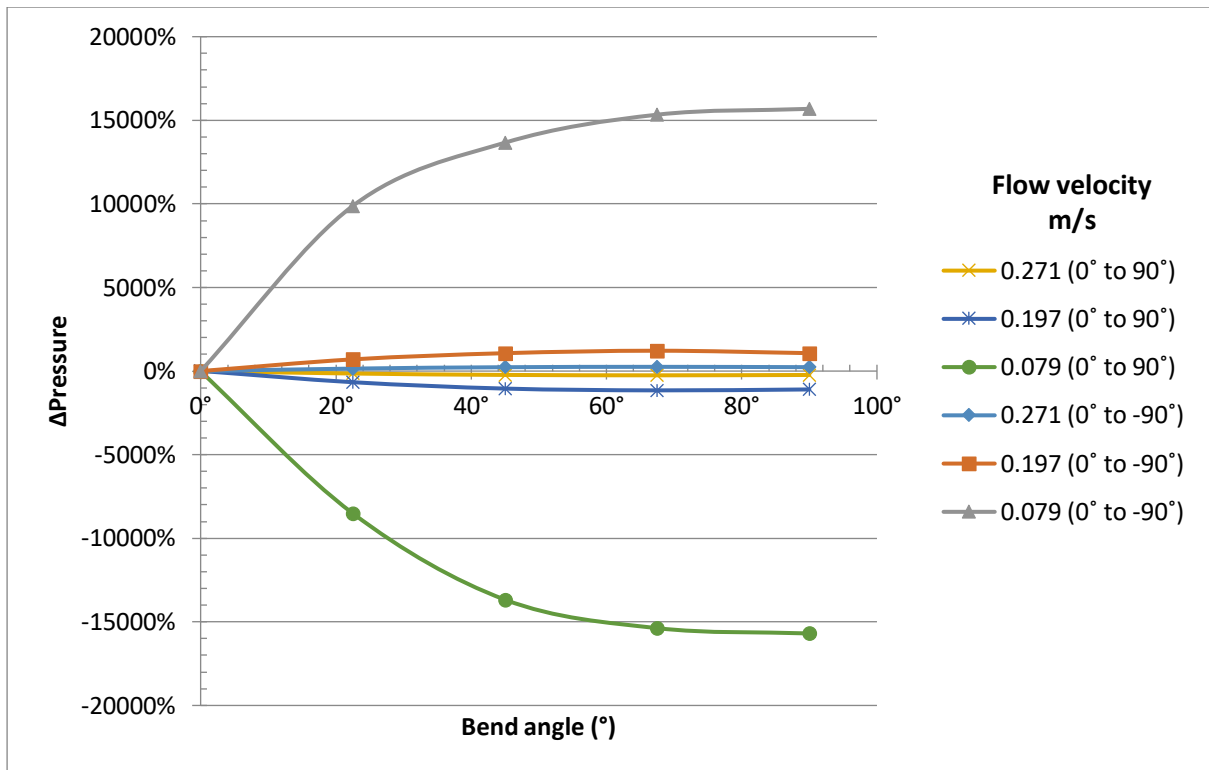


**Figure 6.7 Percentage change in overall pressure drop for plane -90° to 90° and 0° slope with bending**

Pressure changes generally increased from the small bend angles tested and approached constant conditions as bending approached  $\pm 90^\circ$  respectively in both cases of changing plane. This is because with almost no bending or considering a straight pipe section the pressure reading was invariably small with no change in the static level (plane).

The influence of the plane is seen to be similar to the effect of the slope. This means that the combined or effect of total pressure due to the slope and plane remains the sum of the static pressure and dynamic pressure including the extent of bending involved. Considering the bends used in irrigation systems and calculation of the primary losses, the component due to static pressure is catered for in the use of elevation for changes in the total pressure head. The component of dynamic pressure will only be refined with accurate calculation of minor losses due to the bend.

## 6.4 Conclusions

Two phase flow (air and water) in an irrigation system has the effect of increasing the minor losses which also increase with the increase in the bend angle. The effect of two phase flow is more significant with low flow irrigation systems as opposed to higher flow systems as postulated with the disadvantage of increased secondary losses. In the low flow irrigation systems, the minor frictional losses in two phase flow can almost be define as losses only due to the intrusion of air into the system despite the bends. This effect is much more in the case of specialised bends. As the flows in the irrigation system increases, there is a tendency to realise secondary losses only due to the extent of bending despite air in the system. This means as we improve the design of irrigation systems and move more to the low flow systems, air valves become more important at points wherein air entry is potentially realised to reduce the minor or secondary losses. A balance needs to be established for the influence of two phase flow and flow velocity of an irrigation systems in consideration of the primary and secondary losses for optimal or efficient hydraulic performance of irrigation systems.

As the irrigation system comprises of multiple bends, it is safe to calculate pressure losses due to bending (dynamic pressure) independently and add these to the rising and falling main lines (static pressure) with certainty that the component of change in the slope and plane of the bend is catered for.

## CHAPTER 7: CONCLUSIONS AND RECOMMENDATIONS FOR FURTHER RESEARCH

### 7.1 Revisiting the Aims and Objectives

It was possible to establish an Empirical Equation, herein named the *Dayton Equation*, for calculating minor losses for bends ranging from  $0^\circ$  to  $90^\circ$  with respect to varying bend parameters as postulated, providing a simple approach and tool for calculating losses due to bends during the irrigation design procedure. Since smooth pipes were found to have certain similar flow behaviours due to curvature, a multiplier was found to occur in relation to the bend curvature ratio (bend length per diameter, L/D ratio) as the pipe diameter changed. The Empirical Equation's derivation provided for the easy, quick, accurate and precise determination (best approximate) of pressure drop due to bends, dynamically from  $0^\circ$  to  $90^\circ$ , for use in smooth pipe bends for irrigation design. Minor losses can now be determined rapidly, precisely, and accurately as compared to the use of tables which is often erroneous considering the varied bend parameters encountered during the design process. This Equation further clarified the difference between a Short and a Standard radius bend, as well as the principle of saturation as curvature grew past the published Long Radius bend. It also allows for the calculation of frictional loss both inside and outside range of the experimental results published. Because of the Equation's simplicity, an irrigation designer can easily input the changing bend parameters and get reliable results or close estimates. Its compatibility and mathematical approach also allow it to be used as a tool in irrigation design software and other applications.

Development of the successive dynamic hydraulic gradient due to successive pipe bending was realized. The shape of the hydraulic gradient line due the bend angle was the same for different pressure drops owing to varied curvature and flow velocity as postulated. This was achieved by the looking at the resultant of the two extremes of the pressure differentials, the inner and outer pressure within the pipe bend and the peripherals. This together with the available findings from the literature allowed for the generation and normalisation of the dynamic hydraulic gradient. The graphical display expressed findings in the form of a chart for manually determining the dynamic hydraulic gradient and mathematically a MS Excel spread sheet tool from the experimental data for easy handling as postulated.

In comparison to the traditional approaches, the use of the Empirical Equation as reference for comparison established the extent of error and reliability in each case of the traditional methods. The extent of error was very small for the Resistance Coefficient method and generally small with the Valve flow Coefficient method. It was however significant with the Equivalent Length method and increased as the bend angle was reduced in all cases as postulated. The capacity of the Empirical Equation to take into account evolving bend parameters was extremely important, allowing for comparison of all the traditional methods. The shortfalls in the use of traditional methods results in the under- and over-estimation of frictional losses due to bending when designing irrigation systems, which needs to be avoided. Since the Empirical Equation is based on the Resistance Coefficient method, with the relatively small differences seen on comparison, it can again be confidently agreed that it accurately predicts secondary or minor losses in irrigation systems due to bending.

In an irrigation system, two phase flow (air and water) increases the minor losses, which also increases with increase in the bend angle. As opposed to higher flows in irrigation systems, the influence of two phase flow is more noticeable with low flow in an irrigation systems as postulated. Minor frictional losses with the occurrence of two phase flow with low flows in irrigation systems, can almost simply be described as losses entirely due to entry of air into the bends, despite the losses due to the existence of bends. In the case of special bends, this phenomenon is amplified as the bend approaches the straight pipe conditions. With increasing irrigation system flow velocities, secondary losses are more likely to occur only due to the degree of bending despite the presence of air in the system. As irrigation system architecture improves and as we transition toward low-flow irrigation systems, air valves become increasingly critical at points where air penetration is possible to minimize minor or secondary losses. Since the irrigation system has several bends, it is safe to add the sum of individual bends as minor losses to the rising and falling main line losses, ensuring that the slope and plane of individual bends is taken into account due to the effect of the relative liquid depth when elevation is introduced.

## **7.2 Contributions to New Knowledge**

Contributions to new knowledge in light of this research are:

- An Empirical Equation for easy, quick, accurately and precisely determining of minor losses for bends from 0° to 90° with respect to the varied bend parameters was developed;
- The development of the successive dynamic hydraulic gradient due to successive pipe bends formed was done. This was finally expressed as a chart for manually determining the dynamic hydraulic gradient which was also expressed mathematically for use with a MS Excel spread sheet tool. This was done to help in the understanding pressure changes within the bend and peripherals for design of thrust blocks, general understanding pipe erosion due to bends and generation of secondary flow and swirl;
- The Empirical Equation as a reference was used for the comparison of the minor friction losses as determined by the traditional methods. This was achieved by the ability of the Empirical Equation to provide equivalent lengths and coefficients within and outside the range of the published data for comparison of the different equivalent lengths and coefficients. The extent of error identified in the all the traditional method was found to be significant for the Equivalent Length method and much more on bend angle less than 90° for all traditional methods; and
- The effect of two phase flow on pressure loss awakens the critical need for use of air valves in irrigation systems. While the effect of the slope (gradient) and plane (incline) of the bend on single phase pressure loss confirms the correctness of addition of the secondary losses to the primary losses as part of the process in the irrigation design.

### **7.3 Future Possibilities and Recommendations**

Accurately determining the losses due to T pieces, sluice valves, ball valves, reducers, reflux valves and foot valves with screens should be done in the same manner as the bends were pragmatically done. This will also reduce the cost incurred in sizing of pumps due to possible over and under designing.

A relationship between the initial swirl intensity given the value 0.21, which was seen to be from the finest fit amid the data and correlation by Kim *et al.* (2014) due to the pressure drop, should be done in relation to the developed dynamic hydraulic gradient. There is also a need to cater for the next bend or fitting in the design of irrigation systems since losses due to the bending are seen to persist for some 30 to 50 pipe diameters downstream.

Though precise and accurate methods for determining minor losses have been done, future research should also needs to focus on the calculations to include the consideration of the formation of algae in the irrigation pipe lines and bends over the life of an irrigation system.

#### **7.4 Final Comments**

Determination of pressure drop can accurately and precisely be determined for a straight pipe section using the conventional methods Darcy-Weisbach, Colebrook-White / Newton-Raphson, Moody chart, Barr, Wood, Haaland, Swamee - Jain, Hazen-Williams, Lamont and General Exponential formula. However, when a bend is introduced, accuracy and precision becomes questionable since all traditional methods though giving close approximations are not easy to use. Considering empathetically the flow pattern and the transition of fluid flow due to the change in direction of flow as seen in literature, it is evident that pressure loss can be understood to be due to several contributing forces, the bend angle, radius, flow velocity and pipe diameter, and realised in the developed Empirical Equation. The dynamic hydraulic gradient found can be used to understand the forces acting within the bend and peripherals and can be used for future research. In the comparisons made, the extent of error in the traditional methods can be appreciated and complement the use of the developed Empirical Equation. Lastly the effect of two phase flow, slope and plane on bends is better appreciated in the design of irrigation systems.

## REFERENCES

- AKERS, W., DEANS, H. & CROSSER, O. 1958. Condensing heat transfer within horizontal tubes. *Chem. Eng. Progr.*, 54.
- ALBRIGHT, L. 2008. *Albright's chemical engineering handbook*, CRC Press.
- ARC. 2003. *SABI Irrigation Design Manual (ARC-ILI)* [Online]. Available: [http://www.agis.agric.za/agric\\_engineering/pdf/IrrigationDesignPipehydraulics.pdf](http://www.agis.agric.za/agric_engineering/pdf/IrrigationDesignPipehydraulics.pdf) [Accessed 2016 2003].
- AUTEE, A. & GIRI, S. 2016. Experimental study on two-phase flow pressure drop in small diameter bends. *Perspectives in Science*, 8, 621-625.
- AWAD, M. 2016. The science and the history of the two Bejan numbers. *International Journal of Heat and Mass Transfer*, 94, 101-103.
- AZZI, A. & FRIEDEL, L. 2005. Two-phase upward flow 90 bend pressure loss model. *Forschung im Ingenieurwesen*, 69, 120-130.
- BABATOLA, J., OGUNTUASE, A., OKE, I. & OGEDENGBE, M. 2008. An evaluation of frictional factors in pipe network analysis using statistical methods. *Environmental Engineering Science*, 25, 539-548.
- BARASH, L. Y. 2009. Influence of gravitational forces and fluid flows on the shape of surfaces of a viscous fluid of capillary size. *Physical Review E*, 79, 025302.
- BECK, C. 1960. Discussion: "Pressure Losses in Smooth Pipe Bends" (Ito<sup>-</sup>, H., 1960, ASME J. Basic Eng., 82, pp. 131-140).
- BERGER, S., TALBOT, L. & YAO, L. 1983. Flow in curved pipes. *Annual Review of Fluid Mechanics*, 15, 461-512.
- BERLAMONT, J. 2014. Friction Losses in Large-Diameter Pipes. *Journal of Pipeline Systems Engineering and Practice*, 6, 06014004.
- BLANCKAERT, K. 2009. Saturation of curvature-induced secondary flow, energy losses, and turbulence in sharp open-channel bends: Laboratory experiments, analysis, and modeling. *Journal of Geophysical Research: Earth Surface*, 114.
- BRILEY, W. R. 1974. Numerical method for predicting three-dimensional steady viscous flow in ducts. *Journal of Computational Physics*, 14, 8-28.
- BUSCHER, S. 2019. Visualization and modelling of flow pattern transitions in a cross-corrugated plate heat exchanger channel with uniform two-phase distribution. *International Journal of Heat and Mass Transfer*, 144, 118643.
- CHEREMISINOFF, N. P. 1998. *Groundwater Remediation and Treatment Technologies*, Elsevier 101, 388.
- CHIGIER, N. & BEER, J. 1964. Velocity and static-pressure distributions in swirling air jets issuing from annular and divergent nozzles. *Journal of Basic Engineering*, 86, 788-796.
- CHIRGWIN, G. A. & SUTTON, B. 2019. A low-cost, high-precision drip emitter suitable for low-pressure micro-irrigation systems. *Irrigation Science*, 37, 725-735.
- CHISHOLM, D. 1980. Two-phase flow in bends. *International Journal of Multiphase Flow*, 6, 363-367.
- COLEMAN, J. W. & GARIMELLA, S. 1999. Characterization of two-phase flow patterns in small diameter round and rectangular tubes. *International Journal of Heat and Mass Transfer*, 42, 2869-2881.
- CRANE, C. 1957. *Flow of Fluids through Valves, Fittings and Pipes.*, Crane Canada Limited 36, 130.

- CRAWFORD, N., CUNNINGHAM, G. & SPEDDING, P. 2003. Prediction of pressure drop for turbulent fluid flow in 90 bends. *Proceedings of the Institution of Mechanical Engineers, Part E: Journal of Process Mechanical Engineering*, 217, 153-155.
- DAI, B., LI, M. & MA, Y. 2014. Effect of surface roughness on liquid friction and transition characteristics in micro-and mini-channels. *Applied Thermal Engineering*, 67, 283-293.
- DARBY, R., CHHABRA, R. P. & DARBY, R. 2001. *Chemical Engineering Fluid Mechanics, Revised and Expanded*, CRC Press 209, 576.
- DEAN, W. Fluid motion in a curved channel. *Proceedings of the Royal Society of London A: Mathematical, Physical and Engineering Sciences*, 1928. The Royal Society, 402-420.
- DEOBALD, T. L. 1962. An Experimental Investigation of Two-phase Flow Pressure Losses in Pipe Elbows. General Electric Co. Hanford Atomic Products Operation, Richland, Wash. 24-27, 158.
- DHODAPKAR, S., SOLT, P. & KLINZING, G. 2009. Understanding bends in pneumatic conveying systems. *Chem. Eng*, 116, 46-52.
- DOS SANTOS, A. P. P., ANDRADE, C. R. & ZAPAROLI, E. L. 2014. CFD Prediction of the Round Elbow Fitting Loss Coefficient. *World Academy of Science, Engineering and Technology, International Journal of Mechanical, Aerospace, Industrial, Mechatronic and Manufacturing Engineering*, 8, 743-747.
- DUTTA, P., SAHA, S. K., NANDI, N. & PAL, N. 2016. Numerical study on flow separation in 90° pipe bend under high Reynolds number by k-ε modelling. *Engineering Science and Technology, an International Journal*, 19, 904-910.
- ENTING, I. 1987. On the use of smoothing splines to filter CO<sub>2</sub> data. *Journal of Geophysical Research: Atmospheres*, 92, 10977-10984.
- ESCUDIER, M. 2017. *Introduction to Engineering Fluid Mechanics*, Oxford University Press, Page 512.
- FARHAT, C. & LESOINNE, M. 2000. Two efficient staggered algorithms for the serial and parallel solution of three-dimensional nonlinear transient aeroelastic problems. *Computer Methods in Applied Mechanics and Engineering*, 182, 499-515.
- FARSHAD, F., RIEKE, H. & GARBER, J. 2001. New developments in surface roughness measurements, characterization, and modeling fluid flow in pipe. *Journal of Petroleum Science and Engineering*, 29, 139-150.
- FENNER, T., HARRIS, M., LEVENE, M. & BAR-ILAN, J. 2018. A novel bibliometric index with a simple geometric interpretation. *PLoS One*, 13, e0200098.
- FOURAR, M., RADILLA, G., LENORMAND, R. & MOYNE, C. 2004. On the non-linear behavior of a laminar single-phase flow through two and three-dimensional porous media. *Advances in Water resources*, 27, 669-677.
- GHAJAR, A. J. & BHAGWAT, S. M. 2013. Effect of void fraction and two-phase dynamic viscosity models on prediction of hydrostatic and frictional pressure drop in vertical upward gas-liquid two-phase flow. *Heat Transfer Engineering*, 34, 1044-1059.
- GHOBADI, M. & MUZYCHKA, Y. S. 2016. A review of heat transfer and pressure drop correlations for laminar flow in curved circular ducts. *Heat Transfer Engineering*, 37, 815-839.
- GRANT, I. & COTCHIN, C. 1989. Measurements of two-phase pressure change in a series of 900 vertical pipe bends, in a pipe contraction and in a pipe expansion. *HTFS RS*, 788.

- HAIHIO-GROUP. 2020. *Difference between long radius elbows and short radius elbows* [Online]. Available: <https://thepipefitting.com/difference-between-long-radius-elbows-and-short-radius-elbows.html> [Accessed 2020 2020].
- HEWITT, G. & JAYANTI, S. 1992. Prediction of film inversion in two-phase flow in coiled tubes. *Journal of Fluid Mechanics*, 236, 497-511.
- HSU, L.-C., CHEN, Y., CHYU, C.-M. & WANG, C.-C. 2015. Two-phase pressure drops and flow pattern observations in 90° bends subject to upward, downward and horizontal arrangements. *Experimental Thermal and Fluid Science*, 68, 484-492.
- ISMAEL, S. M. 2015. Quantum Chemical QSPR Study of The Parameters Influences on Viscosity ( $\eta$ ) for Some Aniline Derivatives. 2, 6.
- ITO, H. 1960. Pressure losses in smooth pipe bends. *Journal of Basic Engineering*, 82, 131-140.
- IZQUIERDO, J., FUERTES, V., CABRERA, E., IGLESIAS, P. & GARCIA-SERRA, J. 1999. Pipeline start-up with entrapped air. *Journal of Hydraulic Research*, 37, 579-590.
- JAYANTI, S. 2011. Bends, Flow and Pressure Drop. *Thermopedia*. DOI 10.1615/AtoZ.b.bends\_flow\_and\_pressure\_drop, 9-89.
- KALPAKLI, A. & ÖRLÜ, R. 2013. Turbulent pipe flow downstream a 90 pipe bend with and without superimposed swirl. *International Journal of Heat and Fluid Flow*, 41, 103-111.
- KANDLIKAR, S. G., SCHMITT, D., CARRANO, A. L. & TAYLOR, J. B. 2005. Characterization of surface roughness effects on pressure drop in single-phase flow in minichannels. *Physics of Fluids*, 17, 100606.
- KIM, J., YADAV, M. & KIM, S. 2014. Characteristics of secondary flow induced by 90-degree elbow in turbulent pipe flow. *Engineering Applications of Computational Fluid Mechanics*, 8, 229-239.
- LI, Z.-X. 2003. Experimental study on flow characteristics of liquid in circular microtubes. *Microscale Thermophysical Engineering*, 7, 253-265.
- LIANG, Y., ZENG, C., WANG, J.-J., LIU, M.-W., YEH, T.-C. J. & ZHA, Y.-Y. 2017. Constant gradient erosion apparatus for appraisal of piping behavior in upward seepage flow. *Geotechnical Testing Journal*, 40, 630-642.
- LIN, J. M. & PAULEY, L. L. 1996. Low-Reynolds-number separation on an airfoil. *AIAA journal*, 34, 1570-1577.
- LIN, N., LAN, H.-Q., XU, Y.-G., CUI, Y. & BARBER, G. 2015. Coupled effects between solid particles and gas velocities on erosion of elbows in natural gas pipelines. *Procedia Engineering*, 102, 893-903.
- MAHESHWAR, M. 2018. A REVIEW ARTICLE ON MEASUREMENT OF VISCOSITY.
- NET, H. W. C. 2022. *GB/T 20801.3-2020: Translated English of Chinese Standard. (GBT20801.3-2020): Pressure piping code -- Industrial piping -- Part 3: Design and calculation [Tips: BUY here & GET online-reading at GOOGLE. Then, if you need unprotected-PDF for offline-reading, WRITE to Wayne: Sales@ChineseStandard.net], ChineseStandard. Page 30.*  
<https://www.chinesestandard.net>, .
- NEUTRIUM. 2016. *PRESSURE LOSS FROM FITTINGS - EQUIVALENT LENGTH METHOD* [Online]. Available: <https://neutrium.net/fluid-flow/pressure-loss-from-fittings-excess-head-k-method/> [Accessed 2020 2020].
- NPTEL. 2015. *Losses In Pipe Bends* [Online]. Available: [https://nptel.ac.in/content/storage2/courses/112104118/lecture-37/37-2\\_losses\\_pipe\\_bends.htm](https://nptel.ac.in/content/storage2/courses/112104118/lecture-37/37-2_losses_pipe_bends.htm) [Accessed 2016 2015].

- ONO, K., YOKOTA, Y., SAWADA, Y. & KAWABATA, T. 2018. Lateral force–displacement prediction for buried pipe under different effective stress condition. *International Journal of Geotechnical Engineering*, 12, 420-428.
- PADILLA, M., REVELLIN, R. & BONJOUR, J. 2012. Two-phase flow visualization and pressure drop measurements of HFO-1234yf and R-134a refrigerants in horizontal return bends. *Experimental Thermal and Fluid Science*, 39, 98-111.
- PAPAVINASAM, S. 2013. *Corrosion Control in the Oil and Gas Industry*, Elsevier Science, Page 195.
- PEI, P., LI, Y., XU, H. & WU, Z. 2016. A review on water fault diagnosis of PEMFC associated with the pressure drop. *Applied Energy*, 173, 366-385.
- PERMANENT-STEEL-MANUFACTURING. 2017. *The Difference Between A Long Radius Elbow And A Short Radius Elbow* [Online]. Available: <https://www.permanentsteel.com/newsshow/the-difference-between-a-long-radius-elbow-and-a-short-radius-elbow.html> [Accessed 2017 2017].
- PERRY, J. H. 1950. Chemical engineers' handbook. ACS Publications 2, 641.
- POIRIER, D. R. & GEIGER, G. 2016. *Transport Phenomena in Materials Processing*, Springer International Publishing, Page 123.
- POZOS, O., GONZALEZ, C. A., GIESECKE, J., MARX, W. & RODAL, E. A. 2010. Air entrapped in gravity pipeline systems. *Journal of Hydraulic Research*, 48, 338-347.
- PUTNAM, A. 1964. Discussion:“Velocity and Static-Pressure Distributions in Swirling Air Jets Issuing From Annular and Divergent Nozzles”(Chigier, NA, and Bee’ r, JM, 1964, ASME J. Basic Eng., 86, pp. 788–796).
- RÖHRIG, R., JAKIRLIĆ, S. & TROPEA, C. 2015. Comparative computational study of turbulent flow in a 90 pipe elbow. *International Journal of Heat and Fluid Flow*, 55, 120-131.
- SABET, M. 2016. *Industrial Steam Systems: Fundamentals and Best Design Practices*, CRC Press, Page 6.
- SAVVA, A. P. & FRENKEN, K. 2002. Irrigation manual. *Planning, Development Monitoring and Evaluation of Irrigated Agriculture with Farmer Participation, Modules*, 1-14.
- SILVERBERG, P. 2001. Correlate pressure drops through fittings. *Chemical Engineering*, 108, 127.
- SOMMERFELD, M. & LAIN, S. 2015. Parameters influencing dilute-phase pneumatic conveying through pipe systems: A computational study by the Euler/Lagrange approach. *The Canadian Journal of Chemical Engineering*, 93, 1-17.
- SPEDDING, P., BÉNARD, E. & MCNALLY, G. 2004. Fluid flow through 90 degree bends. *Developments in Chemical Engineering and Mineral Processing*, 12, 107-128.
- SPEIGHT, V. 2014. Impact of pipe roughness on pumping energy in complex distribution systems. *Procedia Engineering*, 70, 1575-1581.
- SPELLMAN, F. R. 2013. *Handbook of Water and Wastewater Treatment Plant Operations, Third Edition*, Taylor & Francis, Page 436.
- STEELJRV. 2018. *Long Radius Elbow vs Short Radius Elbow* [Online]. Available: <https://www.steeljrv.com/long-radius-elbow-vs-short-radius-elbow.html> [Accessed 2018 2018].
- SUDO, K., SUMIDA, M. & HIBARA, H. 1998. Experimental investigation on turbulent flow in a circular-sectioned 90-degree bend. *Experiments in Fluids*, 25, 42-49.
- SUN, T., ZHANG, Y. & WANG, Z. 2012. Research on flow in 90° curved duct with round section. *Physics Procedia*, 24, 692-699.

- TEK, M. 1957. Development of a generalized Darcy equation. *Journal of Petroleum Technology*, 9, 45-47.
- TEZUKA, K., MORI, M., SUZUKI, T., ARITOMI, M., KIKURA, H. & TAKEDA, Y. 2008. Assessment of effects of pipe surface roughness and pipe elbows on the accuracy of meter factors using the ultrasonic pulse Doppler method. *Journal of Nuclear Science and Technology*, 45, 304-312.
- THE ENGINEERING TOOL BOX.COM. 2018. *Water - Dynamic and Kinematic Viscosity* [Online]. Available: [https://www.engineeringtoolbox.com/water-dynamic-kinematic-viscosity-d\\_596.html](https://www.engineeringtoolbox.com/water-dynamic-kinematic-viscosity-d_596.html) [Accessed 2018 2018].
- THORLEY, A. 1994. *Guide to the Design of Thrust Blocks for Buried Pressure Pipelines*, Thomas Telford 5, 224.
- VALIANTZAS, J. D. 2005. Modified Hazen–Williams and Darcy–Weisbach equations for friction and local head losses along irrigation laterals. *Journal of Irrigation and Drainage Engineering*, 131, 342-350.
- VASHISTH, S., KUMAR, V. & NIGAM, K. D. 2008. A review on the potential applications of curved geometries in process industry. *Industrial & Engineering Chemistry Research*, 47, 3291-3337.
- WANG, Y., DONG, Q. & WANG, P. 2015. Numerical investigation on fluid flow in a 90-degree curved pipe with large curvature ratio. *Mathematical Problems in Engineering Journal*, 2015, 5, 15.
- WESKE, J. R. 1948. Experimental Investigation of Velocity Distributions of Downstream of Single Duct Bends. 11, 43.
- WILCOX, B. S. 1978. Steam/its generation and use. *Thirty-ninth edition, 3rd printing*.
- WILSON, H. 2012. *Pressure Drop in Pipe Fittings and Valves* [Online]. Available: <https://www.katmarsoftware.com/articles/pipe-fitting-pressure-drop.htm> [Accessed 2016 2012].
- YASMINA, L. & RACHID, L. Evaluation of energy losses in pipes. Congrès français de mécanique, 2015. AFM, Association Française de Mécanique.
- ZARDIN, B., CILLO, G., RINALDINI, C. A., MATTARELLI, E. & BORGHI, M. 2017. Pressure losses in hydraulic manifolds. *Energies*, 10, 310.
- ZHAN, M., YANG, H., HUANG, L. & GU, R. 2006. Springback analysis of numerical control bending of thin-walled tube using numerical-analytic method. *Journal of Materials Processing Technology*, 177, 197-201.